

**STUDIES ON PHWR TRANSIENTS USING MODIFIED
EXPONENTIAL TIME DIFFERENCING METHOD WITH
IMPROVED QUASI STATIC (IQS) MODEL AND
ASSOCIATED DYNAMIC SENSITIVITY ANALYSIS**

By

M. MOHIDEEN ABDUL RAZAK
(Enrolment No. PHYS-02201204019)

Indira Gandhi Centre for Atomic Research, Kalpakkam

*A thesis submitted to the
Board of Studies in Physical Sciences
In partial fulfilment of requirements
for the degree of*

DOCTOR OF PHILOSOPHY

of

HOMI BHABHA NATIONAL INSTITUTE





August 2019

Homi Bhabha National Institute

Recommendations of the Viva Voce Committee

As members of the Viva Voce Committee, we certify that we have read the dissertation prepared by M. Mohideen Abdul Razak entitled "Studies on PHWR transients using modified exponential time differencing method with improved quasi static (IQS) model and associated dynamic sensitivity analysis" and recommend that it may be accepted as fulfilling the thesis requirement for the award of Degree of Doctor of Philosophy.

Chairman - Dr. K. Velusamy  Date: 16/09/2020

Guide / Convener - Dr. K. Devan  Date: 16/9/2020

Technical Advisor - Dr. G.S. Srinivasan  Date: 16/9/2020

Examiner - Dr. P. Mohanakrishnan  Date: 16/9/2020

Member 1- Dr. G. Raghavan  Date: 16/9/2020

Member 2- Dr. M.T. Jose  Date: 16/09/2020

Final approval and acceptance of this thesis is contingent upon the candidate's submission of the final copies of the thesis to HBNI.

I/We hereby certify that I/we have read this thesis prepared under my/our direction and recommend that it may be accepted as fulfilling the thesis requirement.

Date: 16/9/2020

Place: Kalpakam

Signature 

Dr. K. Devan (Guide)

STATEMENT BY AUTHOR

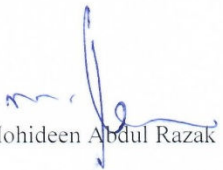
This dissertation has been submitted in partial fulfilment of requirements for an advanced degree at Homi Bhabha National Institute (HBNI) and is deposited in the Library to be made available to borrowers under rules of the HBNI.

Brief quotations from this dissertation are allowable without special permission, provided that accurate acknowledgement of source is made. Requests for permission for extended quotation from or reproduction of this manuscript in whole or in part may be granted by the Competent Authority of HBNI when in his or her judgement the proposed use of the material is in the interests of scholarship. In all other instances, however, permission must be obtained from the author.


M. Mohideen Abdul Razak

DECLARATION

I, hereby declare that the investigation presented in the thesis has been carried out by me. The work is original and has not been submitted earlier as a whole or in part for a degree / diploma at this or any other Institution / University.


M. Mohideen Abdul Razak

List of Publications arising from the thesis

(a) Journals:

1. “The modified exponential time differencing (ETD) method for solving the reactor point kinetics equations”, Mohideen Abdul Razak, M., Devan, K., Sathiyasheela, K., Annals of Nuclear Energy, 2015, vol. 76, 193-199.
2. “The modified exponential time differencing method with IQS model for the neutronic analysis of PHWR transients”, Mohideen Abdul Razak, M., Devan, K., Progress in Nuclear Energy, 2017, vol. 98, 1-10.
3. “Haar wavelet for solving the inverse point kinetics equations and estimation of feedback reactivity coefficient under background noise”, Mohideen Abdul Razak, M., Rathinasamy, N., Nuclear Engineering and Design, 2018, vol. 335, 202-209.

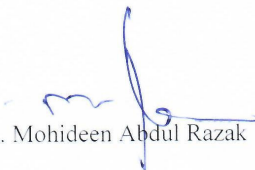
(b) Conference Presentations:

1. “Estimation of Power Transients in Indian Prototype Fast Breeder Reactor (PFBR) with feedback effects using the modified exponential time differencing method”, M. Mohideen Abdul Razak, K. Devan, T. Sathiyasheela, Proceedings of the National Symposium on Radiation Physics (NSRP-20), Mangalore, 2015.

(c) Conference Proceedings:

1. "Design of Finite Impulse Response (FIR) Filters for solving the reactor point kinetics Equations", M. Mohideen Abdul Razak, N. Rathinasamy, DAE-BRNS Symposium on Advances in Reactor Physics (ARP-2017), Anusakthinagar, Mumbai, 2017.

2. "Solution of inverse point kinetics equations using Haar wavelet", M. Mohideen Abdul Razak, N. Rathinasamy, K. Devan, DAE-BRNS Symposium on Advances in Reactor Physics (ARP-2017), Anusakthinagar, Mumbai, 2017.



M. Mohideen Abdul Razak

Dedicated to my parents

ACKNOWLEDGEMENTS

The author expresses his gratitude to Dr. K. Devan, Head, Reactor Neutronics Division (RND), IGCAR, for his highly valuable technical and research guidance during the period of doctoral work. Dr. K. Devan introduced me to reactor kinetics and space-time kinetics. He was my teacher, advisor and philosopher throughout my research work and I am greatly obliged to him for his help. The author expresses his gratitude to Dr. G. S. Srinivasan, Head, SAS, RND, IGCAR, for his persistent encouragement and technical advice on this research work. The author expresses his sincere thanks to doctoral committee members Dr. G. Raghavan, Head, TSS, MPD, IGCAR and Dr. M.T. Jose, RSD, IGCAR. I am highly grateful to my Doctoral Committee Chairman Dr. K. Velusamy, Associate Director, NSAG, IGCAR, for his support.

The author expresses his special thanks to Dr. K. Obaidurrahman, Scientific Officer - F, AERB, Mumbai, for his technical support in the field of transient analysis. Dr. K. Obaidurrahman introduced me to the field of uncertainty and sensitivity analysis in reactor physics and the author expresses his thanks for his technical support in the field of uncertainty and sensitivity analysis. The author expresses his sincere thanks to T. Sathiyasheela, Scientific Officer - G, RND, IGCAR.

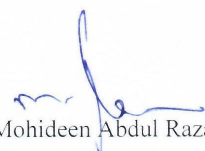
The author expresses his thanks to N. Rathinasamy, Head, TSS, PRPD, for his help and support. The author expresses his special thanks to Dr. A. Moorthi, Scientific Officer - G, PRPD, for his valuable discussions during the research work.

The author sincerely acknowledges the advice rendered by Mr. N. Janarthanan, Scientific Officer - C, Mr. S. Somasundaram, Scientific Officer - E, PRPD. The author would like to express his thanks to P. Ravindra Babu, Scientific Officer - E, BARC-Facilities, Vizag and Mr. S. Dhandapani, Scientific Assistant, PRPD, for their suggestions. The author also expresses his sincere thanks to P. Raghavan, Technical Officer - D and B. Chandrasekar, SO-E, PRPD, for generously sharing the computer facilities. The author acknowledges the assistance rendered by S. Venkatesan, Scientific Assistant, PRPD, in the preparation of art and graphical work.

The author expresses his special thanks to Dr. Suhail Ahmad Khan, Scientific Officer - F, RPDD, BARC, Mumbai, for his help and advice.

The author expresses his thanks to his wife and children for their help.

Above all I express my thanks to The Almighty, God, the most gracious and the most merciful, who gave me strength and knowledge to complete this work. May The Almighty send his blessings to the Holy Prophet Muhammed (peace be upon him), who serves as a splendid model guidance for the entire humanity in the world and may The Almighty extend his blessings to the Holy Prophet's family and his followers.


M. Mohideen Abdul Razak

Abstract

Name of the Student: M. Mohideen Abdul Razak

Name of the CI: IGCAR

Enrolment No.: PHYS-02201204019

Thesis Title: Studies on PHWR transients using modified exponential time differencing method with improved quasi static (IQS) model and associated dynamic sensitivity analysis

Discipline: Physical Sciences

Sub-Area of Discipline: Reactor Physics

Date of viva voce: 16-9-2020

This doctoral work deals with the development of a new computational method, the modified exponential time differencing (ETD) method with improved quasi static (IQS) model, for the estimation of reactor transient and associated dynamic uncertainty and sensitivity analysis. Using this new computational method, the transient can be estimated with good accuracy using large time step. Both the transient estimation as well as the dynamic sensitivity analysis can be performed simultaneously using this computational method. This new computational method is applied to estimate the transients of (i) 3D homogeneous reactor (ii) 3D TWIGL heterogeneous benchmark reactor (iii) 3D LMW heterogeneous benchmark reactor and (iv) CANDU 3D-PHWR (AECL-7236) benchmark reactor. The estimated transients are compared with standard codes. The results are found to be in good agreement. The uncertainty in reactor transient, arising from the uncertainty in macroscopic cross section, is discussed. Both static and dynamic uncertainty and its associated sensitivity analysis are discussed. The sensitivity analysis is performed for (i) 3D homogeneous reactor and (ii) 3D TWIGL heterogeneous benchmark reactor. In the case of static sensitivity analysis, the sensitivity of neutron multiplication factor for various uncertainties in the macroscopic cross section is analyzed and the more influential factor (macroscopic cross section) affecting the neutron multiplication factor is determined. The dynamic uncertainty in transient, arising from the uncertainty in the macroscopic cross section, is estimated by incorporating the IQS model in the forward sensitivity analysis procedure (FSAP). While incorporating the IQS model in FSAP, a new kind of point kinetics equations is developed and its solution with the shape function gives the dynamic uncertainty in transient. The new kind of point kinetics equation is solved using the modified ETD method. In the FSAP with IQS model, only one time scale (single time scale) is adopted to estimate the dynamic uncertainty in reactor transient. The estimated dynamic uncertainty and the results of dynamic sensitivity analysis are found to be in good agreement with the direct solution method. Using this new computational method, the estimation of reactor transient as well as the dynamic sensitivity analysis can be performed simultaneously.

CONTENTS

	Page No
SUMMARY	xii
LIST OF FIGURES	xiv
LIST OF TABLES	xviii
NOMENCLATURE	xx
CHAPTER 1 INTRODUCTION	1
1.1 Introduction	1
1.2 Need for time dependent neutron diffusion equation	2
1.3 Motivation and organization of the thesis	4
CHAPTER 2 SOLUTION OF TIME DEPENDENT NEUTRON DIFFUSION EQUATION	8
2.1 Introduction	8
2.2 Direct Solution Methods	13
2.2.1 Frequency Transform Method	14
2.3 Indirect Solution Methods	15
2.3.1 Modal Expansion Method	15
2.3.2 Flux Factorization Method	17
2.3.2.1 Adiabatic Method	18
2.3.2.2 Quasi static Method	19
2.3.2.3 Improved Quasi Static (IQS) Method	19
2.4 Transient estimation methodology in the IQS scheme	22
2.5 Steps adopted to estimate the transient in the IQS scheme	23
2.6 Summary	24
CHAPTER 3 POINT KINETICS MODEL	25
3.1 Introduction to point kinetics equations	25
3.2 Modified exponential time differencing (ETD) Method	26

3.3	Error analysis of the modified ETD method and convergence of solution	30
3.4	Application to thermal reactors	36
3.4.1	Power transients of thermal reactor caused by step reactivity	36
3.5	Application to Indian Prototype Fast Breeder Reactor (PFBR) transients	37
3.5.1	Step reactivity insertion	37
3.5.2	Ramp reactivity insertion	38
3.6	Inverse point kinetics equations – Solution by modified ETD method	41
3.7	Estimation of temperature coefficient of reactivity of thermal reactor	45
3.8	Estimation of temperature coefficient of reactivity of Indian Prototype Fast Breeder Reactor (PFBR) from simulated transient with various background noise levels	51
3.9	Summary	57

CHAPTER 4 MODIFIED ETD METHOD WITH IQS MODEL 59

4.1	Introduction	59
4.2	3D Homogeneous Reactor Transients	59
4.3	3D TWIGL Benchmark Reactor Transients	66
4.4	3D LMW Benchmark Reactor Transients	72
4.5	CANDU 3D-PHWR (AECL-7236) Benchmark Transients	80
4.5.1	LOCA simulation in CANDU 3D-PHWR	81
4.5.2	Transient estimation and discussion	85
4.5.3	Flux distribution and power tilts in CANDU-PHWR during transient	86
4.6	Summary	98

CHAPTER 5 DYNAMIC UNCERTAINTY QUANTIFICATION AND	
SENSITIVITY ANALYSIS IN REACTOR TRANSIENTS	100
5.1 Introduction to uncertainty quantification and sensitivity analysis in reactor transients	100
5.2 Types of uncertainty analysis	103
5.3 Brute Force Method	106
5.4 Static Adoint Sensitivity Analysis Procedure (ASAP)	114
5.5 Forward Sensitivity Analysis Procedure (FSAP)	115
5.6 Dynamic uncertainty and sensitivity analysis in reactor transient – Forward Sensitivity Analysis Procedure (FSAP) with IQS method	116
5.6.1 Estimation of dynamic uncertainty in flux during transient	121
5.6.2 Dynamic uncertainty and sensitivity analysis in 3D Homogeneous reactor transient	122
5.6.3 Dynamic uncertainty and sensitivity analysis in 3D TWIGL Benchmark reactor transient	127
5.7 Summary	131
CHAPTER 6 SUMMARY AND CONCLUSIONS	132
6.1 Conclusions	132
6.2 Scope for further research	136
REFERENCES	137

Thesis Highlights

Name of the Student: M. Mohideen Abdul Razak

Name of the CI: IGCAR

Enrolment No.: PHYS-02201204019

Thesis Title: Studies on PHWR transients using modified exponential time differencing method with improved quasi static (IQS) model and associated dynamic sensitivity analysis

Discipline: Physical Sciences

Sub-Area of Discipline: Reactor Physics

Date of viva voce: 16-9-2020

A new computational method is developed using modified exponential time differencing (ETD) method with improved quasi static (IQS) model, for the estimation of reactor transient and associated dynamic uncertainty and sensitivity analysis. Using this new computational method, the transient can be estimated with good accuracy using large time step. Both the transient estimation as well as the dynamic sensitivity analysis can be performed simultaneously using this computational method. This new computational method is applied to estimate the transients of (i) 3D homogeneous reactor (ii) 3D TWIGL heterogeneous benchmark reactor (iii) 3D LMW heterogeneous benchmark reactor and (iv) CANDU 3D-PHWR (AECL-7236) benchmark reactor. The estimated transients are found to be in good agreement with standard results. The uncertainty in reactor transient, arising from the uncertainty in macroscopic cross section, is estimated using this method. Both static and dynamic uncertainty and its associated sensitivity analysis can be performed using this method. The sensitivity analysis is performed for (i) 3D homogeneous reactor and (ii) 3D TWIGL heterogeneous benchmark reactor. The sensitivity of neutron multiplication factor for various uncertainties in the macroscopic cross section is analyzed using this method and the more influential factor (macroscopic cross section) affecting the neutron multiplication factor is determined. The dynamic uncertainty in transient, arising from the uncertainty in the macroscopic cross section, is estimated by incorporating the IQS model in the forward sensitivity analysis procedure (FSAP). While incorporating the IQS model in FSAP, a new kind of point kinetics equations is developed and its solution with the shape function gives the dynamic uncertainty in transient. The new kind of point kinetics equation is solved using the modified ETD method. In the FSAP with IQS model, only one time scale (single time scale) is adopted to estimate the dynamic uncertainty in reactor transient. The estimated dynamic uncertainty and the results of dynamic sensitivity analysis are found to be in good agreement with the direct solution method. Using this new computational method, the estimation of reactor transient as well as the dynamic sensitivity analysis can be performed simultaneously.

CHAPTER 1

INTRODUCTION

1.1 Introduction

Energy availability is important for human development and it is the prime factor for economic growth. With increase in population, the economic growth continues to increase and the demand for energy further rises. The rise in demand for energy can be met by burning fossil fuels or from nuclear reactors. The fossil fuels, i.e. coal, gas, oil, will produce large amount of carbon dioxide, which causes environmental pollution. Fossil fuel plants require large amount of coal and gas. With a complete combustion, approx. 8 kWh of heat can be generated from 1 kg of coal, approx. 12 kWh from 1 kg of mineral oil and around 24,000,000 kWh from 1 kg of uranium-235. Thus, 1 kg natural uranium corresponds to nearly 10,000 kg of mineral oil or 14,000 kg of coal and enables the generation of 45,000 kWh of electricity. In contrast to fossil fuel plants (coal, oil and gas), nuclear power plants do not produce any carbon dioxide, methane, or other toxic emissions, which are major contributors to the greenhouse effect.

Compared to other forms of energy, the nuclear energy is cost effective and economical. During the recent decades the nuclear energy has become an essential part of safe and cost effective mode of energy worldwide. The nuclear energy has the potential to support the growing energy need of the industries in the world. Nuclear power currently provides about 11% of the world's electricity, with 12 countries using nuclear power for at least 30% of their national electricity generation. According to International Atomic Energy Agency (IAEA), as of today, there are 449 operational nuclear power reactors in 30 countries, with 56 others under construction in 15 countries. The production of nuclear energy from nuclear reactor is not limited

to power generation only. The production of a wide range of radioactive isotopes for medical and industrial applications, research and development in basic sciences depend on the effective utilization of neutron flux from nuclear reactors. Energy production from nuclear reactor is not free from risk. Ensuring a safe and reliable operation of every nuclear reactor at its rated power over the desired core life is the combined responsibility of suppliers, utilizers and regulators.

The safe and efficient operation of nuclear reactor requires a thorough knowledge of the underlying physical processes taking place in nuclear reactors. The physical process taking place in nuclear reactor is obtained by mathematical modeling and simulation. The principal tools used in this task consist of various numerical methods to estimate the neutron behaviour in the reactor core and understand the space and time dependent physical processes occurring in the core.

1.2 Need for time dependent neutron diffusion equation

A major class of analysis in the reactor core design is the estimation of spatial neutron flux distribution under normal operating and postulated accidental conditions. All nuclear reactors must be designed against postulated initiating events (PIE) and design basis accidents (DBA), which may refer to operational error, reactor start-up accident, sudden ejection of control rod etc. A perturbation in the reactor core due to DBA, during start-up or at steady state, may lead to creation of transient. Sometimes the transient may be detected immediately following the perturbation and in some cases the transient may not be detected immediately. In large reactor cores, a minor perturbation in any localized area may remain unnoticed due to neutron decoupling and this may lead to reactor accident. The power transients taking place in nuclear reactors depend on the kind of reactivity perturbation acting on the reactor and also the power

level at which the reactor is operating. The exact prediction of reactor transient is done by solving the neutron diffusion equation in space and time (space-time kinetics). Accurate estimation of transient will give information about the core power, fuel temperature and hot channel factors. The hot channel factors will in turn give information about the safety margins. But uncertainty always exists in the core output parameters. It is equally important to predict the uncertainty involved in the estimation of reactor transient and other parameters. The prediction of uncertainty in the transient will give information in fixing the hot channel factors and safety margins deterministically. Hence for safe operation of nuclear reactors, the information about the temporal distribution of neutron flux with uncertainty is important. However, the transient can also be predicted using the space-independent reactor model, i.e. the point reactor model, generally known as the point reactor kinetics. But the point reactor model adopts the fundamental mode approximation on space and hence the temporal variation in reactor power and core reactivity, are not very accurately estimated [1]. The point reactor model is applicable for small reactors. In the case of large reactors, due to loosely coupled nature, the neutron flux behaviour during the transient is well studied using the time dependent neutron diffusion equation. In large reactors, a very local perturbation will obviously affect the neutron flux in the immediate vicinity of the perturbation. The distribution of flux, following the perturbation, will give accurate information about the hot channel factors which in turn will determine the limit on core power. Hence for large reactors the estimation of spatial distribution of neutrons is important and this is the reason why the space-time kinetics calculation is widely adopted in the analysis of large reactor cores. Generally the solution of time dependent neutron diffusion equation can be broadly classified into two categories, i.e. direct solution method and indirect solution method. These methods are well described by Sutton and Aviles [1]. In direct method of

solution, the reactor volume is divided into finite meshes and the flux in each mesh is obtained by direct integration or using polynomials ([2]-[4]). The flux factorization method is an indirect method of solving the neutron diffusion equation. Compared to direct methods, the indirect solution methods are faster. The improved quasi static (IQS) model is an indirect method of solving the neutron diffusion equation and it has high efficiency. Due to its high efficiency, the IQS model is adopted in several codes to analyze the transients in large reactors ([5]-[7]). Jain and Gupta [8] developed 3D FAST code based on IQS model to analyze the super-delayed transients in reactors. Several improvements were introduced in the IQS model to estimate the transients in a more effective way. Dahmani et al [9] introduced the theta method in the IQS model to solve the precursor concentration equations and this is adopted in MINOS-CRONOS-3D code. The space-time analysis codes DIF3D [7] and KIKO3D [10] were developed based on IQS model. In this work, we develop a new computational method, the modified exponential time differencing method with IQS model, to estimate the transient and its uncertainty and perform the associated dynamic sensitivity analysis.

1.3 Motivation and organization of the thesis

The computer programs or codes that solve the neutron diffusion equation, both static and dynamic, are generally quite complex and are frequently the result of many years of extensive development. Modern nuclear reactor design depends heavily on efficient computer codes and mathematical models of the reactor core. The motivation for the development of computationally efficient numerical method to solve the neutron diffusion equation and its implementation to realistic reactors is always on the rise. In this regard we develop a new computationally efficient method, the modified exponential time differencing method with improved quasi static model, to

solve the neutron diffusion equation in space and time and analyze the transients. The novelty of this computational method is that the transients can be estimated with good accuracy using large time step thereby reducing the computation time. This new computational method is capable of analyzing the transients in highly heterogeneous reactors. This new computational method is applied to estimate the transients of few international benchmark reactors. The benchmark reactors, considered here, have varying degrees of heterogeneities. The estimated transients are found to be in good agreement with the standard results. The effect of space part in estimating the transient is also discussed. This computational method is also used to perform the dynamic sensitivity analysis in reactor transient. This method adopts one time-scale only (single time scale) to perform the dynamic sensitivity analysis. It serves as one of the fastest and efficient method in analyzing the dynamic uncertainty and sensitivity in reactor transient. The estimation of transient as well as the dynamic sensitivity analysis can be performed simultaneously by using it.

The thesis is organized as follows. **Chapter 2** deals with the different types of techniques to solve the time dependent neutron diffusion equation. It provides discussion on direct method of solution and indirect method of solution. In the indirect solution method, the modal expansion and the flux factorization methods are discussed. It gives detailed discussion on Improved Quasi Static (IQS) model, adopted in the flux factorization technique. Two approximations adopted in the IQS model, i.e. the adiabatic method and the quasi static method are also discussed. Transient estimation methodology adopted in the IQS model is described. **Chapter 3** discusses the development of the modified exponential time differencing (ETD) method to solve the point kinetics equation. The applicability of modified ETD method to solve the point kinetics equations for various kinds of reactivity perturbations are discussed in this chapter. This method

is found to be an efficient method to solve the point kinetics equations for different kinds of reactivity insertions, i.e. step and ramp. This method is applied to Indian Prototype Fast Breeder Reactor (PFBR) to predict the transient for longer duration of time. Using this method, the transient can be estimated with large time step. Its smooth coupling into the IQS model is discussed. The applicability of this method to solve the inverse point kinetics equations to estimate the reactivity from the observed noisy transient, (transient with background noise) is discussed. This method is applied to estimate the temperature coefficient of reactivity of Indian PFBR from the observed power transient with various background noise levels. **Chapter 4** deals with the estimation of transient using the modified ETD method with IQS model for few international benchmark reactors and the accuracy of this new computational method is discussed. The transients in CANDU 3D-PHWR (AECL 7236) benchmark, 3D LMW benchmark, 3D TWIGL benchmark and 3D homogeneous reactors are estimated using this method. In CANDU 3D-PHWR, the transients, following LOCA, are estimated for various micro and macro time steps and the accuracy of this computational method is discussed. The flux distribution and power tilts in CANDU 3D-PHWR during the transient are discussed. The importance of space part in estimating the transient is discussed. It is observed that the effect of space part is more pronounced when the reactor size is large as well as when the perturbation in the cross section is localized, i.e. within confined area. It is observed that when the space part is neglected, the error in the estimation of core power becomes large as the transient duration is increased. In the case of 3D LMW benchmark, the transient, following the control rod ejection accident (REA), is analyzed for longer duration of time. Similarly in 3D TWIGL and 3D homogeneous reactors, the transients following the perturbation in macroscopic cross section are analyzed. The error in the estimation of peaking factors, when the space part is neglected during

the transient, is also discussed. **Chapter 5** deals with the uncertainty quantification and sensitivity analysis in reactor transients. Both static and dynamic sensitivity analysis are discussed here. The propagation of macroscopic cross section uncertainty with time and its impact on core power, peak mesh power and peaking factor during the transient is discussed. In the case of static sensitivity analysis, the sensitivity of neutron multiplication factor with respect to uncertainty in the cross section is analyzed. A linear relation between the sensitivity coefficient and the uncertainty in the cross section is established. The dynamic sensitivity analysis is discussed in detail. The dynamic uncertainty in reactor transient and its associated sensitivity analysis are performed using forward sensitivity analysis procedure (FSAP) with IQS model. While incorporating the IQS model in FSAP, a new kind of point kinetics equation is arrived at and its solution is obtained using the modified ETD method. The dynamic uncertainties in core power, total peaking factor and peak mesh power, during the transient, are analyzed with respect to uncertainty in the cross sections and the dynamic sensitivity coefficients are estimated. The accuracy of dynamic sensitivity coefficient, estimated using FSAP with IQS model is discussed. Simultaneous estimation of transient and its uncertainty is discussed in this chapter. **Chapter 6** gives the conclusions.

CHAPTER 2

SOLUTION OF TIME DEPENDENT NEUTRON DIFFUSION EQUATION

2.1 Introduction

The neutron transport equation deals with the time-dependent angular distribution of neutrons in reactor. The transport equation characterizes the overall reactor behavior and can be obtained by setting up the neutron balance equation [11]. Consider a differential element dV at location ' r ' in space as shown in Fig. 2.1.

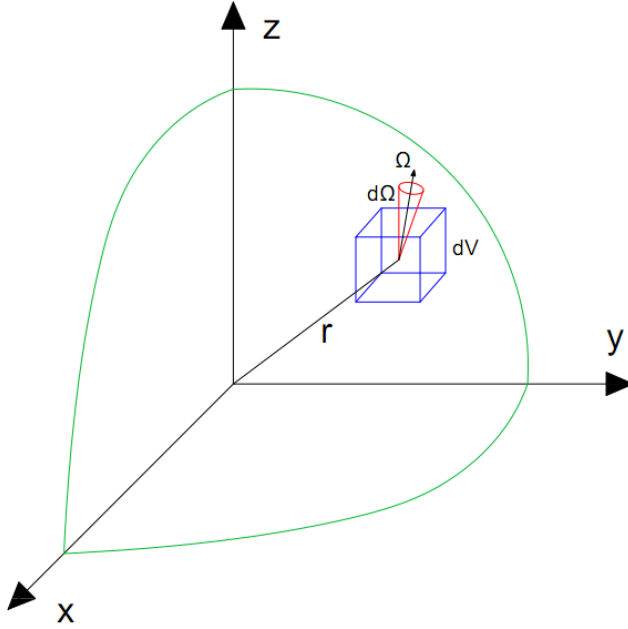


Fig. 2.1. Differential volume dV at location ' r '

We denote the angular neutron number density $N(r, E, \hat{\Omega}, t)$ to represent the number density of neutrons at time t , in unit volume around position r , unit energy interval at E and unit solid

angle in the direction $\widehat{\Omega}$. The neutron balance equation in the differential volume dV is written as

$$\begin{aligned} \text{Rate of change of neutrons (in } dV \text{)} = \\ \text{rate of production of neutrons} - \text{rate of destruction of neutrons} \end{aligned} \quad (2.1)$$

The rate of change of neutrons in a volume element dV at r , within dE at E , within $d\Omega$ at $\widehat{\Omega}$, and at time t can be written as

$$\text{Rate of change of neutrons} = \frac{\partial N(\vec{r}, E, \widehat{\Omega}, t)}{\partial t} dV dE d\Omega \quad (2.2)$$

Neutrons will be removed from the volume element dV by leaking out through the surfaces or by colliding. We use the operator $L(r, E, \widehat{\Omega}, t)$ to represent the neutron destruction process (removal process) in dV at time t and it is given as

$$\begin{aligned} L(r, E, \widehat{\Omega}, t) v N(r, E, \widehat{\Omega}, t) dV dE d\Omega = \\ v \cdot \widehat{\Omega} \cdot \nabla N(r, E, \widehat{\Omega}, t) dV dE d\Omega + \Sigma_t(r, E, \widehat{\Omega}, t) \cdot v N(r, E, \widehat{\Omega}, t) dV dE d\Omega \end{aligned} \quad (2.3)$$

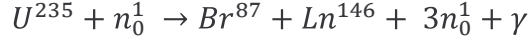
where the first term on the right hand side (RHS) represents the leakage rate and the second term represents the neutron collision rate. Here, Σ_t is the total cross section of the material in volume dV and v is the neutron speed. Meanwhile, in the volume dV , the neutrons are scattered into $d\Omega dE$ from $d\Omega' dE'$ and the scattering process is denoted by the operator S and it is given as

$$\begin{aligned} S(r, E, \widehat{\Omega}, t) v N(r, E, \widehat{\Omega}, t) dV dE d\Omega = \\ \int_0^{4\pi} d\Omega' \int_0^\infty dE' \Sigma_s(r, E' \rightarrow E, \widehat{\Omega}' \rightarrow \widehat{\Omega}, t) v' N(r, E', \widehat{\Omega}', t) dV dE d\Omega \end{aligned} \quad (2.4)$$

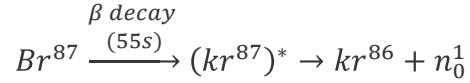
Most importantly, neutrons are generated from fission reactions in dV and it is represented by the operator F as

$$F(r, E, t) v N(r, E, \widehat{\Omega}, t) dV dE d\Omega = \frac{1}{4\pi} \int_0^{4\pi} d\Omega' \int_0^\infty dE' v \Sigma_f(r, E', t) v' N(r, E', \widehat{\Omega}', t) dV dE d\Omega \quad (2.5)$$

where ν is the average number of fission neutrons released per fission. In a typical fission reaction, most of the fission neutrons are released promptly within 10^{-14} s, e.g.



These neutrons are called prompt neutrons. There is also a small fraction of fission neutrons, less than 1%, which are released from fission products after beta decay, e.g.



These neutrons are called delayed neutrons and their release time is determined by the half-life of the beta decay process, ranging from less than a second to a minute. Fission products which produce delayed neutrons are called the delayed-neutron precursors. For a nuclear fission reaction, a multitude of delayed-neutron precursors are produced. For convenience, they are grouped into six groups according to their half-lives. The fraction of neutrons generated per fission, for the i^{th} precursor group, is denoted as β_i and $\beta(\sum_i \beta_i)$, is the total fraction of delayed neutrons generated from all precursors per fission. Therefore, the neutron production rate in dV at time t , with delayed neutrons, can be written as

Rate of production of neutrons =

$$S(r, E, \Omega, t) \nu N(r, E, \Omega, t) dV dE d\Omega + (1 - \beta) \chi_p(E) F(r, E, t) \nu N(r, E, \Omega, t) dV dE d\Omega + \sum_{i=1}^6 \chi_{d,i}(E) \lambda_i C_i(r, t) dV dE d\Omega + Q(r, E, \Omega, t) dV dE d\Omega \quad (2.6)$$

where χ_p is the prompt neutron spectrum, and $\chi_{d,i}$ is the delayed-neutron spectrum for the i^{th} precursor group. We introduce C_i as the number density of the i^{th} precursor group with decay constant λ_i , and Q as the external source. Finally, the continuous neutron transport equation can be written using Eqs. (2.1)-(2.6) as

$$\begin{aligned}
& \frac{\partial N(r, E, \widehat{\Omega}, t)}{\partial t} dV dE d\Omega \\
&= -v \cdot \widehat{\Omega} \cdot \nabla N(r, E, \widehat{\Omega}, t) dV dE d\Omega - \Sigma_t(r, E, \widehat{\Omega}, t) \cdot v N(r, E, \widehat{\Omega}, t) dV dE d\Omega \\
&+ \int_0^{4\pi} d\Omega' \int_0^\infty dE' \cdot \Sigma_s(r, E' \rightarrow E, \Omega' \rightarrow \Omega, t) \cdot v' N(r, E', \widehat{\Omega}', t) dV dE d\Omega \\
&+ \frac{(1-\beta)\chi_p}{4\pi} \int_0^{4\pi} d\Omega' \int_0^\infty dE' \cdot v \Sigma_f(r, E', t) v' N(r, E', \widehat{\Omega}', t) dV dE d\Omega \\
&+ \sum_{i=1}^6 \chi_{d,i}(E) \lambda_i C_i(r, t) dV dE d\Omega + Q(r, E, \widehat{\Omega}, t) dV dE d\Omega
\end{aligned} \tag{2.7}$$

After cancelling $dV dE d\Omega$ on both sides, we get the neutron transport equation, i.e. Boltzman transport equation as

$$\begin{aligned}
& \frac{\partial N(r, E, \widehat{\Omega}, t)}{\partial t} + v \cdot \widehat{\Omega} \cdot \nabla N(r, E, \widehat{\Omega}, t) + \Sigma_t(r, E, \widehat{\Omega}, t) v N(r, E, \widehat{\Omega}, t) \\
&= \int_0^{4\pi} d\Omega' \int_0^\infty dE' \Sigma_s(r, E' \rightarrow E, \Omega' \rightarrow \Omega, t) v' N(r, E', \widehat{\Omega}', t) \\
&+ \frac{(1-\beta)\chi_p}{4\pi} \int_0^{4\pi} d\Omega' \int_0^\infty dE' v \Sigma_f(r, E', t) v' N(r, E', \widehat{\Omega}', t) \\
&+ \sum_{i=1}^6 \chi_{d,i}(E) \lambda_i C_i(r, t) + Q(r, E, \widehat{\Omega}, t)
\end{aligned} \tag{2.8}$$

The above equation (Eq. (2.8)) contains derivatives as well as integrals and hence it is also called as integro-differential equation. The neutron transport equation (Eq. (2.8)) provides an exact description of the neutron angular distribution (say in the energy group ' g ') within the reactor. The solution of Eq. (2.8) yields the angular neutron density $N(r, E, \widehat{\Omega}, t)$, which contains all the information which we desire. For a complete description of neutron behaviour in nuclear

reactors, Eq. (2.8) must be solved for each neutron energy group ' g '. We denote the angular neutron flux, in the energy group ' g ' as $\phi_g(r, E, \Omega, t) = v_g N_g(r, E, \hat{\Omega}, t)$, $N_g(r, E, \hat{\Omega}, t)$ represents the angular neutron density in the energy group ' g ', and v_g is the neutron velocity in the energy group ' g '. The angular current density is represented by $j(r, E, \hat{\Omega}, t) = \hat{\Omega} \cdot \phi_g(r, E, \Omega, t)$

The neutron diffusion equation is obtained from neutron transport equation by assuming few approximations. First we make the assumption that we are interested only in angle integrated flux rather than angular flux. In other words we transform $\phi_g(r, E, \Omega, t)$ to $\phi_g(r, E, t)$ by integration, i.e. $\phi_g(r, E, t) = \int_0^{4\pi} \phi_g(r, E, \Omega, t) d\Omega$. We also denote the neutron current density, in the energy group ' g ' as $\vec{J}_g(r, E, t) = \int_0^{4\pi} j(r, E, \hat{\Omega}, t) d\Omega$, and $\phi_g(r, E, t) = v_g N_g(r, E, t)$. With these assumptions, the neutron transport equation in the energy group ' g ', i.e. Boltzman transport equation, Eq. (2.8) is integrated with respect to angle and it is given as

$$\begin{aligned} \frac{1}{v_g} \frac{\partial \Phi_g}{\partial t} = & -\nabla \cdot (\vec{J}_g) - \Sigma_t^g(r, t) \Phi_g + \sum_{g'=1}^g \Sigma_s^{g' \rightarrow g}(r, t) \Phi_{g'} + (1 - \beta) \chi_p^g \sum_{g'=1}^g v \Sigma_f^{g'}(r, t) \Phi_{g'} + \\ & \sum_{i=1}^6 \chi_{d,i}^g \lambda_i C_i(r, t) + Q \end{aligned} \quad (2.8a)$$

In the above equation, $\Phi_g = \phi_g(r, E, t)$, Σ_t^g is the total cross section in the energy group ' g ', $\Sigma_s^{g' \rightarrow g}$ is the scattering cross section from group $g' \rightarrow g$, $v \Sigma_f^g$ is group fission cross section, $Q(Q(r, E, t))$ is the external neutron source in the energy group ' g '. Using transport theory, the neutron current density, \vec{J}_g , is approximated as $\vec{J}_g = -D_g(r) \vec{\nabla} \Phi_g$ [11]. Under these assumptions, the neutron transport equation becomes the neutron diffusion equation and it is given as

$$\frac{1}{v_g} \frac{\partial \Phi_g}{\partial t} = \vec{\nabla} \cdot (D_g \vec{\nabla} \Phi_g) - \Sigma_t^g(r, t) \Phi_g + \sum_{g'=1}^g \Sigma_s^{g' \rightarrow g}(r, t) \Phi_{g'} + (1 - \beta) \chi_p^g \sum_{g'=1}^g \nu \Sigma_f^{g'}(r, t) \Phi_{g'} + \sum_{i=1}^6 \chi_{d,i}^g \lambda_i C_i(r, t) + Q \quad (2.8b)$$

In terms of operators, the neutron diffusion equation (2.8b) becomes

$$\frac{1}{v_g} \frac{\partial \Phi_g}{\partial t} + L_g \Phi_g = S_g \Phi_g + (1 - \beta) \chi_p F_g \Phi_g + \sum_{i=1}^6 \chi_{d,i} \lambda_i C_i + Q \quad (2.9)$$

In the above equation (Eq. (2.9)), ' L_g ' ($L_g = -\vec{\nabla} \cdot (D_g \vec{\nabla}) + \Sigma_{Rg}$) represents the neutron destruction operator, ' S_g ' represents the production operator by scattering, ' F_g ' ($F_g = \sum_{g'} (\nu \Sigma_{fg'})$) represents the production operator by fission, $\lambda_i C_i$ denote the delayed neutron source and ' Q ', is the external source. The above equation has to be coupled with the precursor concentration equations, which give delayed neutrons. The precursor concentration equations are given by

$$\frac{\partial C_i(r, t)}{\partial t} = \beta_i \sum_{g'=1}^g \nu \Sigma_f^{g'}(r, t) \Phi_{g'} - \lambda_i C_i \quad (2.10)$$

The detailed description of neutron transport theory and diffusion equation can be found in [11]-[14].

2.2 Direct Solution Methods

The neutron diffusion equation (Eq. (2.9)) can be solved directly as well as indirectly. According to direct method, the solution to time-dependent neutron diffusion equation (one group) is written as (from Eq. (2.9))

$$\frac{1}{v} \frac{\partial \Phi}{\partial t} = \frac{1}{v} \frac{\Phi_i^{t+1} - \Phi_i^t}{\Delta t} = -L\Phi + S\Phi + (1 - \beta) \chi_p F\Phi + \sum_{i=1}^6 \chi_{d,i} \lambda_i C_i + Q \quad (2.11)$$

In the above equation Φ_i^{t+1} is the neutron flux at i^{th} mesh at time ' $t + 1$ ' and Φ_i^t is the neutron flux at i^{th} mesh at time ' t '. From the above equation, the time-dependent neutron flux can be estimated as

$$\Phi_i^{t+1} = \Phi_i^t + v\Delta t(-L\Phi_i^t + S\Phi_i^t + (1 - \beta)\chi_p F\Phi_i^t + \sum_{i=1}^6 \chi_{d,i} \lambda_i C_i + Q) \quad (2.12)$$

The constants involved in the RHS are evaluated at ' t '. Since the neutron velocity in thermal reactor is of the order of $\sim 10^5$ cm/s, the time step Δt has to be chosen of the order of $\sim 10^{-6}$ or even less. Using such a small time step for solving the neutron diffusion equation will consume more computation time of the order of several hours and it will introduce lot of round off and truncation errors. For this reason this method is generally not used. Nevertheless this method is the simplest method and using this method the time dependent neutron flux can be obtained.

2.2.1 Frequency Transform Method

It is also another form of direct solution method. This method is widely used in the solution of time dependent neutron diffusion equation. The codes SCOPE2, PARCS, AETNA and SIMULATE3-K adopt this method [15]-[18]. The frequency transform method assumes that in the case of transient, the flux evolves exponentially with time. Under this assumption, the neutron flux can be modeled as

$$\varphi_g(r, t) = \tilde{\varphi}_g(r, t) \exp(\omega(r, t)t) \quad (2.13)$$

Using this assumption, the neutron diffusion equation (Eq. (2.8b)) becomes

$$\begin{aligned} \frac{1}{v_g} \frac{\partial \tilde{\varphi}_g}{\partial t} = & \exp(-\omega(r, t)t) \left(\nabla \cdot (D_g \nabla \Phi_g) - \left[\Sigma_t^g(r, t) + \frac{\omega(r, t)}{v_g} \right] \Phi_g + \sum_{g'=1}^g \Sigma_s^{g' \rightarrow g}(r, t) \Phi_{g'} + \right. \\ & \left. (1 - \beta) \chi_p^g \sum_{g'=1}^g v \Sigma_f^{g'}(r, t) \Phi_{g'} + \sum_{i=1}^6 \chi_{d,i}^g \lambda_i C_i(r, t) + Q \right) \end{aligned} \quad (2.14)$$

The above equation can be solved using explicit or implicit scheme. The solution of Eq. (2.14) gives the time dependent neutron flux. The detailed information about the solution procedure can be obtained from the works of [19].

2.3 Indirect Solution Methods

2.3.1 Modal Expansion Method

To reduce the computational burden and estimate the time dependent neutron flux with reasonable accuracy, indirect methods were devised. Modal synthesis method (or Modal Expansion Method (MEM)) and Improved Quasi Static (IQS) Method come under this category. The key concept in modal expansion method [20]-[22] is that the space-time flux can be factored into a finite sum of spatial shape functions. These shape functions are the spatial modes weighted by a set of time dependent modal amplitudes. The calculation of the space-time flux then reduces to calculating these time-dependent weight factors, which constitute the coupled generalized point kinetics equations. Generally the modes, chosen for the expansion, are the set of λ modes (k-eigen values) or static modes, which are generated from the steady state of reactor before the start of the transient. Higher order lambda modes are generated using subtraction method or filtration method [23]. The detailed calculation of higher order lambda modes can be found in the works of [24]. The accuracy of the time dependent neutron diffusion equation mainly depends on the number of lambda modes chosen for the expansion. As the number of modes increases, the accuracy of the solution will increase.

According to modal synthesis method, the neutron flux, $\Phi_g(r, t)$, corresponding to a perturbation in the core properties, is expanded as a weighted series of fixed number of λ modes which are linearly independent and it is given as [22], [25]

$$\Phi_g(r, t) = \sum_{l=0}^M a_l(t) \Psi_l^g(r) \quad (2.15)$$

where $\Psi_l^g(r)$ is the l^{th} static eigen function corresponding to the eigen value ' λ_l ', for a particular group ' g '. The functions $a_l(t)$ are the amplitude functions or weight functions which are to be evaluated. In principle the choice of shape functions is arbitrary; with the only restriction that the

functions must satisfy the static neutron diffusion equation and they must be linearly independent.

Consider the time dependent neutron diffusion equation (Eq. 2.8b))

$$\frac{1}{v} \frac{\partial \Phi_g}{\partial t} = \nabla \cdot (D_g \nabla \Phi_g) - \Sigma_t^g(r, t) \Phi_g + \sum_{g'=1}^g \Sigma_s^{g' \rightarrow g}(r, t) \Phi_{g'} + (1 - \beta) \chi_p^g \sum_{g'=1}^g v \Sigma_f^{g'}(r, t) \Phi_{g'} + \sum_{i=1}^6 \chi_{d,i}^g \lambda_i C_i(r, t) + Q \quad (2.16)$$

Let the perturbation in the cross section be assumed as $D_g = D_g^0 + \delta D_g$, $\Sigma_g = \Sigma_g^0 + \delta \Sigma_g$ and $v \Sigma_f = v \Sigma_f^0 + \delta(v \Sigma_f)$. This leads to perturbation in the operators as $L = L_0 + \delta L$ and $M = M_0 + \delta M$.

Substituting Eq. (2.15) into Eq. (2.16) and integrating over the volume of reactor after pre multiplying with steady state adjoint flux Ψ_m^* , we get

$$\sum_{l=1}^M \Lambda_{ml} \frac{da_l}{dt} = (\rho_m - \beta) N_m a_m + (1 - \beta) \sum_{l=1}^M A_{ml}^M a_l - \sum_{l=1}^M A_{ml}^L a_l + \sum_{k=1}^6 \lambda_k C_{mk} \quad (2.17)$$

$$\frac{dC_{mk}}{dt} = \beta_k N_m a_m + \beta_k \sum_{l=0}^M A_{ml}^M a_l - \lambda_k C_{mk} \quad (2.18)$$

In the above equations, (Eqs. (2.17)-(2.18)) the constants are given as (following inner product notation)

$$\rho_k = \frac{1 - \lambda_k}{\lambda_k} \quad (2.19)$$

$$\Lambda_{ml} = \langle \Psi_m^*, \frac{1}{v_g} \Psi_l \rangle \quad (2.20)$$

$$A_{ml}^L = \langle \Psi_m^*, \delta L \Psi_l \rangle \quad (2.21)$$

$$A_{ml}^M = \langle \Psi_m^*, \delta M \Psi_l \rangle \quad (2.22)$$

$$C_{mk} = \langle \Psi_m^*, \chi_d^g C_i(r, t) \rangle \quad (2.23)$$

In Eqs. (2.20)-(2.23), Ψ_m^* denotes the steady state adjoint flux corresponding to m^{th} mode. The adjoint flux is obtained by solving the adjoint neutron diffusion equation. The adjoint flux is

referred as the importance function which gives the asymptotic increase or decrease in the neutron flux (in the energy group ‘g’) when a single neutron is introduced at location \vec{r} . Solution of Eqs. (2.17)-(2.18), gives the amplitude coefficients a_l . The detailed derivation can be found in [25]. The amplitude coefficients, a_l , along with the static mode eigen functions can be used to determine the time dependent neutron flux, $\Phi_g(r, t) = \sum_{l=0}^M a_l(t) \Psi_l^g(r)$. This method may be adopted for control studies of large pressurized heavy water reactors [26]-[28].

2.3.2 Flux Factorization Method

This is an indirect method of solving the neutron diffusion equation. The flux factorization method is an efficient computational method for solving the time dependent neutron diffusion equation [29]. The motivation behind the use of the flux factorization method is that in many instances the spatial flux (shape function) is weakly dependent on time and as a result it may not be necessary to re-compute it at every time step. Since the estimation of the shape function is typically very computationally expensive, while computation of the amplitude function is relatively inexpensive, the space-time factorization method can often yield accurate results using far less computer resources than direct methods using a similar spatial treatment.

According to this method the neutron flux of energy group, $\Phi_g(r, t)$, is factored into time part and space part. The time part is called the amplitude function and the space part is called the shape function. The time dependent flux is written as

$$\Phi_g(r, t) = T(t) \Psi_g(r, t) \quad (2.24)$$

$T(t)$ is the amplitude function and $\Psi_g(r, t)$ is the shape function. The amplitude function $T(t)$ is dependent on time only and the shape function $\Psi_g(r, t)$ weakly depends on time. This method

has two approximations, (i) the adiabatic approximation and (ii) the quasi static approximation. The improved quasi-static (IQS) method is an improvement of quasi static approximation and gives accurate solution to the time dependent neutron diffusion equation. Hence the IQS method is adopted by several core calculation codes [5]-[9], [30]. The improved quasi static method does not involve any approximation. Substituting Eq. (2.24) into Eq. (2.8b) we get (neglecting external source Q)

$$\begin{aligned} \frac{1}{v} \frac{\partial \Psi_g}{\partial t} = & \nabla \cdot (D_g \nabla \Psi_g) - \Sigma_r^g(r, t) \Psi_g + \sum_{g'=1}^g \Sigma_s^{g' \rightarrow g}(r, t) \Psi_{g'} + (1 - \beta) \chi_p^g \sum_{g'=1}^g v \Sigma_f^{g'}(r, t) \Psi_{g'} + \\ & \frac{1}{T(t)} \sum_{i=1}^6 \chi_{d,i}^g \lambda_i C_i(r, t) - \frac{\Psi_g}{T(t)} \frac{1}{v} \frac{\partial T(t)}{\partial t} \end{aligned} \quad (2.25)$$

2.3.2.1 Adiabatic Method

In adiabatic method, [29], [31], [32], it is assumed that during the transient, the reactor is assumed to be in steady state in each successive time interval during the transient. Let T be the transient duration and t_1, t_2, t_3 etc. be any time during the transient time interval, i.e. $0 < t_1 < t_2 < t_3 < T$. At ' t_1 ', the reactor is assumed to be in steady state; hence in this case ($t = t_1$) the time derivative of flux is zero, i.e. $\frac{\partial \Phi_g}{\partial t} = 0$. With this assumption, Eq. (2.25) is rewritten as

$$\nabla \cdot (D_g \nabla \Psi_g) - \Sigma_r^g(r, t) \Psi_g + \sum_{g'=1}^g \Sigma_s^{g' \rightarrow g}(r, t) \Psi_{g'} + \frac{\chi_p^g}{k_{eff}} \sum_{g'=1}^g v \Sigma_f^{g'}(r, t) \Psi_{g'} = 0 \quad (2.26)$$

The parameters in the above equation are evaluated at $t = t_1, t_2, t_3$ etc. The above equation is solved to get the shape function $\Psi_g(r, t)$. Using the shape function $\Psi_g(r, t)$, obtained from Eq. (2.26), the parameters in the point kinetics equations are estimated and the point kinetics equations are solved to get the amplitude function i.e. $T(t)$. The product of amplitude function and the shape function gives the actual flux.

2.3.2.2 Quasi Static Method

It is a slightly improved form of adiabatic method. In this method [14], [22], [29], [32] the delayed neutron source is taken into account. Here $\frac{\partial \Psi_g}{\partial t} = 0$ rather than $\frac{\partial \Phi_g}{\partial t} = 0$. The equation to be solved, in this case, is given below

$$\nabla \cdot (D_g \nabla \Psi_g) - \Sigma_r^g(r, t) \Psi_g + \sum_{g'=1}^g \Sigma_s^{g' \rightarrow g}(r, t) \Psi_{g'} + (1 - \beta) \chi_p^g \sum_{g'=1}^g v \Sigma_f^{g'}(r, t) \Psi_{g'} + \frac{1}{T(t)} \sum_{i=1}^6 \chi_{d,i}^g \lambda_i C_i(r, t) - \frac{\Psi_g}{T(t)} \frac{1}{v} \frac{\partial T(t)}{\partial t} = 0 \quad (2.27)$$

The above equation has to be solved along with the point kinetics equations. The product of $T(t)$ and $\Psi_g(r, t)$ gives the actual flux.

2.3.2.3 Improved Quasi Static (IQS) Method

The improved quasi static (IQS) method [21], [28], is an effective method for solving the time dependent neutron diffusion equation. It is an improved form of quasi-static model. In the IQS method, the flux consists of two functions, i.e. amplitude function and shape function. The amplitude function describes the fast time evolution of neutron flux in the reactor. The shape function slowly evolves with time. The IQS method has good computational efficiency to predict reactivity initiated transients. Many numerical space-time codes adopt the IQS scheme to estimate the transients in nuclear reactors. Predictor corrector method can also be employed in the IQS method [33]-[35] to estimate the transients.

Consider the time dependent multi-group neutron diffusion equation (external source $Q = 0$) with delayed neutron precursor groups (Eqs. (2.9) & (2.10))

$$\frac{1}{v_g} \frac{\partial \phi_g(r, t)}{\partial t} + \hat{L} \phi_g(r, t) = S_g \Phi_g(r, t) + \chi_g^p (1 - \beta) \hat{F} \phi_g(r, t) + \sum_{i=1}^M \chi_d^i \lambda_i C_i(r, t) \quad (2.28)$$

$$\frac{\partial C_i(r, t)}{\partial t} = \beta_i \hat{F} \phi_g(r, t) - \lambda_i C_i(r, t) \quad (2.29)$$

where $\hat{L} = -\nabla \cdot (D_g \nabla) + \Sigma_{Rg}$ is the removal operator and $\hat{F} = \sum_{g'} (v \Sigma_{fg'})$ is the fission operator (neutron production operator). In the above equation Σ_{Rg} is the removal cross section and other symbols carry usual meaning. The removal operator \hat{L} and the fission operator \hat{F} are determined by the material properties of the reactor. According to IQS scheme, the time dependent flux, $\phi_g(r, t)$, is written as

$$\phi_g(r, t) = T(t) \psi_g(r, t) \quad (2.30)$$

Substituting Eq. (2.30) into Eqs. (2.28) and (2.29), we get the amplitude function (equation) as [32]

$$\frac{dT(t)}{dt} = \left[\frac{\rho(t) - \beta(t)}{\Lambda} \right] T(t) + \sum_{i=1}^6 \lambda_i C_i(t) \quad (2.31)$$

$$\frac{dC_i(t)}{dt} = \frac{\beta_i(t)}{\Lambda} T(t) - \lambda_i C_i(t) \quad (2.32)$$

and the shape function as

$$\begin{aligned} \frac{1}{v_g} \frac{\partial \psi_g(r, t)}{\partial t} = & \nabla \cdot (D_g \nabla \psi_g(r, t)) - \Sigma_{Rg} \psi_g(r, t) + \chi_g^p (1 - \beta) \sum_{g=1}^G v \Sigma_{fg} \psi_g(r, t) + \sum_{g' \neq g} \Sigma_{g' \rightarrow g} \psi_{g'}(r, t) + \\ & \frac{1}{T(t)} \sum_{i=1}^6 \chi_d^i \lambda_i C_i(r, t) - \frac{1}{v_g} \frac{\psi_g(r, t)}{T(t)} \frac{dT(t)}{dt} \end{aligned} \quad (2.33)$$

The amplitude function, along with the precursor concentration, is known as the point kinetics equation (Eqs. (2.31) and (2.32)). The kinetics parameters $\rho(t)$, $\beta(t)$ and Λ are calculated using the weight function ψ^\dagger and they are given as [32]

$$\begin{aligned} \rho(t) &= \frac{\langle \psi^\dagger (\{\chi_g^p\} \hat{F} - \hat{L}) \psi_g(r, t) \rangle}{\langle \psi^\dagger (\{\chi_g^p\} \hat{F}) \psi_g(r, t) \rangle} \\ \beta_i(t) &= \frac{\langle \psi^\dagger (\beta_i \hat{F}) \psi_g(r, t) \rangle}{\langle \psi^\dagger (\{\chi_g^p\} \hat{F}) \psi_g(r, t) \rangle} \end{aligned}$$

$$\Lambda = \frac{Z}{\langle \psi^\dagger(\{\chi_g^p\}\hat{F}) \psi_g(r, t) \rangle}$$

The weight function is taken as the adjoint flux. To arrive at the amplitude function, we have used the normalization condition $\langle \psi^\dagger \left(\frac{1}{v_g} \right) \psi(r, t) \rangle = \int \psi^\dagger \left(\frac{1}{v_g} \right) \psi(r, t) dV = Z(\text{constant})$. The kinetics parameters $\rho(t)$, $\beta_i(t)$ and Λ are estimated using the adjoint neutron flux ψ^\dagger . The adjoint neutron flux is obtained from the solution of adjoint neutron diffusion equation. As described in section 2.3.1, the adjoint flux is known as the importance function which gives information about the asymptotic neutron flux when a single neutron is introduced at location \vec{r} . When a small change in the neutron flux is introduced at \vec{r} in the reactor, the asymptotic increase or decrease in the flux is estimated by making use of adjoint flux. Hence the worth of control devices and other kinetics parameters are estimated using adjoint flux. The shape function Eq. (2.33) can be numerically solved using implicit scheme with large time step. The detailed description of IQS method is given by [32], Mohideen Abdul Razak [36] and Rakesh Kumar [30].

In IQS model, one has to solve the point kinetics equations and shape functions. The point kinetics equations alone can predict the transient satisfactorily in medium sized thermal reactors as well as in tightly coupled fast reactors. The point kinetics equations are stiff differential equations. A major difficulty in numerically solving the point kinetics equations arises from the stiffness term, which necessitates the requirement of choosing very small time step to solve the equation numerically. In this work, the modified exponential time differencing (ETD) method is used for solving the point kinetics equations with multi group of delayed neutrons and it is coupled in the IQS model to calculate the shape function.

2.4 Transient estimation methodology in the IQS scheme

The transients are estimated by solving the amplitude function and the shape function at two different time scales. Since a fine time step (micro time step, Δt) is required to solve the amplitude function and a large time step (macro time step, ΔT) may be used to solve the shape function, two different time scales are adopted in this method [36], [30]. This is shown in Fig. 2.2. Generally the macro time step will be an integral multiple of micro time step. An initial guess about the shape function at macro time step is assumed. With the assumed shape function, the kinetics parameters and dynamic reactivity are calculated. Using these parameters, the amplitude function is solved using the modified exponential time differencing method. At the end of the micro time step, the shape function is calculated. With the calculated shape function, the dynamic reactivity is checked for convergence. This process is repeated till the dynamic reactivity converges. After the convergence, the shape function is calculated for the next macro time step and so on. In this way the shape function is calculated for the full length of the transient time. The product of amplitude function and shape function gives the actual neutron flux in the reactor.

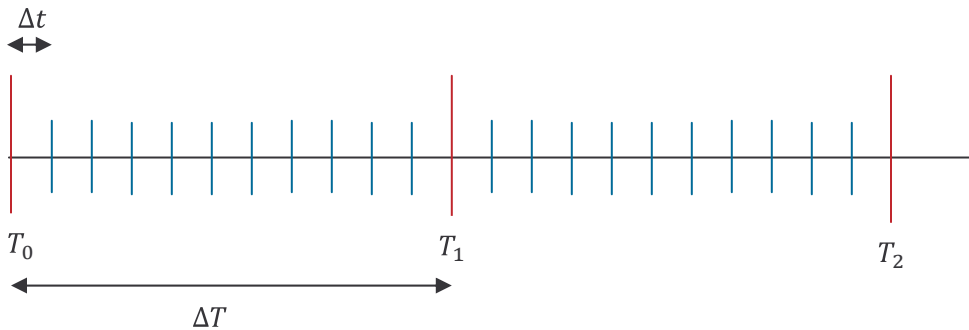


Fig. 2.2. The micro time step (Δt) and the macro time step (ΔT) adopted in the IQS model. T_0 , T_1 , T_2 denote the macroscopic time at which the shape functions are calculated.

2.5 Steps adopted to estimate the transient in the IQS scheme

The macro time steps at which the shape functions are calculated are denoted as T_0 , T_1 , T_2 , T_3 , etc. in Fig. 2.2. The amplitude function is solved using micro time step Δt . The following steps are adopted to estimate the transient in the IQS scheme:

Step 1: The transient is assumed to start $t = T_0$. At macro time T_0 , the shape function is taken as the initial flux (steady state) and the amplitude function is taken as 1.

Step 2: At T_1 , the reactor state is obtained; i.e. position of the control devices, change in the cross section etc. At this time the shape function is assumed to be as that corresponding to T_0 . Using the shape function, the kinetics parameters, i.e. the dynamic reactivity, neutron generation time and delayed neutron fractions are calculated.

Step 3: Using the kinetics parameters, the point kinetics equation is solved using micro time step Δt (Fig. 2.2) and the amplitude function is obtained at T_1 .

Step 4: Using the amplitude function, the shape function is calculated at T_1 and the delayed neutron precursor equation is solved at T_1 .

Step 5: With the shape function, the kinetics parameters, i.e. the dynamic reactivity, neutron generation time and delayed neutron fractions are recalculated.

Step 6: The kinetics parameters are checked for convergence.

Step 7a: If the kinetics parameters have converged then proceed for the calculation of the shape function for the next macroscopic time $t = T_2$ and so on.

Step 7b: If the kinetics parameters have not converged then repeat the steps 3-6 till convergence is obtained.

2.6 Summary

Different solution techniques for solving the time dependent neutron diffusion equation are discussed. The solution of neutron diffusion equation using modal expansion method and flux factorization method are discussed in detail. Two approximations in the flux factorization method are described. From the flux factorization technique, the equation governing the amplitude function (point kinetics equation) and shape function are discussed. The concept of micro time step and macro time step are discussed. The transient estimation methodology and the steps adopted in the IQS model are described.

CHAPTER 3

POINT KINETICS MODEL

3.1 Introduction to Point Kinetics Equations

The point kinetics equations represent the time evolution of power in small reactors. The point kinetics equations are stiff differential equations and special techniques are used to handle the stiffness term while solving the equations. There are different kinds of methodologies available in the literature to solve the stiff point kinetics equations. Hennart and Barrios [37] applied the Pade and Chebyshev type approximation to solve the point kinetics equations. One can use the third order Hermite Polynomial Method (HPM) [38] to solve the point kinetics equations. Hongqiu and Dapu [39] introduced the end floating method (EFM) for solving the point kinetics equations. Aboanber and Nahla [40], [41] developed the analytical inversion method for solving the point kinetics equations with multi-group delayed neutrons. Li et al. [42] introduced a numerical integral method using the better basis function (BBF) for solving the point kinetics equations and investigated the power transients caused by various types of reactivity insertion in thermal reactors. Recently Nahla [43] applied the Taylor series method (TSM) to solve the point kinetics equations.

Here we develop the modified exponential time differencing (ETD) method for solving the point kinetics equations [44]. The advantage of the modified ETD method is that the point kinetics equations can be solved using large time step with good accuracy and the size of the time step can be chosen by satisfying certain criteria. It is proved in this section that this method is capable of estimating the power transients for various types of reactivity perturbations. Its smooth coupling to IQS model is presented to estimate the reactor transients. This method is also

applied to solve the inverse point kinetics equations to estimate the reactivity from the observed power transient with noise.

3.2 Modified exponential time differencing (ETD) method

The Exponential Time Differencing (ETD) methods are time integration techniques that provide accurate solutions to stiff differential equations. The exponential time differencing (ETD) method was originally proposed in the field of computational electrodynamics [45] to solve stiff differential equations. The modified exponential time differencing method is developed by integrating the point kinetics equations over a single time-step using an integrating factor. The power and precursor concentrations in the equations are expanded as a polynomial in derivatives and then integrated. The coefficients of the polynomial, i.e. the ETD coefficients, are obtained from integration of simple function and a recurrence relation between them is also obtained. The recurrence relation is used to determine higher order ETD coefficients. In this method the stiffness term is not involved explicitly in the numerical solution and hence the power transient may be estimated using large time-step. This method is validated to estimate the power transients of thermal reactors as well as the power transients of the 500 MWe Indian Prototype Fast Breeder Reactor (PFBR).

Consider the following stiff differential equation

$$\frac{du}{dt} = cu + F(u, t) \quad (3.1)$$

In the above equation ' c ' is the stiffness constant which may be large and $F(u, t)$ may be a nonlinear term. To numerically solve this kind of stiff differential equation, one should be able to handle the stiffness constant ' c ', by properly choosing the time-step ' h '. To solve Eq. (3.1) using

the exponential time differencing method, it is multiplied by an integrating factor e^{-ct} and integrated over a single time-step, from $t = t_n$ to $t = t_{n+1} = t_n + h$, to get

$$\int_{t_n}^{t_{n+1}} \frac{d}{dt} (ue^{-ct}) dt = \int_{t_n}^{t_{n+1}} F(u, t) e^{-ct} dt \quad (3.2)$$

After integrating, we get (use change of variable as $\tau = t - t_n$)

$$u(t_{n+1}) = u(t_n) e^{ch} + e^{ch} \int_0^h e^{-c\tau} F(u(t_n + \tau), t_n + \tau) d\tau \quad (3.3)$$

where $\tau = t - t_n$. The purpose of transforming Eq. (3.1) into Eq. (3.2) is to remove the explicit dependence of the stiffness constant ' c ' in Eq. (3.1). In the numerical solution, i.e. Eq. (3.3), the stiffness constant appears only in the exponential term. By removing the explicit dependence of the stiffness constant, the solution to Eq. (3.3), may be obtained using large time-step ' h '. Another major critical step in Eq. (3.3) lies in choosing a proper approximation for the integrand $F(u, t)$ in the interval $t_n < t < t_n + h$. If $F(u, t)$ is known a priori for $t < t_n$, then $F(u, t)$ in the interval $t_n < t < t_n + h$ may be obtained using interpolation with its previous values and the integral expression in Eq. (3.3) can be evaluated [46]-[47]. In case if $F(u, t)$ is not known a priori, then $F(u, t)$ in the time interval $t_n < t < t_n + h$ can be obtained from the Taylor series expansion of $F(u, t_n)$.

Now consider the point kinetics equations given by

$$\frac{dp(t)}{dt} = \left(\frac{\rho(t) - \beta}{\Lambda} \right) p(t) + \sum_{i=1}^6 \lambda_i C_i(t) \quad (3.4)$$

$$\frac{dC_i}{dt} = \left(\frac{\beta_i}{\Lambda} \right) p(t) - \lambda_i C_i \quad (i = 1, 2 \dots 6) \quad (3.5)$$

In the above Eqs. (3.4)-(3.5), p is the power, Λ is the prompt neutron generation time, β_i is the effective fraction of the i^{th} group of delayed neutrons, β is the total effective fraction of delayed neutrons ($\beta = \sum_{i=1}^6 \beta_i$), λ_i and C_i are the decay constant and precursor concentration of the i^{th} group of the delayed neutrons respectively. The initial conditions of the point kinetics equations

are chosen as $p(t = 0) = p_0$, $c_i(t = 0) = \frac{\beta_i}{\Lambda \lambda_i} p_0$, p_0 is the steady state power before the occurrence of transient. The neutron generation time, Λ , is of the order of $\sim 10^{-5} s$ for thermal reactors and it is of the order of $\sim 10^{-7} s$ for fast reactors. Here the stiffness constant appears as $\frac{1}{\Lambda}$. To solve the point kinetics equations by the modified ETD method, Eqs. (3.4)-(3.5) are

multiplied by the integrating factor $e^{\frac{t}{\Lambda}}$ and integrated over a single time-step from $t = t_n$ to $t = t_{n+1} = t_n + h$, to get

$$\int_{t_n}^{t_{n+1}} \frac{d}{dt} \left(p e^{\frac{t}{\Lambda}} \right) dt = \int_{t_n}^{t_{n+1}} \left(\frac{\rho(t) - \beta}{\Lambda} \right) p e^{\frac{t}{\Lambda}} dt + \int_{t_n}^{t_{n+1}} \sum_{i=1}^6 \lambda_i C_i(t) e^{\frac{t}{\Lambda}} dt + \frac{1}{\Lambda} \int_{t_n}^{t_{n+1}} p e^{\frac{t}{\Lambda}} dt \quad (3.6)$$

$$\int_{t_n}^{t_{n+1}} \frac{d}{dt} \left(C_i e^{\frac{t}{\Lambda}} \right) dt = \int_{t_n}^{t_{n+1}} \frac{\beta_i}{\Lambda} p e^{\frac{t}{\Lambda}} dt + \left(\frac{1}{\Lambda} - \lambda_i \right) \int_{t_n}^{t_{n+1}} C_i(t) e^{\frac{t}{\Lambda}} dt \quad (3.7)$$

After integrating and rearranging Eqs. (3.6)-(3.7), we get (use change of variable as $\tau = t - t_n$)

$$p(t_{n+1}) = p(t_n) e^{\frac{-h}{\Lambda}} + \int_0^h e^{\frac{\tau-h}{\Lambda}} \frac{\rho(t_n+\tau)}{\Lambda} p(t_n+\tau) d\tau + \left(\frac{1-\beta}{\Lambda} \right) \int_0^h e^{\frac{\tau-h}{\Lambda}} p(t_n+\tau) d\tau + \int_0^h e^{\frac{\tau-h}{\Lambda}} \sum_{i=1}^6 \lambda_i C_i(t_n+\tau) d\tau \quad (3.8)$$

$$C_i(t_{n+1}) = C_i(t_n) e^{\frac{-h}{\Lambda}} + \frac{\beta_i}{\Lambda} \int_0^h e^{\frac{\tau-h}{\Lambda}} p(t_n+\tau) d\tau + \left(\frac{1}{\Lambda} - \lambda_i \right) \int_0^h e^{\frac{\tau-h}{\Lambda}} C_i(t_n+\tau) d\tau \quad (3.9)$$

Here, in the above Eqs. (3.8)-(3.9), we expand $p(t_n + \tau)$ and $C_i(t_n + \tau)$ as a polynomial in derivatives using Taylor series expansion of order ' $S - 1$ '. They are expanded as

$$p(t_n + \tau) = \sum_{k=0}^{S-1} \nabla^k p(t_n) \frac{\tau^k}{k!} \quad (3.10)$$

$$C_i(t_n + \tau) = \sum_{k=0}^{S-1} \nabla^k C_i(t_n) \frac{\tau^k}{k!} \quad (3.11)$$

where $\nabla^k = \frac{d^k}{dt^k}$. The reason for expanding the power and precursor concentrations using

Taylor's series is that it only requires the present value of power and its derivatives and does not require previous power history. The local truncation errors in the Taylor series expansion of $p(t_n + \tau)$ and $C_i(t_n + \tau)$ are termed as $R_1(p)$ and $R_2(C_i)$ respectively and they are given as

$$R_1(p) = \sum_{k=S}^{\infty} \nabla^k p(t_n) \frac{\tau^k}{k!} \quad (3.12)$$

$$R_2(C_i) = \sum_{k=S}^{\infty} \nabla^k C_i(t_n) \frac{\tau^k}{k!} \quad (3.13)$$

Substituting Eqs. (3.10)-(3.11) into Eqs. (3.8)-(3.9), we get

$$\begin{aligned} p(t_{n+1}) &= p(t_n) e^{\frac{-h}{\Lambda}} + \frac{1}{\Lambda} \int_0^h e^{\frac{\tau-h}{\Lambda}} \rho(t_n + \tau) \left(\sum_{k=0}^{S-1} \nabla^k p(t_n) \frac{\tau^k}{k!} \right) d\tau \\ &\quad + \left(\frac{1-\beta}{\Lambda} \right) \int_0^h e^{\frac{\tau-h}{\Lambda}} \left(\sum_{k=0}^{S-1} \nabla^k p(t_n) \frac{\tau^k}{k!} \right) d\tau + \sum_{i=1}^6 \lambda_i \int_0^h e^{\frac{\tau-h}{\Lambda}} \left(\sum_{k=0}^{S-1} \nabla^k C_i(t_n) \frac{\tau^k}{k!} \right) d\tau \end{aligned} \quad (3.14)$$

$$\begin{aligned} C_i(t_{n+1}) &= C_i(t_n) e^{\frac{-h}{\Lambda}} + \frac{\beta_i}{\Lambda} \int_0^h e^{\frac{\tau-h}{\Lambda}} \left(\sum_{k=0}^{S-1} \nabla^k p(t_n) \frac{\tau^k}{k!} \right) d\tau \\ &\quad + \left(\frac{1}{\Lambda} - \lambda_i \right) \int_0^h e^{\frac{\tau-h}{\Lambda}} \left(\sum_{k=0}^{S-1} \nabla^k C_i(t_n) \frac{\tau^k}{k!} \right) d\tau \end{aligned} \quad (3.15)$$

After interchanging the order of summation and integration in Eqs. (3.14)-(3.15), we get

$$\begin{aligned} p(t_{n+1}) &= p(t_n) e^{\frac{-h}{\Lambda}} + \frac{1}{\Lambda} \sum_{k=0}^{S-1} \nabla^k p(t_n) q(k) + \left(\frac{1-\beta}{\Lambda} \right) \sum_{k=0}^{S-1} \nabla^k p(t_n) u(k) \\ &\quad + \sum_{i=1}^6 \lambda_i \sum_{k=0}^{S-1} \nabla^k C_i(t_n) u(k) \end{aligned} \quad (3.16)$$

$$C_i(t_{n+1}) = C_i(t_n) e^{\frac{-h}{\Lambda}} + \frac{\beta_i}{\Lambda} \sum_{k=0}^{S-1} \nabla^k p(t_n) u(k) + \left(\frac{1}{\Lambda} - \lambda_i \right) \sum_{k=0}^{S-1} \nabla^k C_i(t_n) u(k) \quad (3.17)$$

where $q(k)$ is given as

$$q(k) = \int_0^h e^{\frac{\tau-h}{\Lambda}} \rho(t_n + \tau) \frac{\tau^k}{k!} d\tau \quad (3.18)$$

and the ETD coefficient $u(k)$ of order ' k ' is given as

$$u(k) = \int_0^h e^{\frac{\tau-h}{\Lambda}} \frac{\tau^k}{k!} d\tau \quad (3.19)$$

Eqs. (3.16)-(3.17) provide the numerical solution to the power transient and precursor concentrations using the Taylor's series expansion of $p(t_{n+1})$ and $C_i(t_{n+1})$ upto order ' $S - 1$ '.

Substituting $k = 0$ in Eq. (3.19) we get

$$u(0) = \left(1 - e^{\frac{-h}{\Lambda}}\right) \Lambda \quad (3.20)$$

The recurrence relation of the ETD coefficient $u(k)$ (Eq. (3.19)) is given as

$$u(k) = \frac{\Lambda h^k}{k!} - \Lambda u(k-1), \quad k \geq 1 \quad (3.21)$$

3.3 Error analysis of the modified ETD method and convergence of solution

The final global errors involved in the numerical solution of the power transient (Eq. 3.16) and the precursor concentrations (Eq. 3.17) are determined as follows. By increasing the order of the Taylor series expansion of $p(t_n + \tau)$ and $C_i(t_n + \tau)$, Eqs. (3.16)-(3.17) are rewritten as

$$\begin{aligned} p(t_{n+1}) = & p(t_n) e^{\frac{-h}{\Lambda}} + \frac{1}{\Lambda} \sum_{k=0}^{S-1} \nabla^k p(t_n) q(k) + \left(\frac{1-\beta}{\Lambda}\right) \sum_{k=0}^{S-1} \nabla^k p(t_n) u(k) \\ & + \sum_{i=1}^6 \lambda_i \sum_{k=0}^{S-1} \nabla^k C_i(t_n) u(k) + \frac{1}{\Lambda} \sum_{k=S}^{\infty} \nabla^k p(t_n) q(k) + \left(\frac{1-\beta}{\Lambda}\right) \sum_{k=S}^{\infty} \nabla^k p(t_n) u(k) \\ & + \sum_{i=1}^6 \lambda_i \sum_{k=S}^{\infty} \nabla^k C_i(t_n) u(k) \end{aligned} \quad (3.22)$$

$$\begin{aligned}
C_i(t_{n+1}) = & C_i(t_n)e^{\frac{-h}{\Lambda}} + \frac{\beta_i}{\Lambda} \sum_{k=0}^{S-1} \nabla^k p(t_n) u(k) + \left(\frac{1}{\Lambda} - \lambda_i\right) \sum_{k=0}^{S-1} \nabla^k C_i(t_n) u(k) \\
& + \frac{\beta_i}{\Lambda} \sum_{k=S}^{\infty} \nabla^k p(t_n) u(k) + \left(\frac{1}{\Lambda} - \lambda_i\right) \sum_{k=S}^{\infty} \nabla^k C_i(t_n) u(k)
\end{aligned} \tag{3.23}$$

The final global errors $\epsilon_1(p)$ and $\epsilon_2(C_i)$, involved in the computation of the power transient and precursor concentrations, (Eq.(3.22)-(3.23)) are given as

$$\epsilon_1(p) = \frac{1}{\Lambda} \sum_{k=S}^{\infty} \nabla^k p(t_n) q(k) + \left(\frac{1-\beta}{\Lambda}\right) \sum_{k=S}^{\infty} \nabla^k p(t_n) u(k) + \sum_{i=1}^6 \lambda_i \sum_{k=S}^{\infty} \nabla^k C_i(t_n) u(k) \tag{3.24}$$

$$\epsilon_2(C_i) = \frac{\beta_i}{\Lambda} \sum_{k=S}^{\infty} \nabla^k p(t_n) u(k) + \left(\frac{1}{\Lambda} - \lambda_i\right) \sum_{k=S}^{\infty} \nabla^k C_i(t_n) u(k) \tag{3.25}$$

These global errors $\epsilon_1(p)$ and $\epsilon_2(C_i)$ arise due to the truncation errors $R_1(p)$ and $R_2(C_i)$. For step (constant) and slowly varying reactivity insertions, Eqs. (3.22)-(3.23) are further simplified as follows. In this case $q(k) \sim \rho(t_n) u(k)$, $u(0) \sim \Lambda$ and $u(k) \sim \frac{\Lambda h^k}{k!}$ for $k \geq 1$ (since $\left(\frac{1}{\Lambda}\right) \gg 1$ and $\Lambda^{k+1} \ll \frac{\Lambda h^k}{k!}$). Substituting $q(k)$ and $u(k)$ into Eqs. (3.22)-(3.25), we get

$$p(t_{n+1}) = p(t_n)e^{\frac{-h}{\Lambda}} + (1 - \beta + \rho(t_n)) \sum_{k=0}^{S-1} \nabla^k p(t_n) \frac{h^k}{k!} + \Lambda \sum_{i=1}^6 \lambda_i \sum_{k=0}^{S-1} \nabla^k C_i(t_n) \frac{h^k}{k!} + \epsilon_1(p) \tag{3.26}$$

$$C_i(t_{n+1}) = C_i(t_n)e^{\frac{-h}{\Lambda}} + \beta_i \sum_{k=0}^{S-1} \nabla^k p(t_n) \frac{h^k}{k!} + (1 - \Lambda \lambda_i) \sum_{k=0}^{S-1} \nabla^k C_i(t_n) \frac{h^k}{k!} + \epsilon_2(C_i) \tag{3.27}$$

and the final global errors $\epsilon_1(p)$ and $\epsilon_2(C_i)$ are given as

$$\epsilon_1(p) = (1 - \beta + \rho(t_n)) \sum_{k=S}^{\infty} \nabla^k p(t_n) \frac{h^k}{k!} + \Lambda \sum_{i=1}^6 \lambda_i \sum_{k=S}^{\infty} \nabla^k C_i(t_n) \frac{h^k}{k!} \quad (3.28)$$

$$\epsilon_2(C_i) = \beta_i \sum_{k=S}^{\infty} \nabla^k p(t_n) \frac{h^k}{k!} + (1 - \Lambda \lambda_i) \sum_{k=S}^{\infty} \nabla^k C_i(t_n) \frac{h^k}{k!} \quad (3.29)$$

Eqs. (3.26)-(3.27) represent the numerical solution to the power transient and the precursor concentrations for step and slowly varying reactivity insertions. Eqs. (3.28)-(3.29) represent the global errors involved in the computation of power transient and the precursor concentrations.

The numerical solution of the power transient $p(t_{n+1})$ and precursor concentrations $C_i(t_{n+1})$, (Eqs. (3.26)-(3.27)), converge if the global errors $\epsilon_1(p)$ and $\epsilon_2(C_i)$, (Eqs. (3.28)-(3.29)), become

small as the order of the ETD coefficients is increased, i.e. $\lim_{k \rightarrow \infty} \nabla^k p(t_n) \frac{h^k}{k!} \rightarrow 0$ and

$\lim_{k \rightarrow \infty} \nabla^k C_i(t_n) \frac{h^k}{k!} \rightarrow 0$. At a first glance, the global errors $\epsilon_1(p)$ and $\epsilon_2(C_i)$ can be made to

approach zero by choosing $h < 1$. However the time-step h and its upper bound are determined

as follows. For step and slowly varying reactivity insertion, $\nabla^k p(t_n)$ and $\nabla^k C_i(t_n)$ can be written

in matrix form as

$$\begin{bmatrix} \nabla^k p(t_n) \\ \nabla^k C_1(t_n) \\ \nabla^k C_2(t_n) \\ \nabla^k C_3(t_n) \\ \nabla^k C_4(t_n) \\ \nabla^k C_5(t_n) \\ \nabla^k C_6(t_n) \end{bmatrix} = \begin{pmatrix} \frac{\rho - \beta}{\Lambda} & \lambda_1 & \lambda_2 & \lambda_3 & \lambda_4 & \lambda_5 & \lambda_6 \\ \frac{\beta_1}{\Lambda} - \lambda_1 & 0 & 0 & 0 & 0 & 0 & 0 \\ \frac{\beta_2}{\Lambda} & 0 - \lambda_2 & 0 & 0 & 0 & 0 & 0 \\ \frac{\beta_3}{\Lambda} & 0 & 0 - \lambda_3 & 0 & 0 & 0 & 0 \\ \frac{\beta_4}{\Lambda} & 0 & 0 & 0 - \lambda_4 & 0 & 0 & 0 \\ \frac{\beta_5}{\Lambda} & 0 & 0 & 0 & 0 - \lambda_5 & 0 & 0 \\ \frac{\beta_6}{\Lambda} & 0 & 0 & 0 & 0 & 0 - \lambda_6 & 0 \end{pmatrix} \begin{bmatrix} \nabla^{k-1} p(t_n) \\ \nabla^{k-1} C_1(t_n) \\ \nabla^{k-1} C_2(t_n) \\ \nabla^{k-1} C_3(t_n) \\ \nabla^{k-1} C_4(t_n) \\ \nabla^{k-1} C_5(t_n) \\ \nabla^{k-1} C_6(t_n) \end{bmatrix} \quad (3.30)$$

By making use of Eq. (3.4)-(3.5), Eq. (3.30) is rearranged as

$$\begin{bmatrix} \nabla^k p(t_n) \\ \nabla^k C_1(t_n) \\ \nabla^k C_2(t_n) \\ \nabla^k C_3(t_n) \\ \nabla^k C_4(t_n) \\ \nabla^k C_5(t_n) \\ \nabla^k C_6(t_n) \end{bmatrix} = \left(\begin{pmatrix} \frac{\rho - \beta}{\Lambda} & \lambda_1 & \lambda_2 & \lambda_3 & \lambda_4 & \lambda_5 & \lambda_6 \\ \frac{\beta_1}{\Lambda} - \lambda_1 & 0 & 0 & 0 & 0 & 0 & 0 \\ \frac{\beta_2}{\Lambda} & 0 - \lambda_2 & 0 & 0 & 0 & 0 & 0 \\ \frac{\beta_3}{\Lambda} & 0 & 0 - \lambda_3 & 0 & 0 & 0 & 0 \\ \frac{\beta_4}{\Lambda} & 0 & 0 & 0 - \lambda_4 & 0 & 0 & 0 \\ \frac{\beta_5}{\Lambda} & 0 & 0 & 0 & 0 - \lambda_5 & 0 & 0 \\ \frac{\beta_6}{\Lambda} & 0 & 0 & 0 & 0 & 0 - \lambda_6 & 0 \end{pmatrix} \right)^k \begin{bmatrix} p(t_0) \\ C_1(t_0) \\ C_2(t_0) \\ C_3(t_0) \\ C_4(t_0) \\ C_5(t_0) \\ C_6(t_0) \end{bmatrix} \quad (3.31)$$

and

$$\begin{bmatrix} \nabla^k p(t_n) \\ \nabla^k C_1(t_n) \\ \nabla^k C_2(t_n) \\ \nabla^k C_3(t_n) \\ \nabla^k C_4(t_n) \\ \nabla^k C_5(t_n) \\ \nabla^k C_6(t_n) \end{bmatrix} \frac{h^k}{k!} = \begin{pmatrix} \frac{\rho-\beta}{\Lambda} & \lambda_1 & \lambda_2 & \lambda_3 & \lambda_4 & \lambda_5 & \lambda_6 \\ \frac{\beta_1}{\Lambda} - \lambda_1 & 0 & 0 & 0 & 0 & 0 & 0 \\ \frac{\beta_2}{\Lambda} & 0 & -\lambda_2 & 0 & 0 & 0 & 0 \\ \frac{\beta_3}{\Lambda} & 0 & 0 & -\lambda_3 & 0 & 0 & 0 \\ \frac{\beta_4}{\Lambda} & 0 & 0 & 0 & -\lambda_4 & 0 & 0 \\ \frac{\beta_5}{\Lambda} & 0 & 0 & 0 & 0 & -\lambda_5 & 0 \\ \frac{\beta_6}{\Lambda} & 0 & 0 & 0 & 0 & 0 & -\lambda_6 \end{pmatrix}^k \frac{h^k}{k!} \begin{bmatrix} p(t_0) \\ C_1(t_0) \\ C_2(t_0) \\ C_3(t_0) \\ C_4(t_0) \\ C_5(t_0) \\ C_6(t_0) \end{bmatrix} \quad (3.32)$$

Eq. (3.32) is rewritten in matrix form as

$$[Y^k(t_n)] = B^k [Y^0(0)], \quad (3.33)$$

where $[Y^k(t_n)] = [\nabla^k p(t_n) \ \nabla^k C_1(t_n) \ \nabla^k C_2(t_n) \ \nabla^k C_3(t_n) \ \nabla^k C_4(t_n) \ \nabla^k C_5(t_n) \ \nabla^k C_6(t_n)]^T \frac{h^k}{k!}$,

$$[Y^0(t_n)] = [p(t_0) \ C_1(t_0) \ C_2(t_0) \ C_3(t_0) \ C_4(t_0) \ C_5(t_0) \ C_6(t_0)]^T, \ B^k = A^k \left(\frac{h}{k!^{1/k}} \right)^k$$

$$\text{and } A = \begin{pmatrix} \frac{\rho - \beta}{\Lambda} & \lambda_1 & \lambda_2 & \lambda_3 & \lambda_4 & \lambda_5 & \lambda_6 \\ \frac{\beta_1}{\Lambda} & -\lambda_1 & 0 & 0 & 0 & 0 & 0 \\ \frac{\beta_2}{\Lambda} & 0 & -\lambda_2 & 0 & 0 & 0 & 0 \\ \frac{\beta_3}{\Lambda} & 0 & 0 & -\lambda_3 & 0 & 0 & 0 \\ \frac{\beta_4}{\Lambda} & 0 & 0 & 0 & -\lambda_4 & 0 & 0 \\ \frac{\beta_5}{\Lambda} & 0 & 0 & 0 & 0 & -\lambda_5 & 0 \\ \frac{\beta_6}{\Lambda} & 0 & 0 & 0 & 0 & 0 & -\lambda_6 \end{pmatrix} \quad (3.34)$$

For convergence of the numerical solution to the power transient and precursor concentrations, $[Y^k(t_n)] \rightarrow 0$ as $k \rightarrow \infty$. In other words, $\lim_{k \rightarrow \infty} [Y^k(t_n)] \rightarrow 0$ if $\lim_{k \rightarrow \infty} B^k \rightarrow 0$. This is possible if the magnitude of the largest eigen value of $B < 1$. Let $\gamma_1, \gamma_2, \gamma_3, \gamma_4, \gamma_5, \gamma_6, \gamma_7$ be the eigen values of A and let the magnitude of the largest eigen value of A be $\gamma_{max} = \max \{ |\gamma_1|, |\gamma_2|, |\gamma_3|, |\gamma_4|, |\gamma_5|, |\gamma_6|, |\gamma_7| \}$. Since $B = A \frac{h}{(k!)^{1/k}}$, the largest eigen value of B is $\gamma_{max} \frac{h}{(k!)^{1/k}}$. Hence convergence is possible if $\gamma_{max} \frac{h}{(k!)^{1/k}} < 1$. So the time-step h is chosen as

$$h < \left(\frac{1}{\gamma_{max}} \right) (k!)^{1/k} \quad (3.35)$$

The upper bound for the time-step ' h ' is given as

$$h = \left(\frac{1}{\gamma_{max}} \right) (k!)^{1/k} \quad (3.36)$$

where $k > S - 1$. With this time-step, the global errors $\epsilon_1(p)$ and $\epsilon_2(C_i) \rightarrow 0$ as $k \rightarrow \infty$ i.e. both $\nabla^k p(t_n) \frac{h^k}{k!}$ and $\nabla^k C_i(t_n) \frac{h^k}{k!} \rightarrow 0$ as $k \rightarrow \infty$. The detailed description of modified ETD method is given by Mohideen Abdul Razak [44].

3.4 Application to thermal reactors

The modified exponential time differencing method is applied to solve the point kinetics equations with six groups of delayed neutrons for both thermal and fast reactors. The power transients for step and ramp reactivity perturbations are computed and the results are discussed. In all the power transient computations, discussed here by this method, the time-step is chosen to satisfy Eq. (3.35).

3.4.1 Power transients of thermal reactor caused by step reactivity

The modified ETD method is applied to estimate the power transients of the thermal reactor described by Nahla [43]. The decay constants of the neutron precursors and the delayed neutron fractions for the thermal reactor are given as $\lambda_1 = 0.0127s^{-1}$, $\lambda_2 = 0.0317s^{-1}$, $\lambda_3 = 0.115s^{-1}$, $\lambda_4 = 0.311s^{-1}$, $\lambda_5 = 1.4s^{-1}$, $\lambda_6 = 3.87s^{-1}$, $\beta_1 = 0.000285$, $\beta_2 = 0.0015975$, $\beta_3 = 0.00141$, $\beta_4 = 0.0030525$, $\beta_5 = 0.00096$, $\beta_6 = 0.000195$, and $\Lambda = 5.0 \times 10^{-4}s$. An external step reactivity $\rho_0 = -1\%$ is applied and the resulting power transient is analyzed. Table 3.1 shows the values of the power transients obtained from modified ETD method using a time-step $h = 0.1s$. Table 3.1 also shows the power transients obtained from the Taylor Series Method (TSM) along with the exact values given by Nahla [43]. The relative errors, $|(X_{cal} - X_{exact})/X_{exact}|$, are shown in brackets in Table 3.1. The comparison is made till 1s as the exact values are available till 1s only. From the comparison of results in Table 3.1, the accuracy of this method is assured.

Consider another example of thermal reactor described by [42] with the following parameters. $\lambda_1 = 0.0127s^{-1}$, $\lambda_2 = 0.0317s^{-1}$, $\lambda_3 = 0.115s^{-1}$, $\lambda_4 = 0.311s^{-1}$, $\lambda_5 = 1.4 s^{-1}$, $\lambda_6 = 3.87 s^{-1}$, $\beta_1 = 0.000266$, $\beta_2 = 0.001491$, $\beta_3 = 0.001316$, $\beta_4 = 0.002849$, $\beta_5 = 0.000896$, $\beta_6 = 0.000182$, and $\Lambda = 2.0 \times 10^{-5}s$. A step reactivity $\rho_0 = 0.003$ is inserted and the power transient is computed using the modified ETD method ($h = 0.01s$, $S = 7$) (Eq. 3.36). The results are compared with the Taylor Polynomial Method (TPM), the better basis function method (BBF) and the End Floating Method (EFM) referred by [42]. The results are shown in Table 3.2. The relative errors are shown in brackets in Table 3.2. It is observed from Table 3.2 that the power transient computed by this method is more accurate. In this case also the comparison is made till 1s as the exact values [42] are available till 1s only. The point kinetics equations can also be solved using finite impulse response (FIR) filters [48].

3.5 Application to Indian Prototype Fast Breeder Reactor (PFBR) transients

3.5.1 Step reactivity insertion

As an example of fast reactor, consider the 500 MWe Indian Prototype Fast Breeder Reactor (PFBR) at Kalpakkam [49]. The decay constants of the neutron precursors and the delayed neutron fraction for the PFBR are given as $\lambda_1 = 0.0129s^{-1}$, $\lambda_2 = 3.12s^{-1}$, $\lambda_3 = 0.1344s^{-1}$, $\lambda_4 = 0.3448s^{-1}$, $\lambda_5 = 1.3922 s^{-1}$, $\lambda_6 = 3.7491 s^{-1}$, $\beta_1 = 0.00008246$, $\beta_2 = 0.00076817$, $\beta_3 = 0.00066296$, $\beta_4 = 0.0012849$, $\beta_5 = 0.00057615$, $\beta_6 = 0.00017213$, and $\Lambda = 4.1 \times 10^{-7}s$. A step reactivity of 50 pcm is inserted in the PFBR. Assuming the maximum order of ETD coefficient is 5, ($S = 6$ in Eqs. (3.26)-(3.27)), in this case, the upper limit for the time-step (Eq. 3.36) is found to be $h = 3.5 \times 10^{-4}$. By choosing $h = 0.0001$, the power transient is computed using the modified ETD method and the Cohen's method [50] for an initial period of 100s. The results are given in Table 3.3. The power transient computed by

this method is in good agreement with the Cohen's method. This ensures that the modified ETD method is capable of estimating the power transient with good accuracy for longer duration of time for a typical fast breeder reactor. The power transients obtained using the modified ETD method and the Cohen's method are shown in Fig. 3.1. A maximum relative error of $1.18\text{E-}4$ is observed during the transient time. The modified ETD method can be used to estimate the transients with feedback also [51].

3.5.2 Ramp reactivity insertion

Consider another power transient of the Indian PFBR, caused by a ramp reactivity of 1pcm/s . Table 3.4 shows the power transient computed using the modified ETD method and the Cohen's method for an initial period of 100s. The relative errors are also shown in Table 3.4. The power transient estimated by this method is in good agreement with the Cohen's method. A maximum relative error of $1.83\text{E-}04$ is observed during this transient time. From Table 3.4 it is observed that this method is capable of estimating the power transient for fast reactors with ramp reactivity input for longer duration of time. Fig. 3.2 shows the power transients computed using the modified ETD method and the Cohen's method. This method can also be used to estimate the transients of typical PFBR for oscillatory reactivity insertion [44].

From the comparison of results, it is established that the modified ETD method can be used to solve stiff point kinetics equations with good accuracy and this shows that it can be smoothly coupled in the IQS model to estimate the transients.

Table 3.1. The power transient of thermal reactor computed by the modified ETD method and the TSM method [43] ($\rho_0 = -1\%$). The relative errors are shown in the parenthesis.

Time (s)	Exact Values	Modified ETD	TSM
		$h = 0.1s$	$h = 0.1s$
0.0	1.0000000	1.0000000	1.0000000
0.1	0.5205643	0.5205643(0.0)	0.5206784 ($2.2E - 4$)
0.2	0.4880113	0.4880113(0.0)	0.488022 ($2.25E - 5$)
0.4	0.4702262	0.4702262(0.0)	0.470226 ($2.10E - 7$)
0.6	0.4562794	0.4562794(0.0)	0.4562793 ($2.2E - 7$)
0.8	0.4441506	0.4441506(0.0)	0.4441505 ($2.3E - 7$)
1.0	0.4333335	0.4333335(0.0)	0.4333334 ($2.3E - 7$)

Table 3.2. The power transient of thermal reactor computed by the modified ETD method and other methods [42] ($\rho_0 = 0.003$). The relative errors are shown in the parenthesis.

Time (s)	Exact Values	Mod. ETD	TPM	BBF	EFM
		$h = 0.1s$		$h = 0.1s$	
0.0	1.00000	1.00000	1.00000	1.00000	1.0000
0.2	1.851268	1.851268	1.851246	1.851250	1.851252
		(0.0)	($1.2E-6$)	($9.7E-6$)	($8.6E-6$)
0.4	1.947593	1.947593	1.947581	1.947585	1.947586
		(0.0)	($6.2E-6$)	($4.1E-6$)	($3.6E-6$)
0.6	2.037922	2.037922	2.037915	2.037917	2.037918
		(0.0)	($3.4E-6$)	($2.5E-6$)	($2.0E-6$)
0.8	2.124832	2.124832	2.124827	2.124829	2.124829
		(0.0)	($2.4E-6$)	($1.4E-6$)	($1.4E-6$)
1.0	2.209841	2.209841	2.209838	2.209839	2.209839
		(0.0)	($1.4E-6$)	($9.1E-7$)	($9.1E-7$)

Table 3.3. The power transient of the Indian Prototype Fast Breeder Reactor (PFBR) computed by the modified ETD method and the Cohen's method [50] (step reactivity = 50 pcm).

Time (s)	Mod. ETD Method $h = 0.0001s$	Cohen $h = 0.0001s$	Relative Error
0.0	1.000000	1.000000	0
10.0	2.451082	2.451120	1.55E-05
20.0	4.522973	4.523096	2.72E-05
30.0	8.237472	8.237786	3.81E-05
40.0	14.926962	14.927707	4.99E-05
50.0	26.986656	26.988310	6.13E-05
60.0	48.736440	48.739983	7.27E-05
70.0	87.969711	87.977112	8.41E-05
80.0	158.746774	158.761943	9.55E-05
90.0	286.434427	286.465074	1.07E-04
100.0	516.798131	516.859342	1.18E-04

Table 3.4. The power transient of the Indian Prototype Fast Reactor (PFBR) computed by the modified ETD method and other method [50] for positive ramp reactivity of 1pcm/s.

Time (s)	Mod. ETD Method $h = 0.0001s$	Cohen $h = 0.0001s$	Relative Error
0.0	1.000000	1.000000	0.0
10.0	1.102048	1.102051	2.72E-06
20.0	1.353823	1.353832	6.65E-06
30.0	1.860535	1.860560	1.34E-05
40.0	2.895502	2.895566	2.21E-05
50.0	5.189995	5.190173	3.43E-05
60.0	10.939190	10.939743	5.05E-05
70.0	27.769447	27.771452	7.22E-05
80.0	87.199901	87.208655	1.00E-04
90.0	348.924903	348.972575	1.37E-04
100.0	1839.603459	1839.939691	1.83E-04

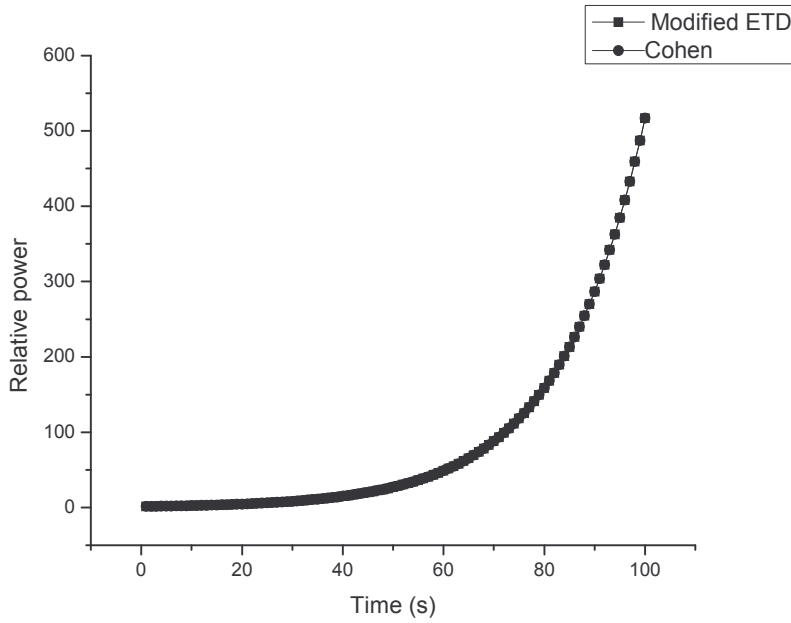


Fig. 3.1. The power transient of the Indian Prototype Fast Breeder Reactor (PFBR) computed by the modified ETD method (solid line) and the Cohen's method [50] (dot) for step reactivity $\rho(t) = 50 \text{ pcm}$.

3.6 Inverse point kinetics equations – Solution by modified ETD method

The modified exponential time differencing (ETD) method is tested to solve the inverse point kinetics equations to estimate the reactivity from the observed power transient with noise. The inverse point kinetics equations are stiff differential equations. The solution of inverse point kinetics equation is helpful in estimating the reactivity, feedback reactivity and the temperature coefficient of reactivity from the observed power transient. Generally background noise interferes in the measurement of the power transient and in real-time scenario, it becomes equally important to solve the inverse point kinetics equation with feedback and background noise to estimate the kind of reactivity acting on the reactor.

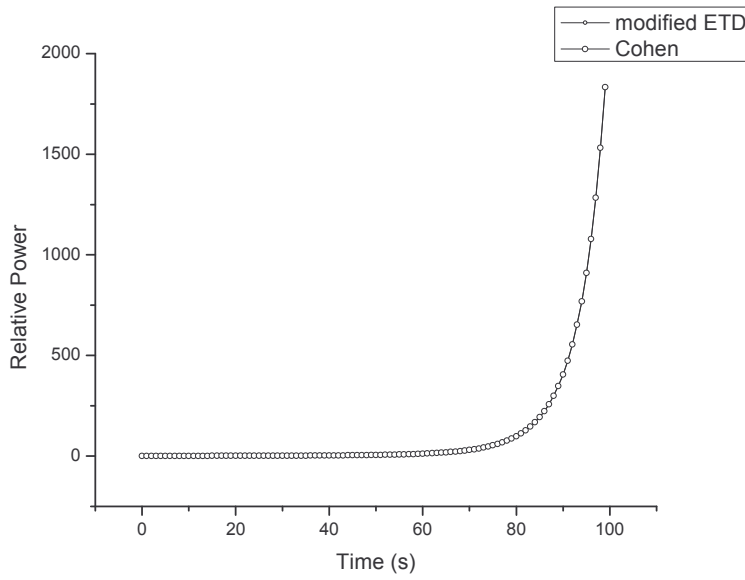


Fig. 3.2. The power transient of the Indian Prototype Fast Breeder Reactor (PFBR) computed by the modified ETD method (solid line) and the Cohen's method [50] (dot) for positive ramp reactivity of 1pcm/s.

The solution of inverse point kinetics equation requires the discretization of integral term associated with the precursor concentration. This discretization requires the power history [52]-[54]. One can use discrete Laplace transform technique to solve the inverse point kinetics equation [55]. Hamming method [56] can also be used to solve the inverse point kinetics equation without requiring power history.

Here we apply the modified ETD method to solve the inverse point kinetics equations with noise and estimate the reactivity required for the desired power transient in thermal as well as in Indian Prototype Fast Breeder Reactor (PFBR). This method is used to estimate various types of reactivity perturbations from the observed power transient. This method is also applied to estimate the temperature coefficient of reactivity from the power transients of thermal and

simulated power transient of Indian PFBR. In the case of Indian PFBR, the temperature coefficient of reactivity is estimated from synthetic power transients with various background noise levels. It is observed that as the background noise level is increased in the measurement of power transient, the accuracy in the estimation of temperature coefficient of reactivity is reduced and it is a natural phenomenon. But even in high background noise also, the temperature coefficient of reactivity can be accurately estimated by beamforming [57] the power transients from different channels. Beamforming is done by summing the signals from different channels with appropriate time delay. In the case of Indian PFBR, the synthetic power transients with high background noise levels are beamformed and the beamformed power transient is used to estimate the temperature coefficient of reactivity. While beamforming the power transients from different channels, it is assumed that there is no time delay between the channels. The estimated temperature coefficient of reactivity of the Indian PFBR, after beamforming, is found to be in good agreement with the reference value. It is also shown that as the number of channels in the beamforming is increased, the accuracy in the estimation of temperature coefficient of reactivity is improved. From the comparison of results, it is established that the modified ETD method can be used to estimate the feedback reactivity and temperature coefficient of reactivity to a good accuracy from the observed power transients in thermal as well as simulated transients in fast reactors with high background noise.

The reactivity $\rho(t)$ necessary for causing the desired power transient $P(t)$ can be obtained from the inverse point kinetics equation as [11]

$$\rho(t) = \beta + \frac{\Lambda}{P(t)} \frac{dP(t)}{dt} - \frac{\Lambda}{P(t)} \sum_{j=1}^6 \lambda_j C_j(t) \quad (3.37)$$

$$\frac{dC_j(t)}{dt} = \frac{\beta_j(t)}{\Lambda} P(t) - \lambda_j C_j(t), \quad j = 1, 2, 3 \dots 6 \quad (3.38)$$

Solution of Eqs. (3.37) and (3.38) gives the reactivity required for the desired power transient $P(t)$.

Consider the thermal reactor described by Daniel Suescun Diaz et al [55]. The kinetic parameters of the reactors are given as λ_i (0.0127, 0.0317, 0.115, 0.311, 1.4 and 3.87 s^{-1}), β_i (0.000266, 0.001491, 0.001316, 0.002849, 0.000896 and 0.000182) and $\Lambda = 2.0 \times 10^{-5} \text{ s}$. The desired power transient is assumed to be $P(t) = \exp(\omega t)$, $\omega = 0.12353$. The reactivity required for this power transient is calculated using the modified exponential time differencing (ETD) method and it is shown in Fig. 3.3a. The reference solution is taken from Daniel Suescun Diaz et al., [56]. Fig. 3.3b shows the relative error (%) in the estimation of reactivity. Fig. 3.4a shows the reactivity computed for the power transient $P(t) = \exp(\omega t)$, $\omega = 11.6442$ using modified ETD method. Fig. 3.4b shows the relative error.

Consider the 500 MWe Indian Prototype Fast Breeder Reactor (PFBR) at IGCAR, Kalpakkam [49]. The decay constants and delayed neutron fractions of the PFBR are given as λ_i (0.0129, 3.12, 0.1344, 0.3448, 1.3922 and 3.7491 s^{-1}), β_i (0.00008236, 0.00076817, 0.00066296, 0.0012849, 0.00057615 and 0.00017213) and $\Lambda = 4.1 \times 10^{-7} \text{ s}$. The reactivity required for the desired power transient, $P(t) = 1.44836 \times \exp\left(\frac{t}{17.06302}\right) - 0.16335$, $0 \leq t \leq 50 \text{ s}$, [44], is calculated using the modified ETD method and it is shown in Fig. 3.5a. The relative error in the estimation of reactivity is shown in Fig. 3.5b. The estimation of reactivity from power transient can also be performed using Haar wavelets [58].

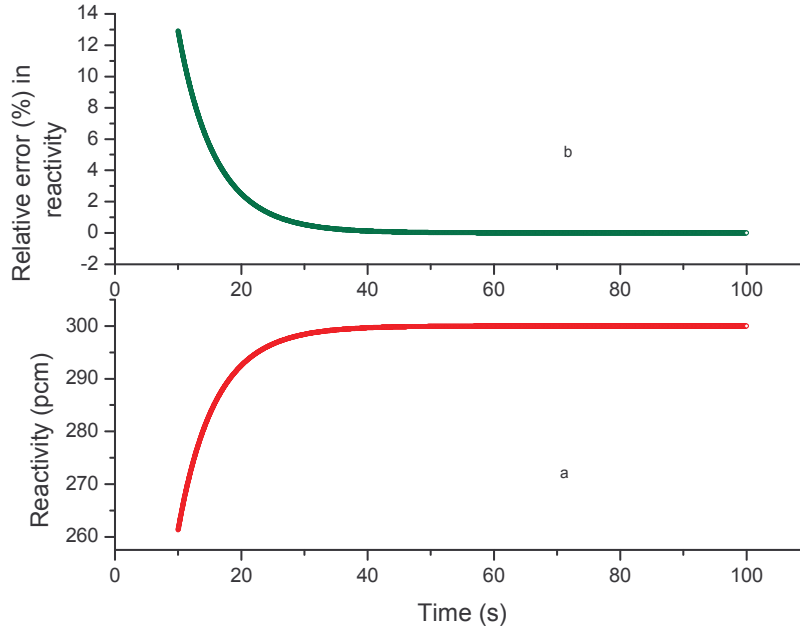


Fig. 3.3. (a) The reactivity computed using modified ETD method for the desired power transient $P(t) = \exp(\omega t)$ with $\omega = 0.12353$. (b) The relative error (%) between the reference solution [56] and the solution obtained using modified ETD method.

3.7 Estimation of temperature coefficient of reactivity of thermal reactor

In this case, the inverse point kinetics equation is solved with feedback using modified ETD method and the temperature coefficient of reactivity is estimated. Consider the supercritical process in a pressurized water reactor [59]. This reactor is modeled by one group of delayed neutron precursor and the kinetics parameters are given as $\beta = 0.0065$, $l = 1.0 \times 10^{-4} \text{ s}$, $\lambda = 0.07741 \text{ s}^{-1}$. In this reactor the supercritical process is initiated by giving an external step reactivity, $\rho_{ex} = \frac{\beta}{2}$. The temperature rise in the reactor is assumed to follow the relation [59]

$$\frac{dT(t)}{dt} = K_c n(t) \quad (3.39)$$

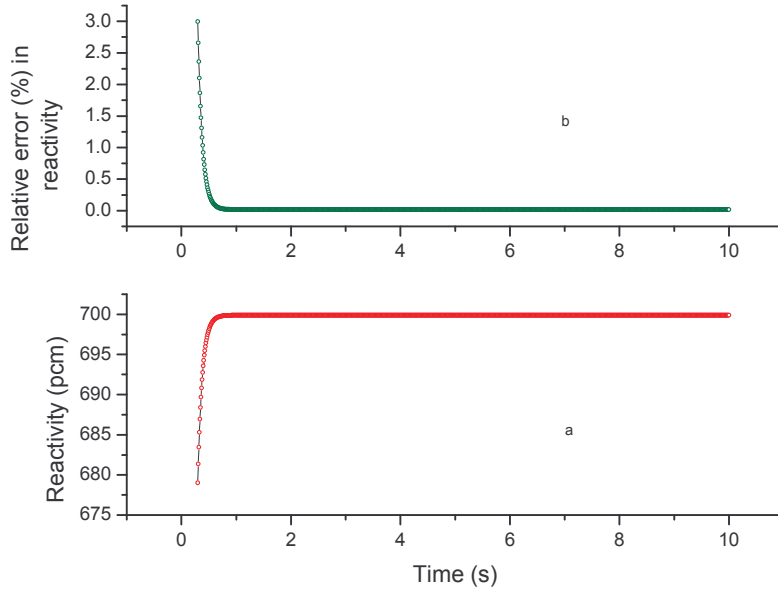


Fig. 3.4. (a) The reactivity computed using modified ETD method for the desired power transient $P(t) = \exp(\omega t)$ with $\omega = 11.6442$. (b) The relative error (%) in the estimation of reactivity.

In the above equation $n(t)$ is the neutron density and K_c is the inverse of thermal capacity of reactor [59] and it is given as $K_c = 0.05 \text{ } ^\circ K/MWs$. Before the start of supercritical process, the reactor is assumed to be in the steady state of initial power of 10 MW. Following the step reactivity, the increase in neutron density (power) and temperature are given Figs. 3.6 and 3.7 [59].

From the observed neutron density (Fig. 3.6) and temperature (Fig. 3.7), the inverse point kinetics equations are solved using the modified ETD method to obtain the net reactivity, feedback reactivity and temperature coefficient of reactivity. The estimated net reactivity is shown in Fig. 3.8. The feedback reactivity is calculated as $\rho_{fb} = \rho_{net} - \rho_{ext}$ and it is given in Fig. 3.9.

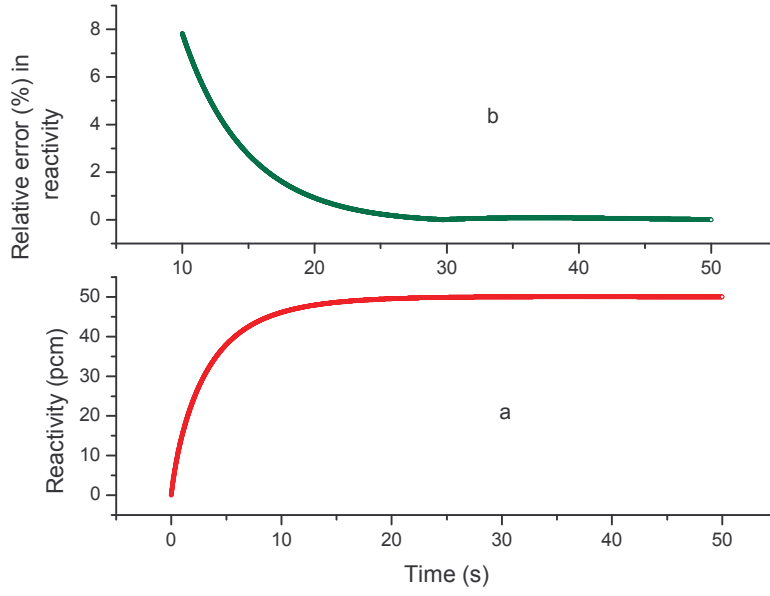


Fig. 3.5. (a) The reactivity computed using modified ETD method for the desired power transient $P(t) = 1.44836 \times \exp\left(\frac{t}{17.06302}\right) - 0.16335$, $0 \leq t \leq 50s$ for Indian PFBR. (b) The relative error (%) in the estimation of reactivity.

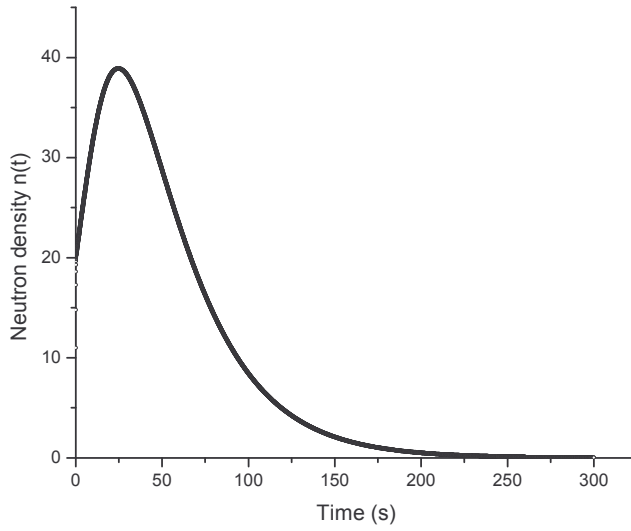


Fig. 3.6. The neutron density $n(t)$ (with adiabatic feedback) with time for the external reactivity $\rho_{ex} = \frac{\beta}{2}$.

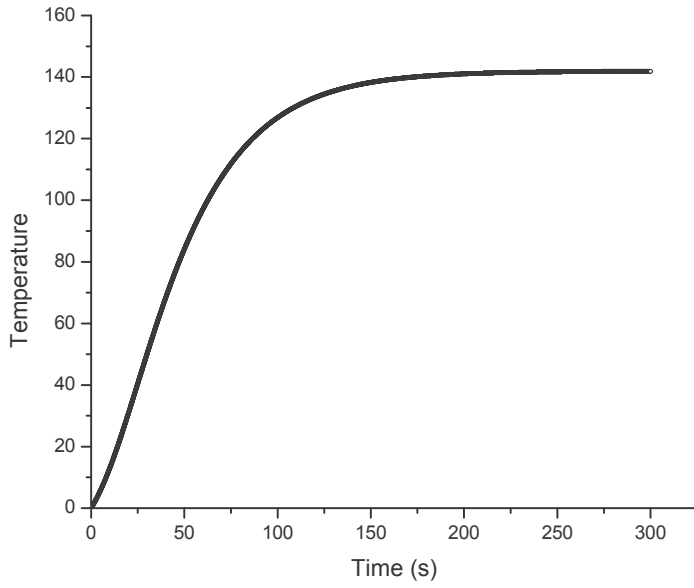


Fig. 3.7. The variation of temperature with time.

Table 3.5. The temperature coefficient of reactivity $\left(\frac{\Delta k/k}{^{\circ}\text{C}}\right)$ obtained using the modified ETD method along with the reference [59]

Parameter	Reference	modified ETD method
Temperature coefficient of reactivity $\left(\frac{\Delta k/k}{^{\circ}\text{C}}\right)$	-5.0×10^{-5}	-5.0284×10^{-5}

From Figs. 3.7 and 3.9, the temperature coefficient of reactivity, $\frac{\partial \rho_{fb}}{\partial T}$, is estimated and it is given in Fig. 3.10.

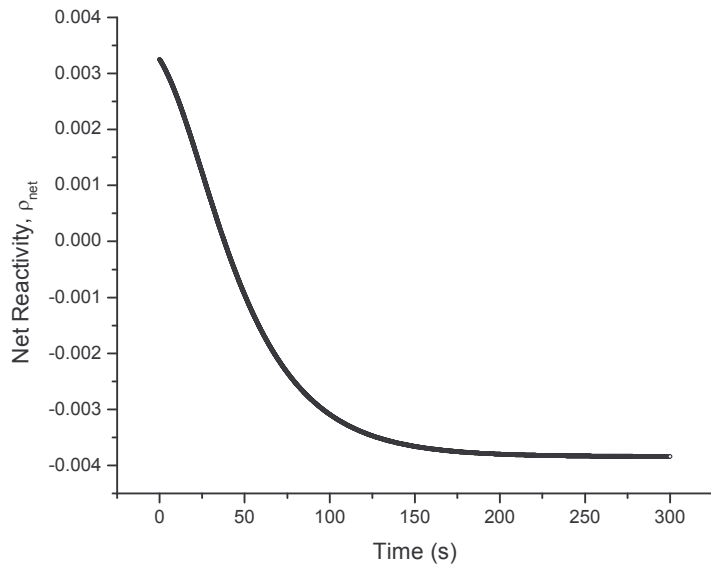


Fig. 3.8. The variation of estimated net reactivity with time.

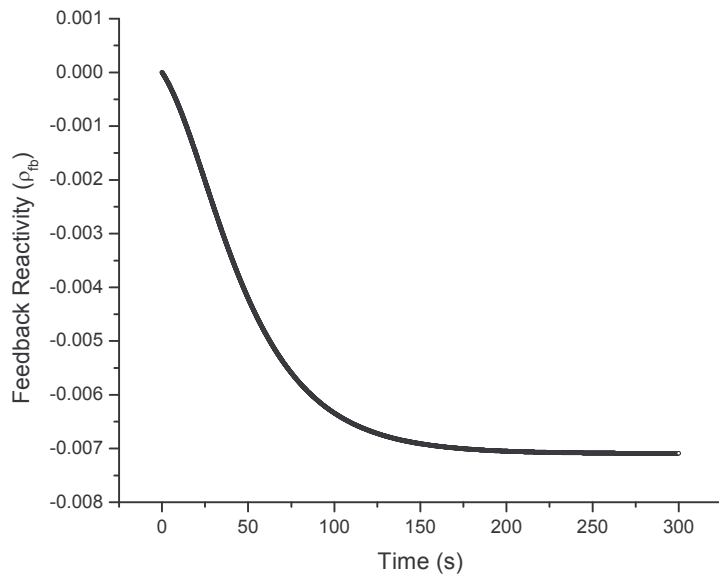


Fig. 3.9. The variation of estimated feedback reactivity (ρ_{fb}) with time.

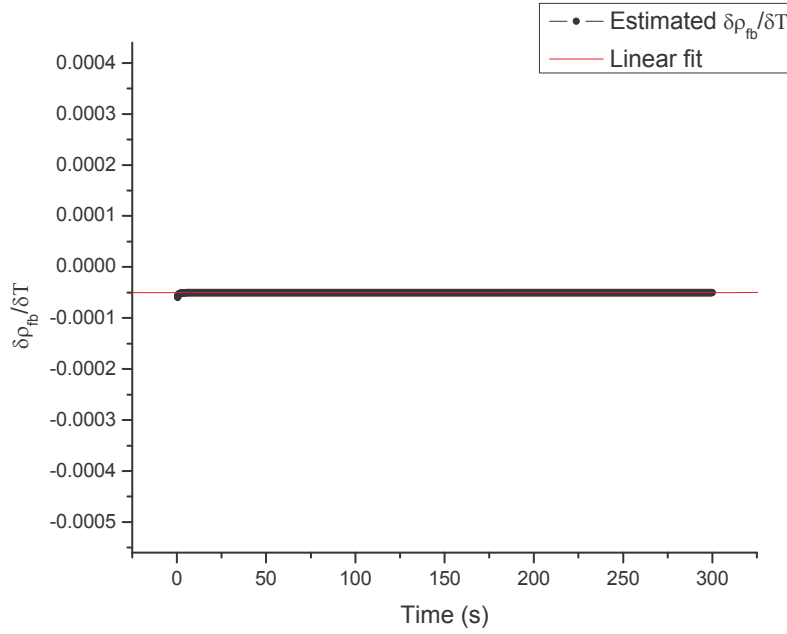


Fig. 3.10. The variation of feedback temperature coefficient of reactivity, i.e. $\left(\frac{\partial\rho_{fb}}{\partial T}\right)$ with time.

The linear fit is also shown.

From Fig. 3.10, it is observed that the temperature coefficient of reactivity is independent of time in this case and it can be linearly fitted as

$$\frac{d\rho_{fb}}{dT} = C_1 + C_2 t \quad (3.40)$$

The parameters of the fit, C_1 and C_2 , are found using least square error minimization technique and they are found to be $C_1 = -5.0284 \times 10^{-5} \left(\frac{\Delta k/k}{^\circ C}\right)$ and $C_2 = 1.4765910^{-9} \left(\frac{\Delta k/k}{^\circ C s}\right)$. The constant, C_1 , gives the temperature coefficient of reactivity and it is given in Table 3.5.

From Eq. (3.40) the adiabatic feedback reactivity with temperature can be written as (neglecting C_2)

$$\rho_{fb} = -5.0284 \times 10^{-5} (T - T_0)$$

where T_0 is the initial temperature. The estimated temperature coefficient of reactivity, i.e. -5.0284×10^{-5} is found to be in good agreement with the reference value. The estimation of reactivity can also be performed using Haar wavelets [60].

In the recent years, wavelet approach has become an important field in the numerical solution of differential equations. Different types of wavelets and approximating functions can be used in numerical solution of initial and boundary value problems [61], [62]. Wavelets are basis functions, constructed from translation and dilation of mother wavelet. Haar wavelets are effective in solving ordinary and partial differential equations [63]. The Haar wavelet approach can be adopted in solving the inverse point kinetics equation for reactivity calculation. The Haar wavelet transforms the inverse point kinetics equations into a set of linear equations and these equations can be solved easily [60].

3.8 Estimation of temperature coefficient of reactivity of Indian Prototype Fast Breeder Reactor (PFBR) from simulated transient with various background noise levels

Here we apply the modified ETD method to solve the inverse point kinetics equations to estimate the temperature coefficient of reactivity of Indian PFBR from simulated transient with background noise. Consider the Indian Prototype Fast Breeder Reactor (PFBR) at IGCAR, Kalpakkam [49]. The decay constants of the delayed neutron precursors and the delayed neutron fraction of the Indian PFBR are given as $\lambda_1 = 0.0129s^{-1}$, $\lambda_2 = 3.12s^{-1}$, $\lambda_3 = 0.1344s^{-1}$, $\lambda_4 = 0.3448s^{-1}$, $\lambda_5 = 1.3922 s^{-1}$, $\lambda_6 = 3.7491 s^{-1}$, $\beta_1 = 0.00008246$, $\beta_2 = 0.00076817$, $\beta_3 = 0.00066296$, $\beta_4 = 0.0012849$, $\beta_5 = 0.00057615$, $\beta_6 = 0.00017213$, and $\Lambda = 4.1 \times 10^{-7}s$. In this case, first, synthetic power transients with temperature feedback are generated by

applying a step reactivity of 50 pcm for various background noise levels. The rate of variation of temperature with power and the feedback reactivity of the Indian PFBR are given as [64]

$$\frac{\partial T(t)}{\partial t} = \left(0.130005 \frac{^{\circ}K}{MWs}\right) p(t) \quad (3.41)$$

$$\frac{\partial \rho_{fb}}{\partial T} = -1.835 \text{ pcm}/^{\circ}K \quad (3.42)$$

In the above equations, (Eqs. (3.41)-(3.42)), ' T ' is the temperature, ' P ' is the power and ρ_{fb} is the feedback reactivity. The synthetic power transients with the above temperature feedback are generated by solving the point kinetics equations using the modified ETD method. At the beginning of simulation process, the initial temperature is assumed to be 673°K. During the simulation process, the background noise in the power transient is incorporated as

$$\tilde{p}(t) = p(t)(1 + \alpha S(T)) \quad (3.43)$$

In the above Eq. (3.43), $p(t)$ is the true power transient (without noise), α is the percentage of noise i.e. $\alpha = 0, 1\%, 2\%$, etc., and $s(t)$ is the background noise. The background noise is simulated by generating random numbers of uniform distribution in the interval $[-1, 1]$. Here the simulation is performed for various noise levels i.e. $\alpha = 0, 2\%, 4\%$. The simulated power transients ($\tilde{p}(t)$) for 4% noise, for five different channels (CH1-CH5), are shown in Fig. 3.11. From Fig. 3.11, it is obvious that the noise present in different channels is different. First the inverse point kinetics equations are solved using the modified ETD method with simulated power transients ($\tilde{p}(t)$) with no noise ($\alpha = 0\%$), to estimate the temperature coefficient of reactivity. The simulated power transient ($\alpha = 0\%$) and temperature rise are shown in Figs. 3.12 and 3.13. Using the simulated power transient and temperature (Figs. 3.12 and 3.13), the net reactivity and the feedback reactivity ($\alpha = 0\%$) are estimated and they are shown in Figs. 3.14 and 3.15 respectively. From Figs. 3.13 and 3.15, the temperature coefficient of reactivity is estimated and it is shown in Fig. 3.16. The curve shown in Fig. 3.16 is linearly

fitted and the constants of the linear fit are found using least square error minimization technique. The slope of the linear fit is 2.352×10^{-8} and the intercept is -1.8195×10^{-5} . The ‘y’ intercept of the fit gives the temperature coefficient of reactivity and it is found to be $-1.8195 \text{ pcm}/^{\circ}\text{K} (\alpha = 0\%)$ which is in good agreement with $-1.835 \text{ pcm}/^{\circ}\text{K}$ [64]. In a similar manner, various background noise levels are incorporated in the power transient (Eq. (3.43)) and the inverse point kinetics equations are solved to estimate the reactivity and temperature coefficient of reactivity. The estimated temperature coefficient of reactivity for various background noise levels is given in Table 3.6. With 4% noise, the temperature coefficient of reactivity is found to be $-2.2166 \text{ pcm}/^{\circ}\text{K}$, which has an error of 20.8%. The error in the estimation of temperature coefficient of reactivity can be reduced by beamforming the power transients from different channels and the beamformed power transient can be used in solving the inverse point kinetics equations. With 4% noise and with five-channel and ten-channel beamforming, the temperature coefficient of reactivity is estimated and it is given in Table 3.6. With 4% noise and with five-channel beamforming (5CH-BF), the error in the estimation of temperature coefficient of reactivity is found to be 11.6% and with ten-channel beamforming (10CH-BF), the error is found to be 1.79%. This is given in Table 3.6. By increasing the number of channels in the beamforming, the error in the estimation of temperature coefficient of reactivity can be reduced. The detailed description of estimating the reactivity from power transient of Indian PFBR for various background noise levels can be found in the work of [60].

Table 3.6. The temperature coefficient of reactivity $\left(\frac{pcm}{^{\circ}K}\right)$ of the Indian PFBR, obtained using the modified ETD method for various background noise levels with beamforming. The reference value [64] is also given.

Parameter	Reference	Noise level(α)				
		0%	2% *NBF	4% *NBF	4% 5-channel beamforming	4% 10-channel beamforming
Temp.coeff. of reactivity $\left(\frac{pcm}{^{\circ}K}\right)$	-1.835	-1.8195	-1.6825	-2.2166	-1.6218	-1.8021

*NBF- No beamforming

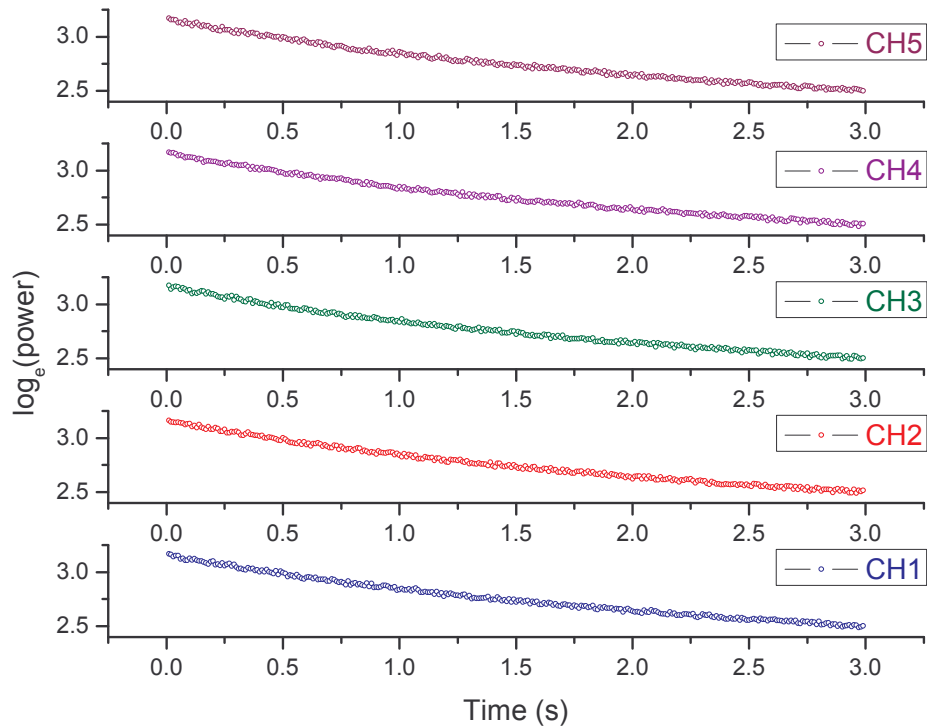


Fig. 3.11. The synthetic power transients at different channels with 4% background noise.

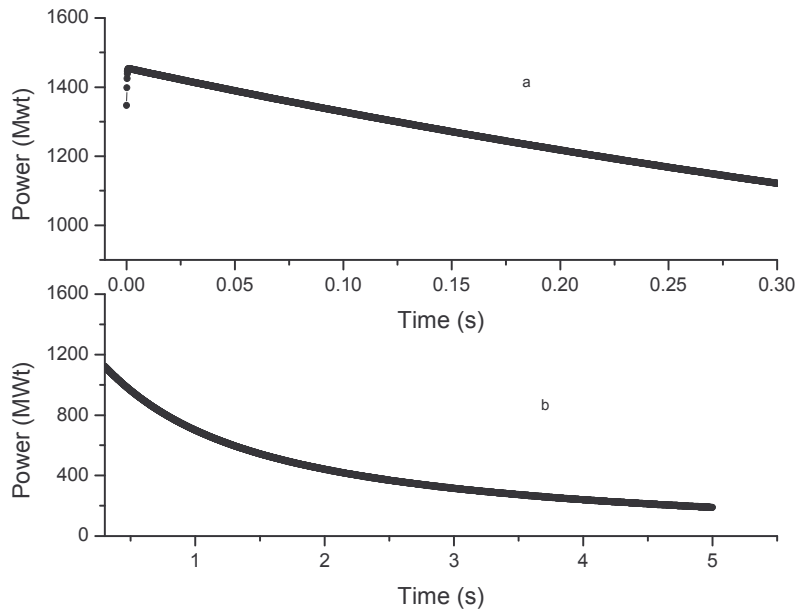


Fig. 3.12. The power transient following a step reactivity of 50 pcm, $0 \leq t \leq 0.3s$, is shown in trace 'a'. The power transient $0.3s \leq t \leq 5.0s$ is shown in trace 'b'. Trace 'b' is the continuation of trace 'a'.

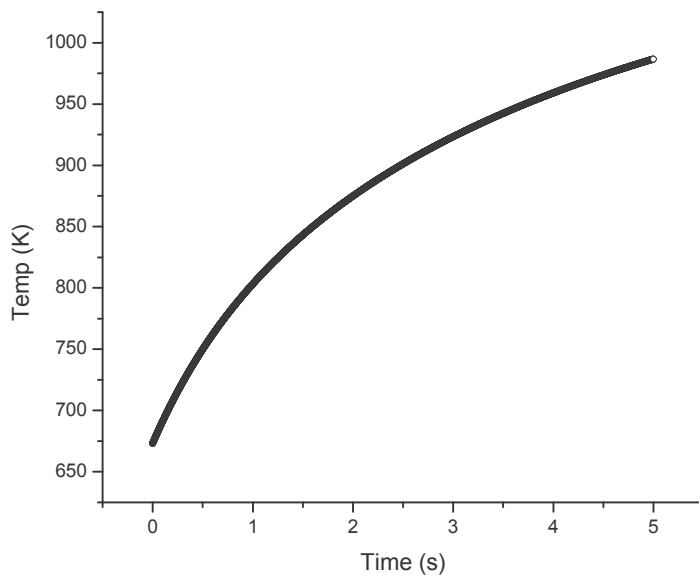


Fig. 3.13. The variation of temperature with time.

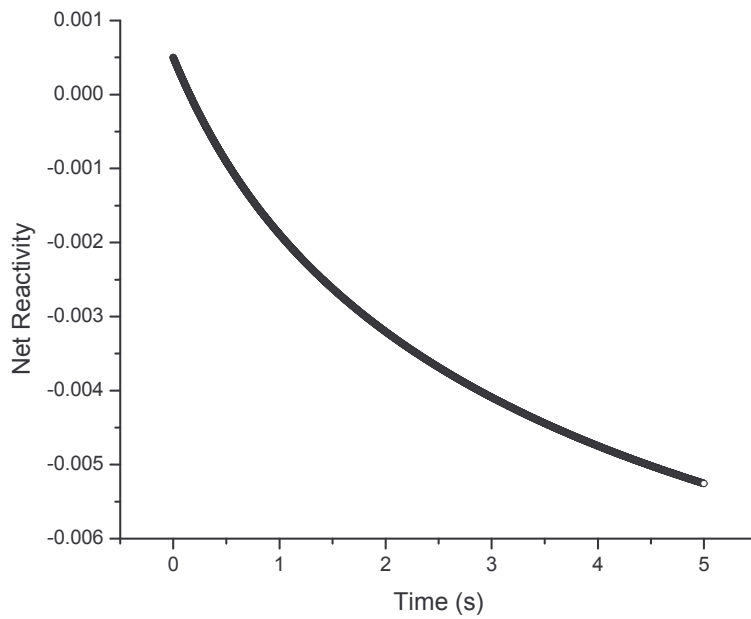


Fig. 3.14. The variation of net reactivity causing the power transient.

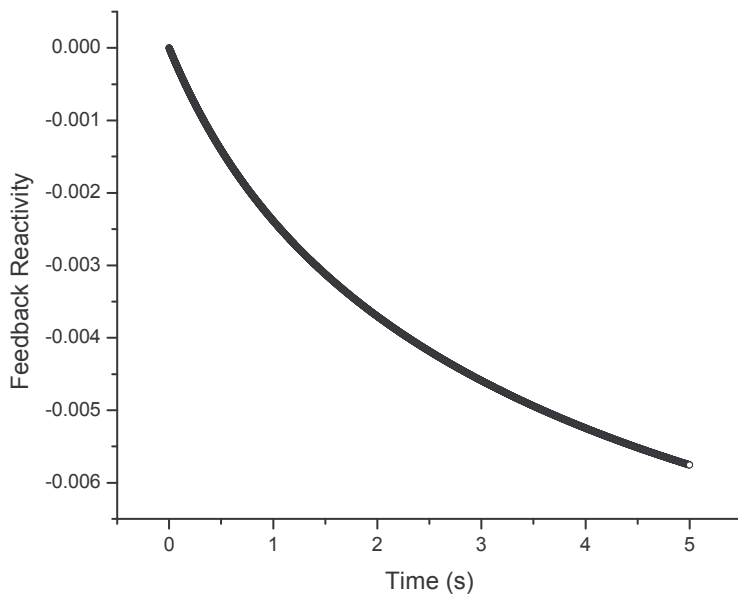


Fig. 3.15. The variation of feedback reactivity involved in the power transient.

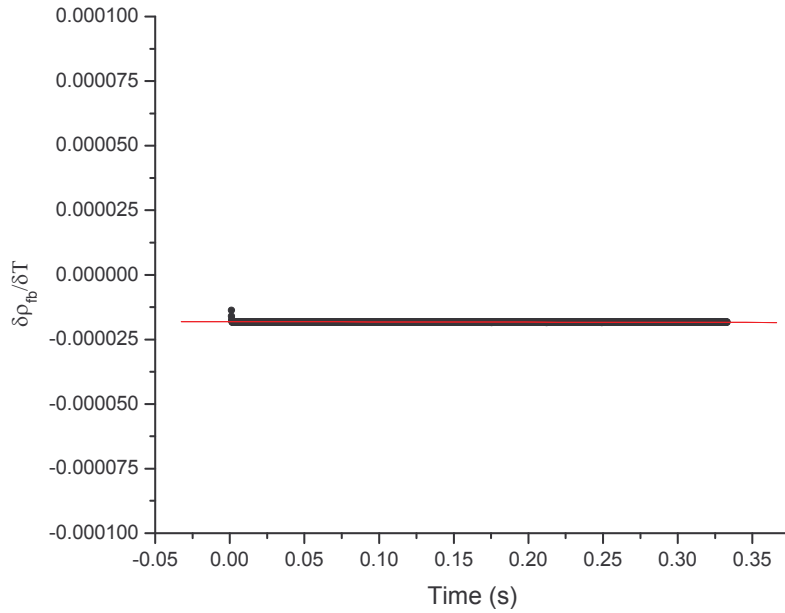


Fig. 3.16. The estimated variation of the feedback temperature coefficient of reactivity, $\frac{\partial \rho}{\partial T}$, with time (no noise). The linear fit is found to be $y = -1.8195 \times 10^{-5} + (2.352 \times 10^{-8})t$. The feedback temperature coefficient of reactivity is found to be $-1.8195 \frac{pcm}{^\circ K}$.

3.9 Summary

The modified exponential time differencing (ETD) method for solving the point kinetics equations is described in detail. A novel technique to choose the time step for solving the point kinetics equations is established. The modified ETD method is applied to estimate the power transient in few thermal reactors for different types of reactivity perturbations and the results are discussed. The results indicate that using the modified ETD method, the transient can be estimated with good accuracy with large time step. The applicability of modified ETD method to estimate the transient of typical fast reactor is also discussed. The transient of 500 MWe Indian PFBR, estimated by this method is discussed. The applicability of this method to estimate the temperature coefficient of reactivity from the simulated transient with background noise is also

discussed. As the modified ETD method is capable of estimating the transient for various types of reactivity perturbations, this method can be safely coupled with the improved quasi static IQS) method to estimate the space effects in the transients.

CHAPTER 4

MODIFIED ETD METHOD WITH IQS MODEL

4.1 Introduction

As discussed in chapter 2, the transients are estimated by solving the amplitude function and the shape function. The amplitude function is solved using the modified exponential time differencing (ETD) method and the shape function is solved using the implicit scheme. The implicit scheme is given by

$$\frac{\partial \psi(r, t)}{\partial t} = \frac{\psi(r, t) - \psi(r, t - \delta t)}{\delta t}$$

Since the shape function is a slowly varying function of time, a large time step (macro time step) can be used to solve the shape function. The product of amplitude function and shape function gives the actual neutron flux in the reactor. The methodology to estimate the transient using the IQS model is described in chapter 2. Here we apply the modified ETD method with IQS model to estimate the transients of the following reactors.

4.2 3D Homogeneous Reactor Transients

It is a three dimensional homogeneous reactor of cubic size of length 200 cm [65], [66]. The material composition is uniform throughout the core. The material composition is given in Table 4.1. Flux zero boundary conditions are used while solving the neutron diffusion equation. Here the reactor is subjected to two independent perturbations. First the reactor is subjected to a perturbation in the thermal absorption cross section given by $\Delta \Sigma_{a2}(t) = -0.369 \times 10^{-4}$. The perturbation remains constant in time and the perturbation is applied throughout the reactor. The fast and thermal flux, following this perturbation, are estimated by the modified ETD method

with IQS model and they are given in Table 4.2. The transients are estimated till 0.4s as the results are available till 0.4s only [65]. The second perturbation is caused by increase in thermal absorption cross section given by $\Delta\Sigma_{a2}(t) = 0.369 \times 10^{-4}$. The second perturbation also remains constant in time and it is applied throughout the reactor. The fast and thermal flux, following this negative reactivity perturbation, are estimated by this method and they are given in Table 4.3. Here also the transients are estimated till 0.4s only as the results are available till 0.4s [65]. The micro time step for calculating the amplitude function was chosen as described in chapter 3 (Eq. (3.35)). Since this reactor has one group of delayed neutron, the matrix A (Eq. (3.35)) assumes the dimension of 2×2 . Assuming that the order of Taylor series expansion is taken up to 3, ($S = 3$), the largest eigen value (in magnitude) of the matrix A is found to be 2.467 in the case of positive reactivity perturbation. Using the relation (Eq. (3.35)), the micro time step in this case is found to be $h \leq 0.7$. Similarly in the case of negative reactivity perturbation, the dynamic reactivity remains constant and the largest eigen value is found to be 18.224 and hence the micro step is found to be $h \leq 0.1$ in this case. Since the results (Table 4.2 and 4.3) are available at a time interval of 0.05s, we have taken the micro time step as well as macro time step as 0.05s ($\Delta t = \Delta T = 0.05s$) for estimating the transient under positive and negative reactivity perturbations. The fast and thermal flux estimated by this method and other standard codes [65] are given in Table 4.2 and 4.3. The fast and thermal flux, computed by this method, are in good agreement with other standard codes. The significance of space part (shape function), in estimating the transient, is determined as follows. For both perturbations, the core power is estimated with space-time kinetics and point kinetics. The relative error (%) in the core power, when space part is neglected, is estimated and it is given in Fig. 4.1 and Fig. 4.2 for positive and negative reactivity perturbations. It is observed, during the transient, that a maximum error of

0.12% is observed in the case of positive perturbation (Fig. 4.1) and a maximum error of 0.18% is observed in the case of negative perturbation (Fig. 4.2). The relative error is found to increase with time for both positive and negative perturbations.

The total peaking factors (3D peaking factor) are calculated for positive and negative perturbations and they are given in Table 4.4 and 4.5 respectively. When the space part is neglected, the error in the estimation of peaking factors is observed to be small during the transient. This is shown in Table 4.6 for positive and negative perturbations. This may be due to the reason that the perturbations are applied throughout the reactor. The total peaking factor is found to be 3.68 (corrected to two decimal places). For a bare homogeneous cubic reactor, the theoretical value of total peaking factor is 3.88 (corrected to two decimal places), whereas in this example the peaking factor is found to be 3.68. The reason for this is as follows: here a mesh size of 20 cm is taken [65], [66] to estimate the transient. Under this condition, the flux shape will not exactly match with the theoretical cosine function. But as the mesh size is reduced, the flux shape improves and approaches the cosine function and the total peaking factor also approaches the theoretical value of 3.88. A case study was performed to estimate the total peaking factor for various mesh sizes and it is given in Table 4.7. From Table 4.7, it can be observed that as the mesh size is reduced, the peaking factor approaches the value of 3.88.

Table 4.1 Two group constants for 3D Homogeneous Reactor

Group 1	Group 2
$D_1 = 1.35 \text{ cm}$	$D_2 = 1.08 \text{ cm}$
$\Sigma_{a1} = 0.001382 \text{ cm}^{-1}$	$\Sigma_{a2} = 0.0054869 \text{ cm}^{-1}$
$\nu = 2.41$	$\nu = 2.41$
$\Sigma_{f1} = 0.00242 \text{ cm}^{-1}$	$\Sigma_{f2} = 0.00408 \text{ cm}^{-1}$
$\Sigma_{1 \rightarrow 2} = 0.0023 \text{ cm}^{-1}$	$\Sigma_{1 \rightarrow 2} = 0.0 \text{ cm}^{-1}$
$\nu_1 = 3.0 \times 10^7 \text{ cm s}^{-1}$	$\nu_2 = 2.2 \times 10^5 \text{ cm s}^{-1}$
$\lambda = 0.08 \text{ s}^{-1}$	$\beta = 0.0064$

Table 4.2 The fast and thermal flux estimated by the modified ETD method with IQS model at the centre of 3D Homogeneous Reactor for positive reactivity perturbation. The fast and thermal flux computed by other standard codes [65] are also given.

Time (s)	Fast flux				Thermal flux			
	AMF	NT-FMM	NT-AM	Modified ETD+IQS	AMF	NT-FMM	NT-AM	Modified ETD+IQS
0.0	2.229	2.229	2.229	2.229	0.816	0.816	0.816	0.816
0.05	3.071	3.071	3.071	3.074	1.127	1.127	1.127	1.127
0.10	3.830	3.828	3.830	3.835	1.407	1.406	1.407	1.408
0.15	4.516	4.510	4.516	4.524	1.660	1.658	1.660	1.662
0.20	5.138	5.124	5.137	5.147	1.890	1.885	1.889	1.892
0.30	6.216	6.176	6.215	6.232	2.287	2.273	2.287	2.292
0.40	7.118	7.033	7.116	7.139	2.620	2.589	2.619	2.626

Table 4.3 The fast and thermal flux computed by the modified ETD method with IQS model at the centre of 3D Homogeneous Reactor for negative reactivity perturbation. The fast and thermal flux computed by other standard codes [65] are also given.

Time (s)	Fast flux				Thermal flux			
	AMF	NT-FMM	NT-AM	Modified ETD+IQS	AMF	NT-FMM	NT-AM	Modified ETD+IQS
0.0	2.229	2.229	2.229	2.229	0.816	0.816	0.816	0.816
0.05	1.645	1.645	1.645	1.671	0.601	0.601	0.601	0.612
0.10	1.409	1.409	1.409	1.431	0.514	0.514	0.514	0.522
0.15	1.313	1.312	1.313	1.326	0.478	0.478	0.478	0.483
0.20	1.273	1.271	1.273	1.280	0.464	0.463	0.464	0.466
0.30	1.247	1.243	1.247	1.248	0.454	0.453	0.454	0.454
0.40	1.240	1.234	1.240	1.239	0.451	0.449	0.451	0.451

Table 4.4. Total peaking factor (3D peaking factor) during transient for positive reactivity perturbation

Time	Total peaking factor (Space-time Kinetics)	Total peaking factor (Point kinetics)
0.0	3.688562	3.688562
0.05	3.688604	3.688562
0.1	3.688590	3.688562
0.15	3.688580	3.688562
0.2	3.688577	3.688562
0.25	3.688572	3.688562
0.3	3.688570	3.688562
0.35	3.688569	3.688562
0.4	3.688566	3.688562

Table 4.5. Total peaking factor (3D peaking factor) during transient for negative reactivity perturbation

Time	Total peaking factor (Space-time Kinetics)	Total peaking factor (Point kinetics)
0.0	3.688562	3.688562
0.05	3.688749	3.688562
0.1	3.688733	3.688562
0.15	3.688702	3.688562
0.2	3.688665	3.688562
0.25	3.688634	3.688562
0.3	3.688614	3.688562
0.35	3.688597	3.688562
0.4	3.688586	3.688562

Table 4.6. Error in the peaking factor during the transient

Time	Relative error in total peaking factor (positive perturbation)	Relative error in total peaking factor (negative perturbation)
0.0	0	0
0.05	1.14E-3	0.00507
0.1	7.59098E-4	0.00464
0.15	4.87993E-4	0.00380
0.2	4.06661E-4	0.00279
0.25	2.71108E-4	0.00195
0.3	2.16886E-4	0.00141
0.35	1.89775E-4	9.4887E-4
0.4	1.08443E-4	6.5065E-4

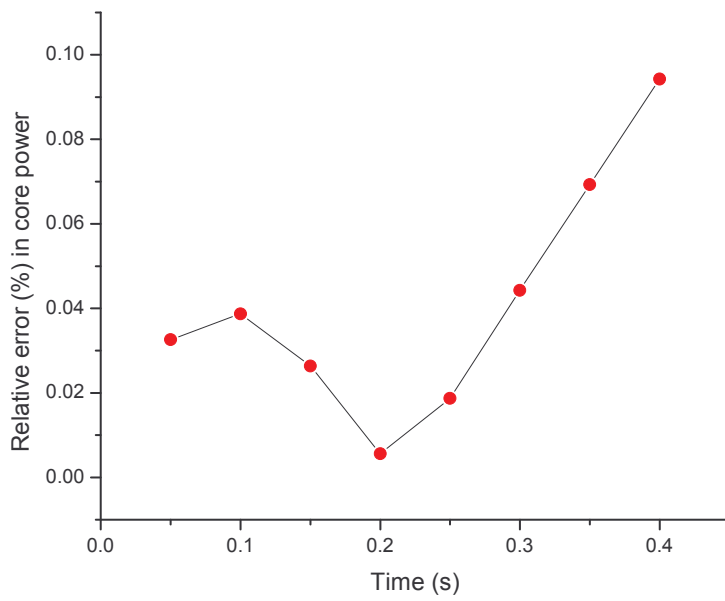


Fig. 4.1 The relative error in reactor core power when the shape function is neglected (in the case of positive reactivity perturbation).

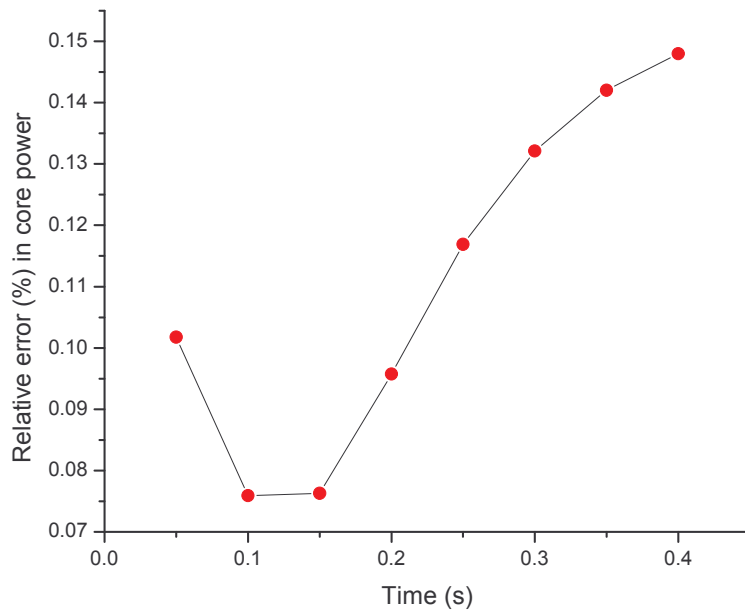


Fig. 4.2 The relative error in reactor core power when shape function is neglected (in the case of negative reactivity perturbation).

Table 4.7. Total peaking factor for various mesh sizes. The theoretical value is 3.88.

Mesh size (cm)	Total peaking factor (Space-time kinetics)
20	3.68
10	3.82
5	3.85

4.3 3D TWIGL Benchmark Reactor Transients

It is an extension of original 2D TWIGL Benchmark [67] problem in 3D geometry. It is also one of the widely studied problem [19], [65], [66], [68]. It is a three dimensional heterogeneous cubic reactor. It is a seed blanket reactor and has side length of 160 cm. One quadrant of the reactor core is shown in Fig. 4.3. An axial blanket of 24 cm thickness is present at the top and bottom of the core. The material composition of the core is given in Table 4.8. Two neutron energy groups and one delayed neutron group are assumed here. Flux zero boundary conditions are applied while solving the diffusion equation. The k_{eff} value for the unperturbed state of reactor is computed and it is given in Table 4.9 along with the reference [69]. Four regions containing the fuel material 1 (Fuel-1) are perturbed by a linear ramp followed by step perturbation in the thermal absorption cross section and it is given as [66]

$$\Delta\Sigma_{a2}(t) = -\frac{0.0045}{0.2}t, \quad 0 \leq t \leq 0.2s$$

$$\Delta\Sigma_{a2}(t) = -0.0045, \quad t > 0.2s$$

Here the perturbation in the cross section occurs only in some confined area. The thermal flux, following the transient, is estimated by this method at different location of the reactor and it is given in Table 4.9. The thermal flux computed by other standard codes is also given in Table 4.10 [65], [66]. The thermal flux is calculated till 0.3s as the reference results are available till 0.3s only. From Table 4.10, it is observed that the thermal flux obtained by this method is in

good agreement with other standard codes. The core power is estimated with space part and without space part (point kinetics). The relative error in the core power when the space part is neglected is shown in Fig. 4.4. It is observed from Fig. 4.4 that an error of 10% is observed in the core power, at $t = 3.0s$, when the space part is neglected. The axial power profile (radially integrated axial power) is estimated with space part as well as without space part and it is given in Fig. 4.5. From Figs. 4.4 and 4.5, it is observed that the space part (shape function) has significant role in estimating the core power. In 3D TWIGL reactor, the effect of space part, in estimating the transient, is more pronounced.

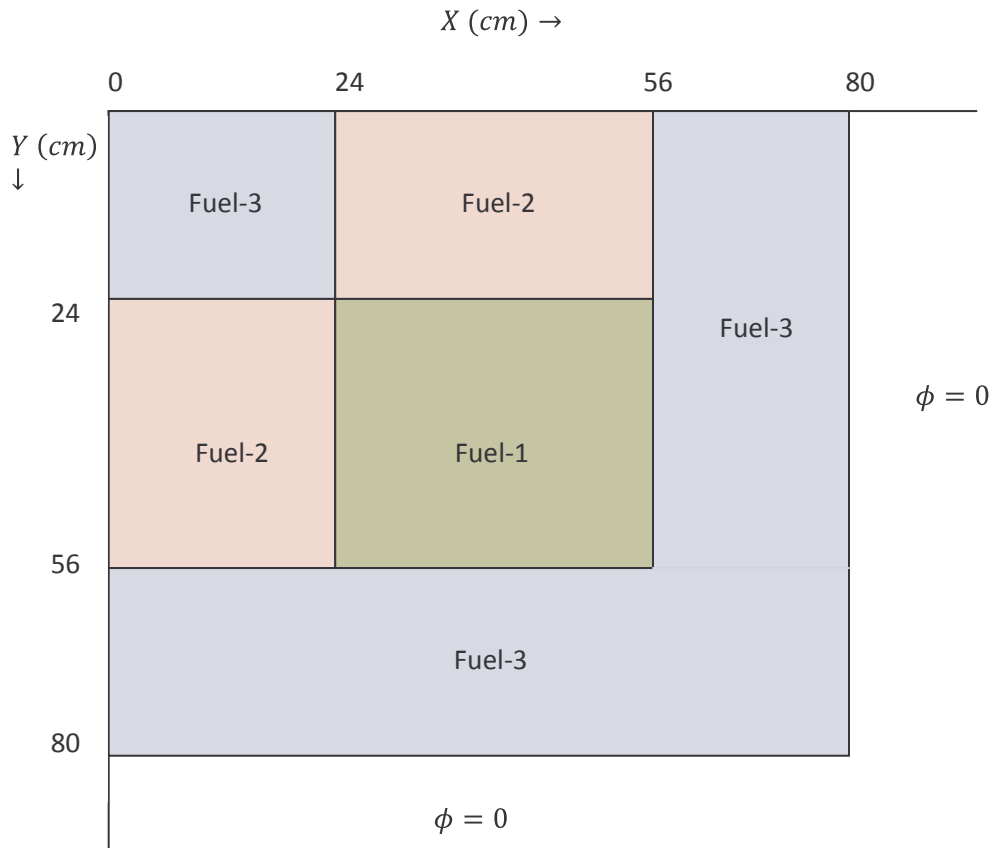


Fig. 4.3. One quadrant of 3D-TWIGL reactor. The different fuel regions and boundary conditions are shown.

The total peaking factors are also calculated during the transient and they are given in Table 4.11. It is observed that the variations in the peaking factors are observed when the space part is neglected while computing the transient. The error in the estimation of peaking factors when space part is neglected is given in Table 4.11. It is to be noted that a maximum error of 1.4 % observed in the total peaking factor during the transient time when the space part is neglected. The 10% error in the core power and 1.4% error in the peaking factor may arise due to the reason that the perturbation in the cross section is localized; and it implies that in such cases, the significance of space part is more important.

Table 4.8. Two group constants for 3D TWIGL Reactor at different regions

Region No.	Group 1	Group 2
1 & 2	$D_1 = 1.4 \text{ cm}$ $\Sigma_{a1} = 0.01 \text{ cm}^{-1}$ $\nu = 2.4$ $\Sigma_{f1} = 0.0035 \text{ cm}^{-1}$ $\Sigma_{1 \rightarrow 2} = 0.01 \text{ cm}^{-1}$ $\nu_1 = 1.0 \times 10^7 \text{ cm s}^{-1}$	$D_2 = 0.4 \text{ cm}$ $\Sigma_{a2} = 0.15 \text{ cm}^{-1}$ $\nu = 2.4$ $\Sigma_{f2} = 0.1 \text{ cm}^{-1}$ $\Sigma_{1 \rightarrow 2} = 0.0 \text{ cm}^{-1}$ $\nu_2 = 2.0 \times 10^5 \text{ cm s}^{-1}$
3	$D_1 = 1.3 \text{ cm}$ $\Sigma_{a1} = 0.008 \text{ cm}^{-1}$ $\nu = 2.4$ $\Sigma_{f1} = 0.0015 \text{ cm}^{-1}$ $\Sigma_{1 \rightarrow 2} = 0.01 \text{ cm}^{-1}$ $\nu_1 = 1.0 \times 10^7 \text{ cm s}^{-1}$ $\lambda = 0.08 \text{ s}^{-1}$	$D_2 = 0.5 \text{ cm}$ $\Sigma_{a2} = 0.05 \text{ cm}^{-1}$ $\nu = 2.4$ $\Sigma_{f2} = 0.03 \text{ cm}^{-1}$ $\Sigma_{1 \rightarrow 2} = 0.0 \text{ cm}^{-1}$ $\nu_2 = 2.0 \times 10^5 \text{ cm s}^{-1}$ $\beta = 0.0075$

Table 4.9. Comparison of k_{eff}

Parameter	Estimated	Reference [69]
k_{eff}		
k_{eff}	1.06371	1.06398

Table 4.10. The thermal flux of 3D TWIGL reactor, estimated by modified ETD+IQS method and other standard codes [65] for positive reactivity perturbation.

Time (s)	Method	Thermal flux at different locations					
		(0,80,16)	(40,40,16)	(0,80,80)	(40,40,80)	(0,80,44)	(40,40,144)
0.0	3DKIN	0.347	0.244	1.279	0.421	0.347	0.244
	AMF	0.347	0.244	1.279	0.421	0.347	0.244
	NT-FMM	0.347	0.244	1.279	0.421	0.347	0.244
	NT-AM	0.347	0.244	1.279	0.421	0.347	0.244
	Modified	0.347	0.244	1.279	0.421	0.347	0.244
	ETD+IQS						
0.05	3DKIN	0.398	0.284	1.467	0.496	0.395	0.283
	AMF	0.400	0.284	1.478	0.498	0.401	0.285
	NT-FMM	0.396	0.281	1.461	0.492	0.396	0.282
	NT-AM	0.396	0.281	1.461	0.492	0.396	0.282
	Modified	0.401	0.282	1.477	0.491	0.400	0.284
	ETD+IQS						
0.10	3DKIN	0.483	0.349	1.780	0.616	0.479	0.348
	AMF	0.487	0.350	1.800	0.621	0.488	0.352
	NT-FMM	0.479	0.345	1.769	0.610	0.479	0.345
	NT-AM	0.479	0.345	1.769	0.610	0.479	0.345
	Modified	0.490	0.345	1.802	0.607	0.489	0.351
	ETD+IQS						

0.15	3DKIN	0.619	0.454	2.284	0.809	0.615	0.452
	AMF	0.626	0.457	2.319	0.820	0.629	0.459
	NT-FMM	0.610	0.445	2.255	0.797	0.610	0.445
	NT-AM	0.610	0.445	2.255	0.797	0.610	0.445
	Modified	0.633	0.446	2.320	0.793	0.630	0.458
	ETD+IQS						
0.20	3DKIN	0.867	0.643	3.197	1.162	0.860	0.640
	AMF	0.882	0.651	3.269	1.184	0.887	0.656
	NT-FMM	0.841	0.621	3.109	1.126	0.841	0.621
	NT-AM	0.841	0.621	3.109	1.126	0.841	0.621
	Modified	0.891	0.622	3.257	1.131	0.888	0.653
	ETD+IQS						
0.25	3DKIN	0.994	0.737	3.666	1.330	0.987	0.734
	AMF	0.997	0.736	3.686	1.333	0.998	0.737
	NT-FMM	0.980	0.724	3.623	1.311	0.980	0.724
	NT-AM	0.980	0.724	3.623	1.311	0.980	0.724
	Modified	0.997	0.706	3.630	1.270	0.987	0.732
	ETD+IQS						
0.30	3DKIN	0.991	0.735	3.655	1.326	0.984	0.732
	AMF	1.008	0.745	3.727	1.348	1.009	0.745
	NT-FMM	1.004	0.741	3.710	1.342	1.004	0.741
	NT-AM	1.004	0.741	3.710	1.342	1.004	0.741
	Modified	1.010	0.720	3.681	1.295	1.006	0.745
	ETD+IQS						

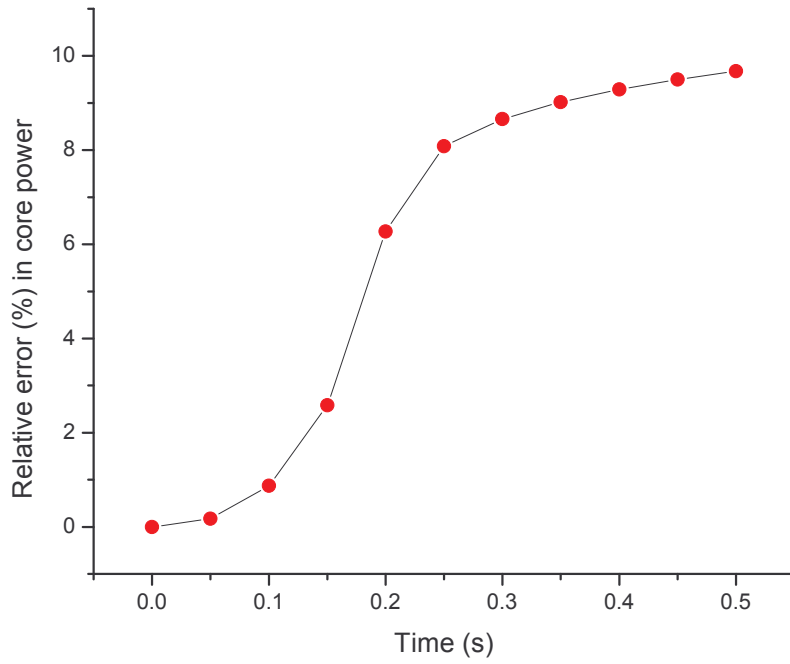


Fig. 4.4. The relative error (%) in core power (3D TWIGL) when the space part is neglected.

Table 4.11. Total peaking factor estimated with space-time kinetics and in the absence of space part. The error in the peaking factor, when space part is neglected, is also shown.

Time	Total PF (Space-time Kinetics)	Total PF (Point kinetics)	Relative error (%) in Total PF
0.0	3.914752	3.914752	0
0.05	3.905088	3.914752	0.24747
0.1	3.894653	3.914752	0.51607
0.15	3.883672	3.914752	0.80027
0.2	3.872078	3.914752	1.1021
0.25	3.865069	3.914752	1.28544
0.3	3.859865	3.914752	1.42199

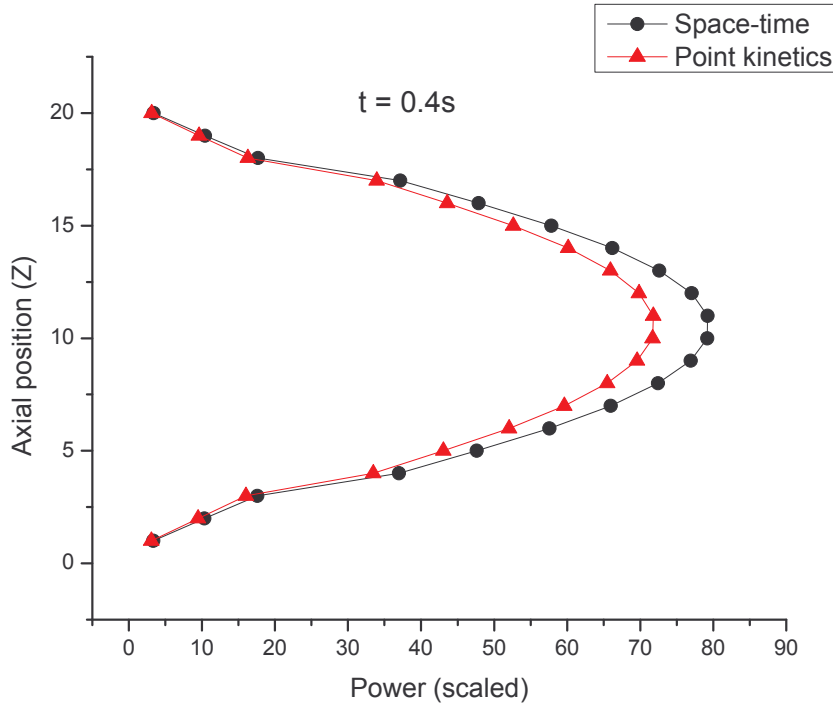


Fig. 4.5. The variation of axial power (radially integrated) profile at $t = 0.4s$.

4.4 3D LMW Benchmark Reactor Transients

The Langenbuch, Maurer and Werner (LMW) problem simulates an operational transient involving control rod movement [9], [17], [19], [70], [71]. In this benchmark, the control rod ejection accident (REA) is analyzed and the transient following the REA is estimated for longer duration of time. The control rod ejection accident is a design-basis accident which must be evaluated as part of deterministic safety analysis. This problem is a 3D transient benchmark without thermal-hydraulics feedback. The core dimensions are given as $200cm \times 200cm \times 160cm$. The core is composed of two kinds of fuel assemblies. One quadrant of the core is shown in Fig. 4.6. The control rod positions before and after the transient are shown in Fig. 4.7 and 4.8. There are axial reflectors with 20-cm width. Here the number of neutron energy groups

is two and the number of delayed precursor groups is six. The macroscopic cross section data and the delayed neutron precursor data are given in Table 4.12 and 4.13. This problem is widely studied for the cusping effect of control rod movement [17]. Before the transient, one bank of control rods is inside the core while the second bank of control rods is located in the reflector. The transient is caused by withdrawal and insertion of two control rod banks. The control rods of group 1 are inserted from the upper water reflector to the axial mid-plane of the core, and the control rods of group 2 are set in the upper axial reflector in the initial state. The transient is initiated by withdrawing the control rods of the rod group 1 at a constant speed of 3 cm/s until they are fully withdrawn. At 7.5 s into the transient, the control rods of the rod group 2 starts moving inside at the same speed and continue to move in for 40 s. The transient is initiated by withdrawing a bank of four partially inserted control rods at the rate of 3 cm/s over the time interval from 0 to 26.7 s. The second bank of control rods is inserted at the same rate over the time from 7.5 to 47.5s. The transient is followed for 60 s. These complicated control rod motions lead to significant shape changes and large cusping effects. The detailed description of control rod movement can be obtained from the works of [17], [19]. The numerical solution of this problem had been obtained using several nodal computer codes [1], [20]. The computed k_{eff} is given in Table 4.14 along with the reported values. The reported values are taken from [17], [19], [68]. The core power following the transient is given in Fig. 4.9. In Fig. 4.9, the core power is compared with the SKETCH code [72]. It is observed that during the transient the core power increases, reaches a maximum and then starts decreasing. The core power is also estimated by neglecting the space part and it is given in Fig. 4.10. The relative error in the estimation of core power, when the space part is neglected, is given in Fig. 4.11. It is observed from Figs. 4.10 and 4.11 that the effect of space part is significant in computing the

power. The power density $\left(\frac{W}{cm^3}\right)$ is computed for various micro and macro time steps and they are given in Table 4.15. The power density is compared with that of SKETCH code (Table 4.15). It is observed from Table 4.15 that as the micro and macro time step is varied, the change in the power transient is observed to be small.

The total peaking factors are calculated during the transient and they are given in Table 4.16. The error in the estimation of peaking factors when the space part is neglected is given in Table 4.16. It is to be noted that a maximum error of 3.26% is observed in the total peaking factor during the transient, when the space part is neglected.

Table 4.12. Material composition for LMW Benchmark reactor

Material Zone	Energy group	D (cm)	$\Sigma_a(cm^{-1})$	$\nu\Sigma_f$	$\Sigma_{1\rightarrow 2}$
1	1	1.423913	0.01040206	0.006477691	0.01755550
	2	0.356306	0.08766217	0.112732800	
2	1	1.423913	0.01095206	0.006477691	0.01755550
	2	0.356306	0.09146217	0.112732800	
3	1	1.425611	0.01099263	0.007503284	0.01717768
	2	0.350574	0.09925634	0.137800400	
4	1	1.634227	0.00266057	0.0	0.02759693
	2	0.264002	0.04936351	0.0	

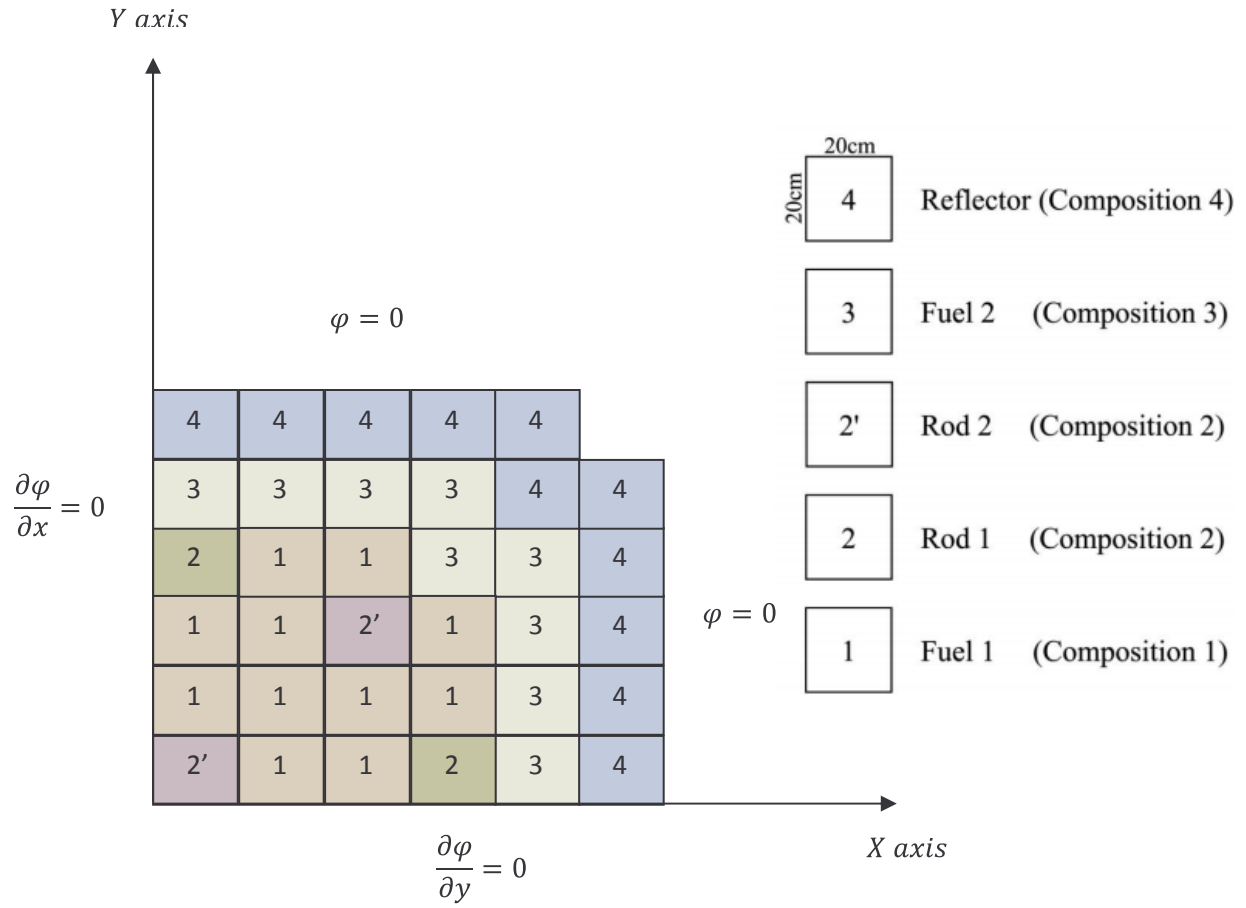


Fig. 4.6. One quadrant of the LMW core. The boundary conditions are also shown. The control rods and fuel material composition numbers are shown in the inset.

Table 4.13. Delayed neutron precursor data

Group no.	β_i	$\lambda_i(s^{-1})$	Group no.	β_i	$\lambda_i(s^{-1})$
1	0.0002470	0.0127	4	0.0026455	0.3110
2	0.0013845	0.0317	5	0.0008320	1.4000
3	0.0012220	0.1150	6	0.0001690	3.8700

Table 4.14. Estimated k_{eff} along with the reference [17], [19], [68].

S.N	Parameter	Estimated k_{eff}	Reference-1 QUANDRY	Reference-2 SPANDEX	Reference-3 SIMULATE	Reference-4 CONQUEST
1	k_{eff}	0.99981	0.99974	0.99971	0.99974	0.99966

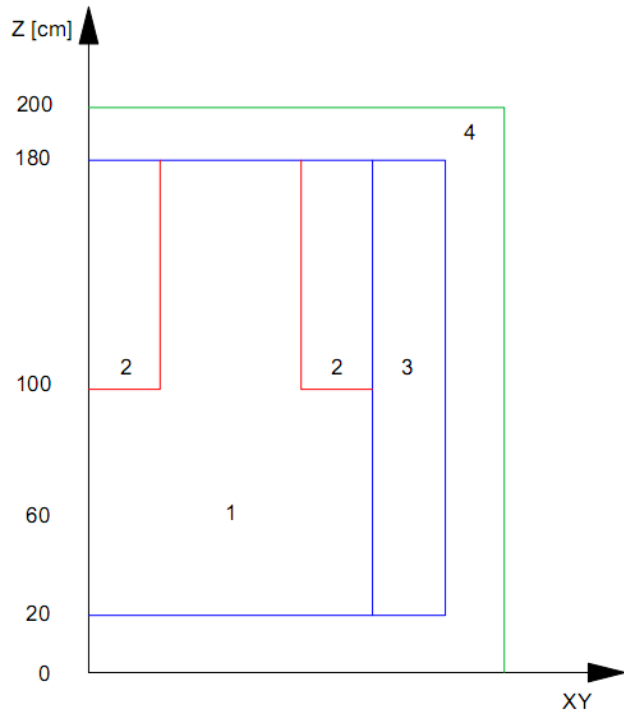


Fig. 4.7. The axial position of control rod before transient

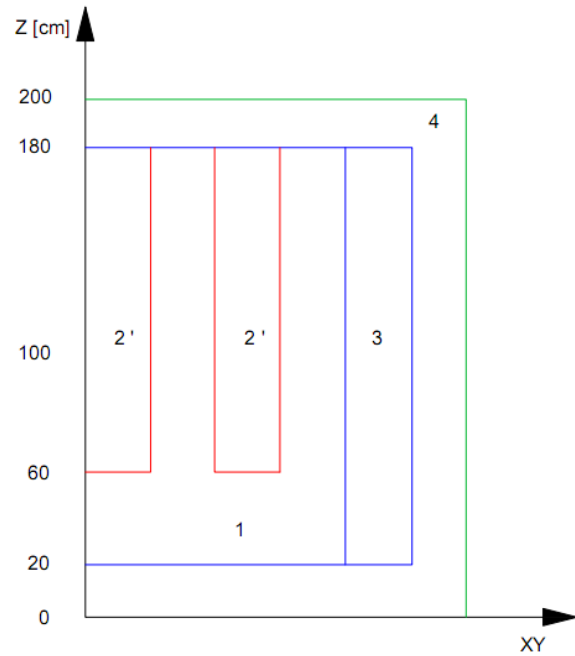


Fig. 4.8. The axial position of control rod at the end of transient.

Table 4.15. Comparison of core power density with SKETCH code [72]. Power density $\left(\frac{W}{cm^3}\right)$ for various macro and micro time steps along with the SKETCH code.

Time (s)	0	10.0	20.0	30.0	40.0	50.0	60.0
Power density $\left(\frac{W}{cm^3}\right)$ (SKETCH CODE, [72])	150	201	257	207	122	76	58
Modified ETD+IQS method							
$\Delta t = 1.0E - 3$ $\Delta T = 0.5$	150.00	200.57	251.68	204.02	124.38	80.44	63.04
$\Delta t = 2.0E - 3$ $\Delta T = 0.5$	150.00	200.57	251.71	204.06	124.38	80.48	63.07
$\Delta t = 2.0E - 3$ $\Delta T = 1.0$	150.00	201.82	254.69	205.06	123.86	79.87	62.64
$\Delta t = 2.5E - 3$ $\Delta T = 1.0$	150.00	202.99	258.72	206.89	123.02	80.07	63.24
$\Delta t = 5.0E - 3$ $\Delta T = 1.0$	150.00	201.83	254.72	205.07	123.83	79.83	62.60
$\Delta t = 1.0E - 2$ $\Delta T = 1.0$	150.00	201.84	254.70	205.04	123.83	79.83	62.59

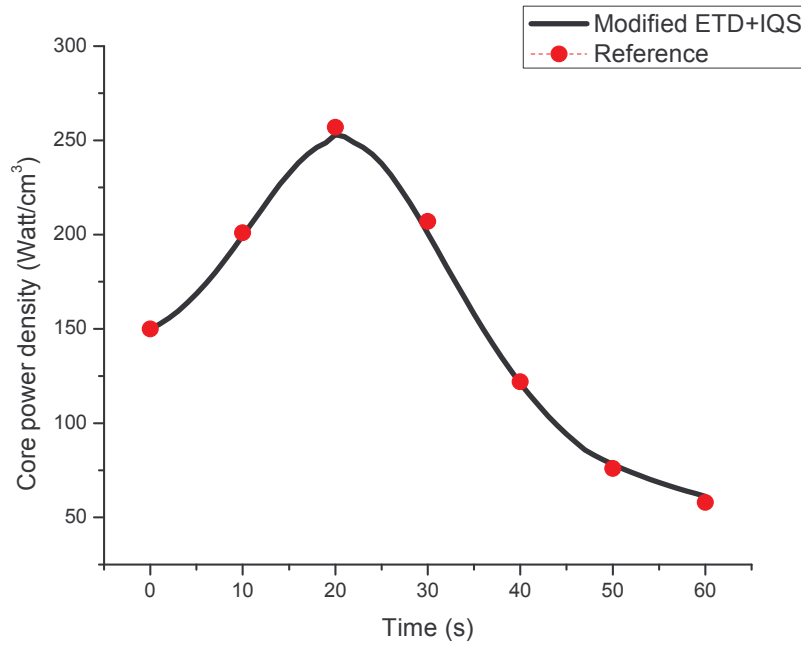


Fig. 4.9. The core power density (W/cm^3) with time. The reference data is taken from SKETCH code [72].

Table 4.16. Total peaking factor during the transient. The relative error in the estimation of total peaking factor when space part is neglected.

Time	Space-Time Kinetics Total PF	Point Kinetics Total PF	Relative error (%) in Total PF
0.0	3.312788	3.312788	0
10	3.308672	3.312788	0.1244
20	3.308173	3.312788	0.1395
30	3.300141	3.312788	0.38323
40	3.208119	3.312788	3.26263
50	3.210680	3.312788	3.18026
60	3.210717	3.312788	3.17907

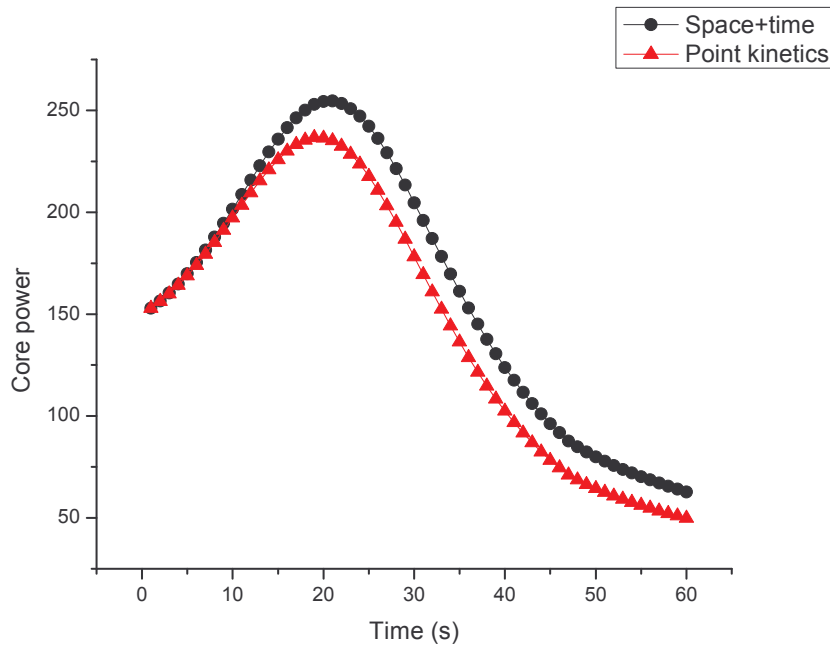


Fig. 4.10. 3D LMW core power estimated with space-time kinetics and point kinetics.

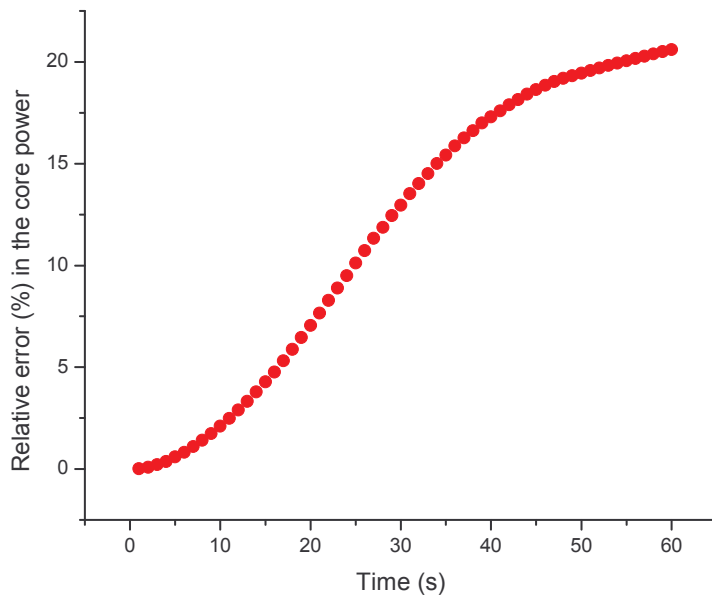


Fig. 4.11. Relative error (%) in the estimation of core power when the space part is neglected.

4.5 CANDU 3D-PHWR (AECL 7236) Benchmark Transients

It is a benchmark reactor transient proposed by ATOMIC ENERGY OF CANADA LIMITED [73]. It is a realistic 3D CANDU PHWR space-time kinetics benchmark problem [73] in Cartesian geometry. This is one of the widely studied benchmark problem [8], [28], [30], [74]. The geometrical description of the CANDU core is as follows: This core contains two radial fuel zones (inner core and outer core) surrounded by heavy water reflector as shown in Fig. 4.12. The axial length of the core in the horizontal Z direction is 600 cm. Along the horizontal direction (Z axis) the material distribution is uniform. The height and width of the core are 780 cm. The core is divided into a total of $18 \times 18 \times 10$ meshes. It has reflective symmetry in all XY , YZ and XZ planes passing through the centre of the reactor. The vertical cross section ($0 < Z < 300$ cm) of the core is shown in Fig. 4.13. The horizontal cross section of the core at $Y = 390$ cm is shown in Fig. 4.14. The vertical cross section for $300 < Z < 600$ cm is shown in Fig. 4.15. The core composition is given in Table 4.17. Under normal operating conditions, the fissile component in the inner core is slightly less than that of the outer core. The two group cross section data for the core are given in Table 4.18. The decay constants of the delayed neutron precursors and the delayed neutron fractions are given in Table 4.19. Here the transients are modeled using two energy groups and zero flux boundary condition is assumed. The k_{eff} value is estimated and it is given in Table 4.20 along with the reference values. One can follow the sub-space iteration scheme to estimate the eigen value (mode) and other lower modes [74]. The eigen value can also be obtained using Orthomin(1) algorithm [75].

4.5.1 LOCA simulation in CANDU 3D-PHWR

Here the transient is caused by the occurrence of LOCA. The LOCA is simulated by decreasing the thermal absorption cross section in regions 5, 6, 10, 11, 17, 18, 22 and 23 (Figs. 4.13 and 4.15). The rate of decrease of thermal absorption cross section is given by [73]

$$\frac{\partial \Sigma_2}{\partial t} = \begin{cases} -1.0 \times 10^{-4} (cms)^{-1} & \text{for } t \leq 0.4 \text{ s} \\ -8.88889 \times 10^{-6} (cms)^{-1} & \text{for } t > 0.4 \text{ s} \end{cases}$$

To arrest the positive reactivity insertion, shut down devices are inserted asymmetrically and the insertion of shut down devices creates an incremental thermal absorption cross section [73], given by

$$\Delta \Sigma_2 = 6.15 \times 10^{-4} cm^{-1}$$

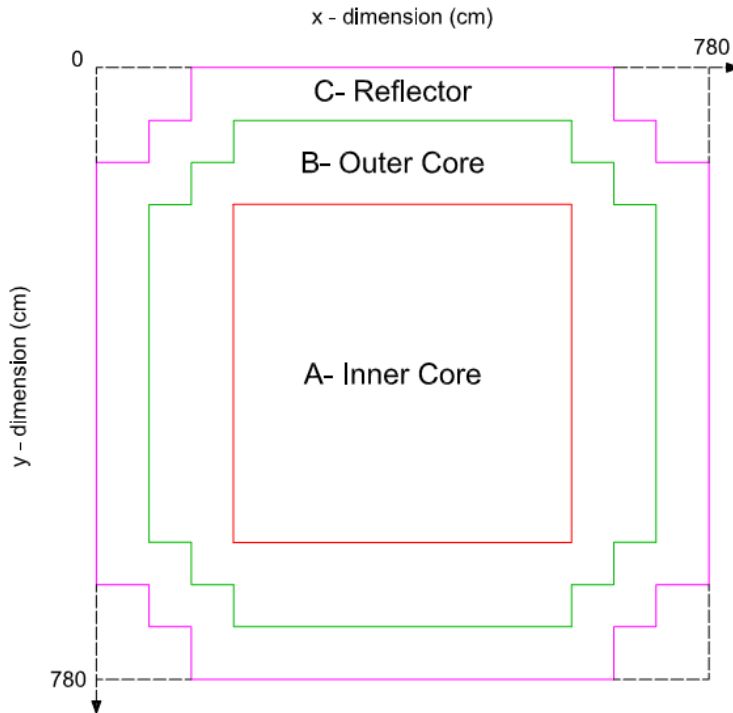


Fig. 4.12. Vertical cross section of CANDU 3D-PHWR

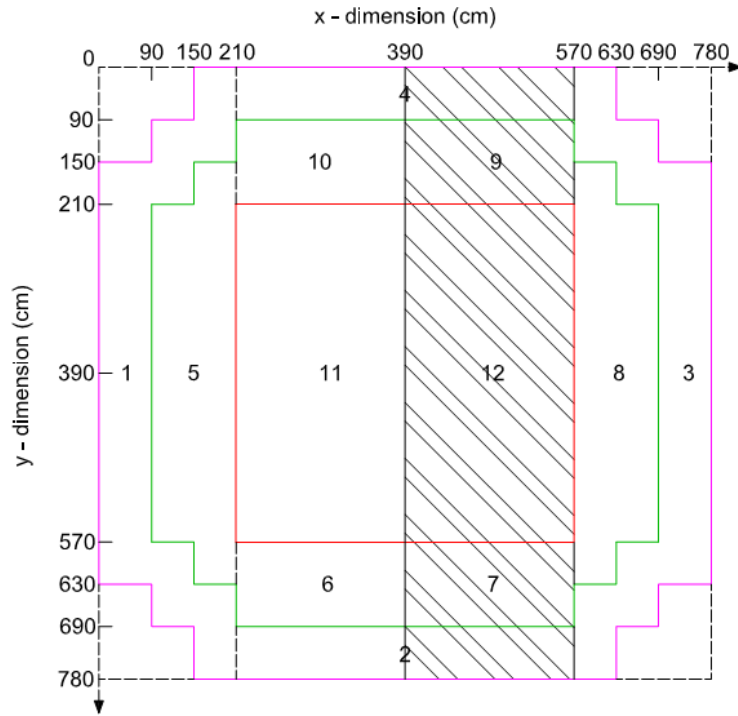


Fig. 4.13. Vertical cross section (at $Z = 0$) of CANDU 3D-PHWR. The shaded regions indicate the area where the absorber is inserted.

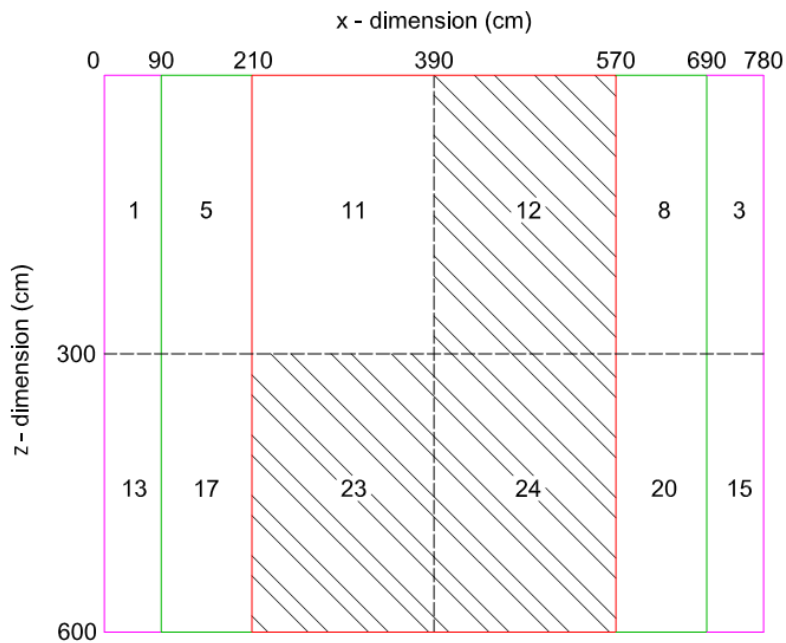


Fig. 4.14. Horizontal cross section (at $Y = 390 \text{ cm}$) of CANDU 3D-PHWR. The shaded regions indicate the area where the absorber is inserted.

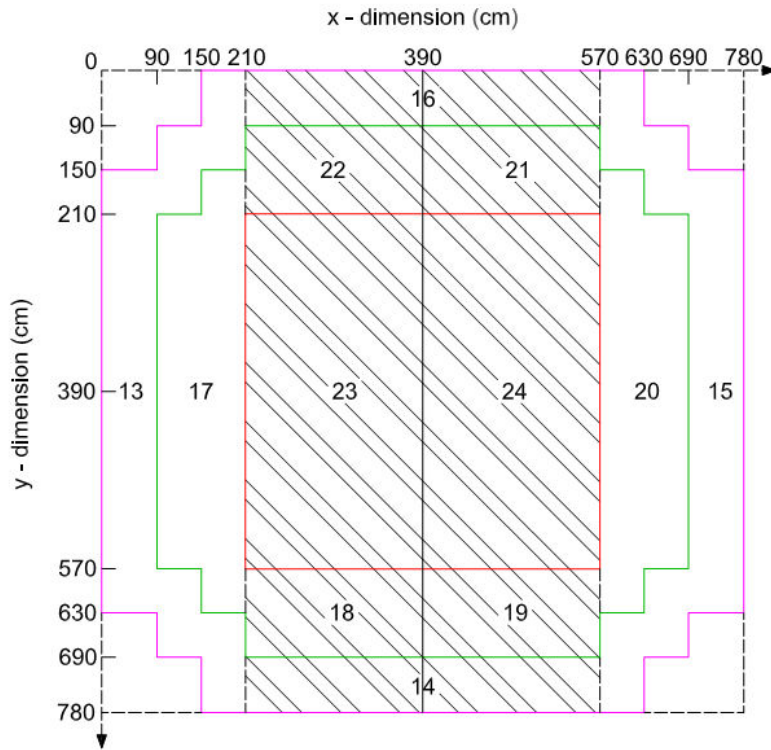


Fig. 4.15. Vertical cross section of CANDU 3D-PHWR at $Z = 600 \text{ cm}$. The shaded regions indicate the area where the absorber is inserted.

Table 4.17. Material composition of CANDU 3D-PHWR at different regions

Region Name	Material Composition (Fresh fuel)
A-Inner core &	Fuel: natural UO_2 at 600°C
B-Outer core	Coolant: 99.7% D_2O at 270°C Moderator: 99.7% D_2O at 60°C
C-Reflector	99.7% D_2O at 60°C

Table 4.18. Two group constants for CANDU 3D-PHWR

Region No.	D_g	$\nu\Sigma_{fg}$	Σ_i	$\Sigma_{1\rightarrow 2}$
1,2,3,4,13, 14,15,16	$D_1 = 1.3100 \text{ cm}$ $D_2 = 0.8695 \text{ cm}$	$\nu\Sigma_{f1} = 0.0$ $\nu\Sigma_{f2} = 0.0$	$\Sigma_1 = 1.018 \times 10^{-2}$ $\Sigma_2 = 2.117 \times 10^{-4}$	1.018E-2
5-10, 17-22	$D_1 = 1.2640 \text{ cm}$ $D_2 = 0.9328 \text{ cm}$	$\nu\Sigma_{f1} = 0.0$ $\nu\Sigma_{f2} = 4.723 \times 10^{-3}$	$\Sigma_1 = 8.154 \times 10^{-3}$ $\Sigma_2 = 4.014 \times 10^{-3}$	7.368E-3
11,12, 23,24	$D_1 = 1.2640 \text{ cm}$ $D_2 = 0.9328 \text{ cm}$	$\nu\Sigma_{f1} = 0.0$ $\nu\Sigma_{f2} = 4.562 \times 10^{-3}$	$\Sigma_1 = 8.154 \times 10^{-3}$ $\Sigma_2 = 4.100 \times 10^{-3}$	7.368E-3

Table 4.19. Delayed neutron fractions and precursor decay constants

Delayed neutron group no.	β_i	$\lambda_i \text{ (s}^{-1}\text{)}$
1	4.17E-04	1.244E-2
2	1.457E-3	3.063E-2
3	1.339E-3	1.139E-1
4	3.339E-3	3.079E-1
5	8.970E-4	1.198E+0
6	3.200E-4	3.212E+0
$v_1 = 1.0 \times 10^7 \text{ cm/s}, \quad v_2 = 3.0 \times 10^5 \text{ cm/s}$		

The incremental thermal absorption cross section is created in the regions 2, 4 7, 9, 12, 14, 16, 18, 19 and 21-24 (Figs 4.13-4.15). The regions where absorbers are inserted are shown as shaded areas in Figs. 4.13-4.15. The absorber insertion starts at 0.6s with a constant velocity of 520 cm/s in the Y direction. The moving absorber boundary is parallel to the XZ plane. The

change in cross section is additive whenever the perturbations overlap. The transient lasts for 2.5 s.

4.5.2 Transient estimation and discussion

The combined effect of LOCA and asymmetric insertion of shutdown devices create super delayed transients. This benchmark problem was initially solved using the CERKIN code [73] and it is taken as the reference. The initial k_{eff} is found to be 1.003555 and other reported k_{eff} values are given in Table 4.20. A micro time step of 0.1ms is adopted here to solve the amplitude function and the shape functions are estimated at macro time steps 0.0125s, 0.250s, 0.5s and 0.1s. The relative core power, following the transients, is estimated for the full length of the transient for each macro time step using the modified ETD with IQS model. The estimated relative core power is compared with that of benchmark result [73]. The relative core power computed with the macro time step 0.0125s is shown in Fig. 4.16 along with the benchmark result. A relative error of 2.02% is observed in the computation of peak power. Fig. 4.17 shows the relative power estimated using the macro time step 0.025s. A relative error of 1.53% is observed in the estimation of peak power. Figs. 4.18 & 4.19 show the relative powers for the macro time steps 0.05s and 0.1s and the relative errors are found to be 0.94% and 0.98% respectively. The variation of normalized thermal flux in the XZ plane at $Y = 360cm$, $Z = 270cm$ at $T = 2.5s$ is shown in Fig. 4.20. From the comparison of results, it is observed this method is capable of estimating the transient to a good accuracy. The error in the estimation of core power, when different macro time steps are used, is given in Fig. 4.21. The core power is estimated with space part and without space part. The relative error (%) between them is computed and given in Fig. 4.22. The detailed description of the transient, estimated using modified ETD method with IQS model is given by Mohideen Abdul Razak [36].

Table 4.20. Comparison of initial k_{eff} with other standard codes

Parameter	Estimated k_{eff}	Benchmark [73]	TRIKIN [30]	Modak and Jain [74]
k_{eff}	1.003555	1.003550	1.00355119	1.0035548

4.5.3 Flux distribution and power tilts in CANDU-PHWR during transient

The thermal flux distribution at $270 < Z < 300$ before the transient is shown in Fig. 4.23a. As the transient takes place, the flux distribution starts changing and this causes the power tilt. The thermal flux distributions at $t = 0.5s, 1.0s, 1.5s, 2.0s$ and $2.5s$, in the plane $270 < Z < 300$, are shown in Figs. 4.23b-4.23f. In a similar manner the fast flux distribution before the transient ($270 < Z < 300$) is given in Fig. 4.24a. The fast flux distributions at $t = 0.5s, 1.0s, 1.5s, 2.0s$ and $2.5s$, in the plane $270 < Z < 300$, are shown in Figs. 4.24b-4.24f.

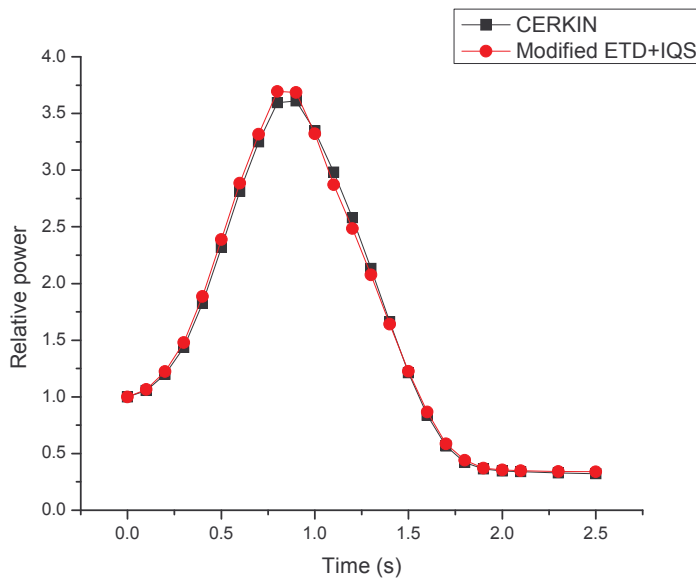


Fig. 4.16. Relative Power of CANDU 3D-PHWR computed with macro time step 0.0125s.

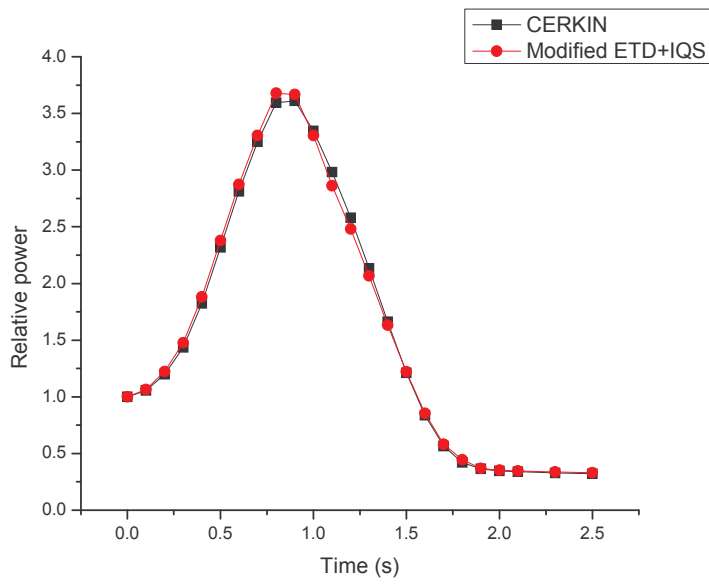


Fig. 4.17. Relative Power of CANDU 3D-PHWR computed with macro time step 0.0250s.

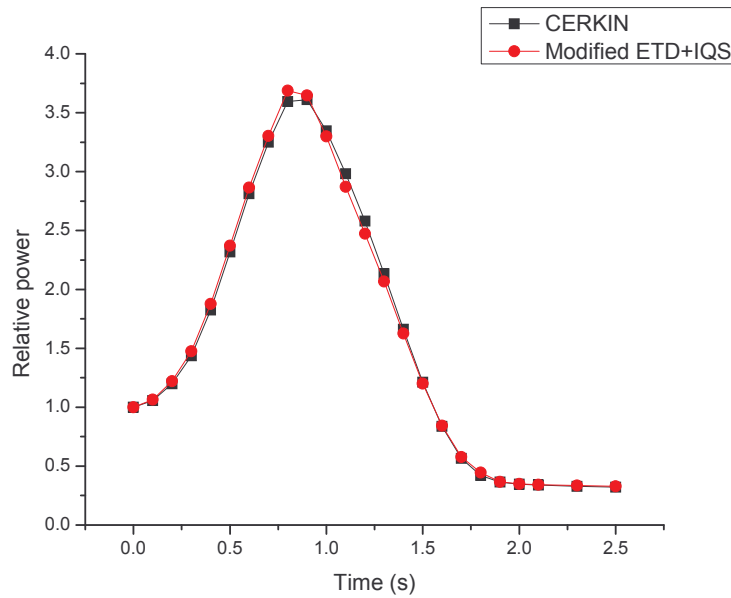


Fig. 4.18. Relative Power of CANDU 3D-PHWR computed with macro time step 0.05s.

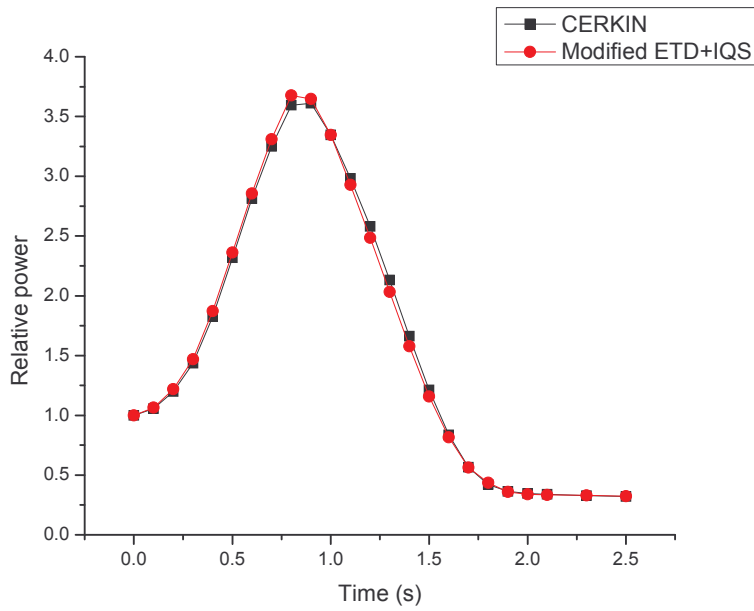


Fig. 4.19. Relative Power of CANDU 3D-PHWR computed with macro time step 0.1s.

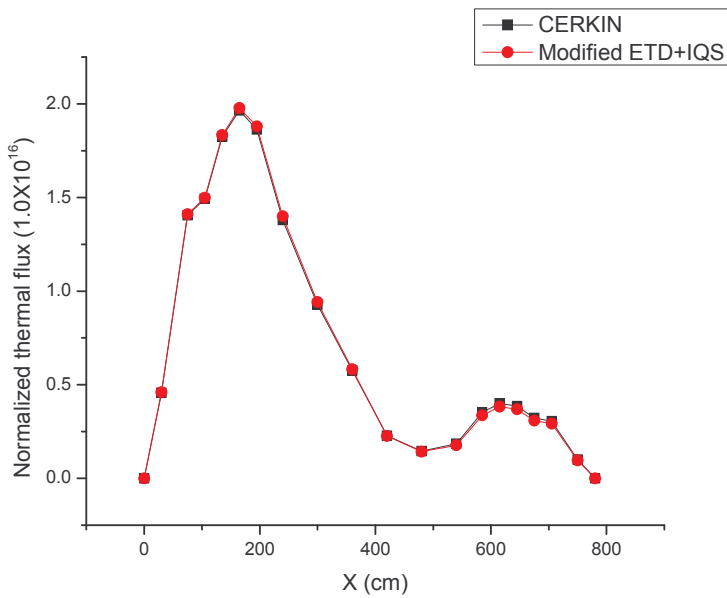


Fig. 4.20. Normalized thermal flux in XZ plane, at $Y = 360\text{ cm}$, $Z = 270\text{ cm}$, $T = 2.5\text{ s}$.

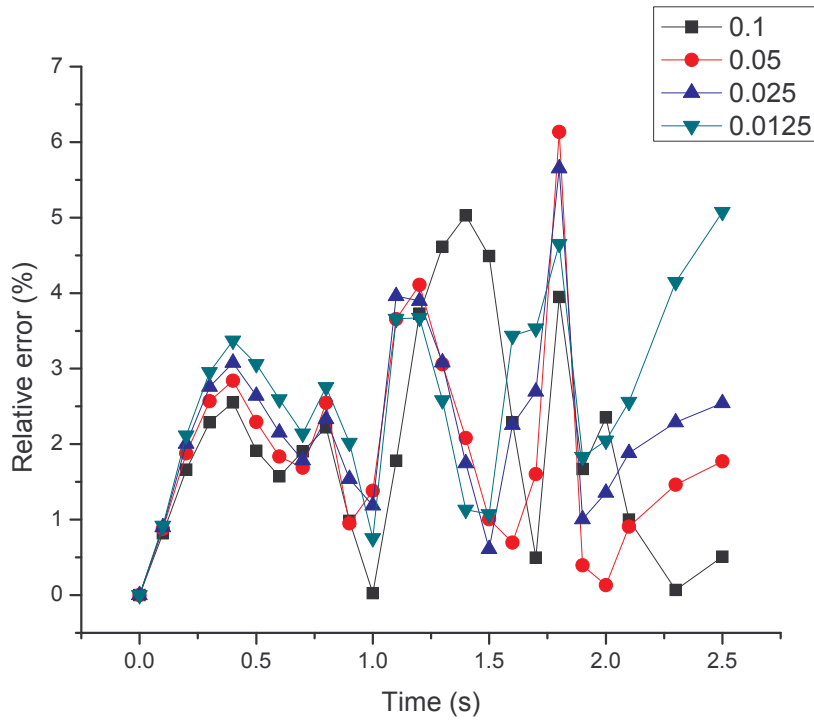


Fig. 4.21. The relative error (%) in core power for various macro time steps.

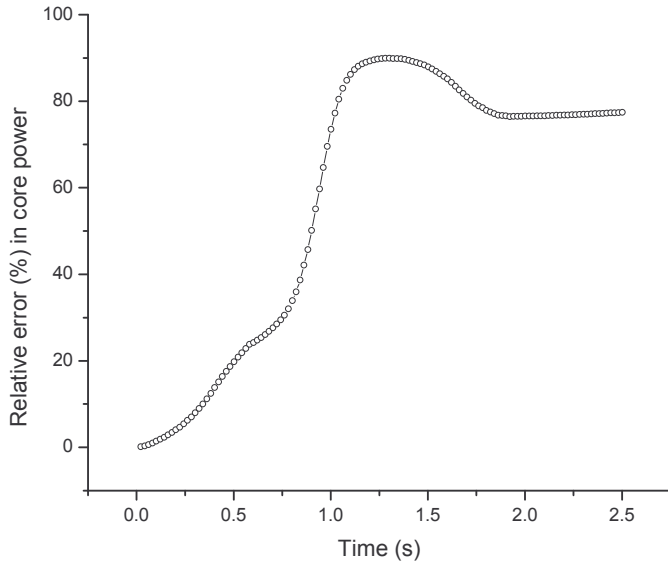


Fig. 4.22. Relative error (%) in core power (modified ETD+IQS) when space part is neglected.

The power tilt is computed as

$$\text{Power tilt (top to bottom)} = \frac{\text{power in upper part} - \text{power in lower part}}{\text{total power}}$$

$$\text{Power tilt (side to side)} = \frac{\text{power in left side} - \text{power in right side}}{\text{total power}}$$

$$\text{Power tilt (front to back)} = \frac{\text{power in front part} - \text{power in back part}}{\text{total power}}$$

The initial power tilt is observed to be

$$\text{Power tilt (top-bottom) (\%)} = 7.4947502\text{E-}04$$

$$\text{Power tilt (side-side) (\%)} = 2.7080099\text{E-}03$$

$$\text{Power tilt (front - back) (\%)} = 2.1282263\text{E-}03$$

The variation of power tilt during the transient is given in Figs. 4.25-4.27.

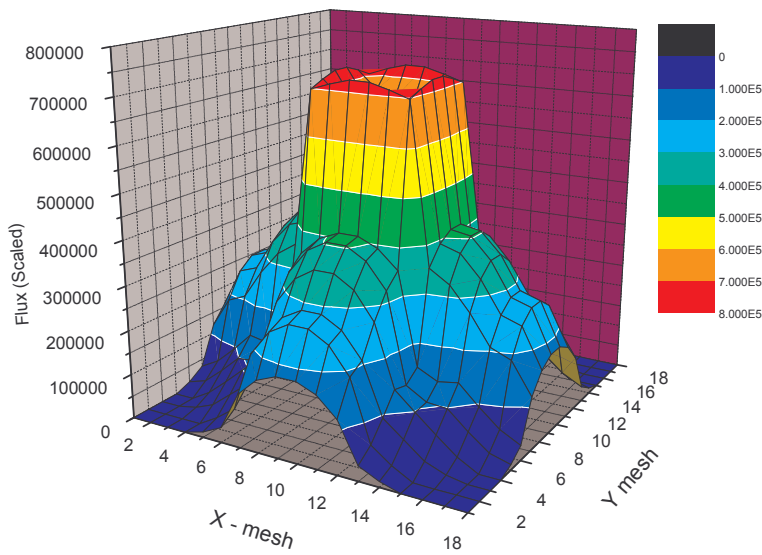


Fig. 4.23a. The thermal flux distribution ($270 < Z < 300$) in CANDU PHWR at $t = 0$ s.

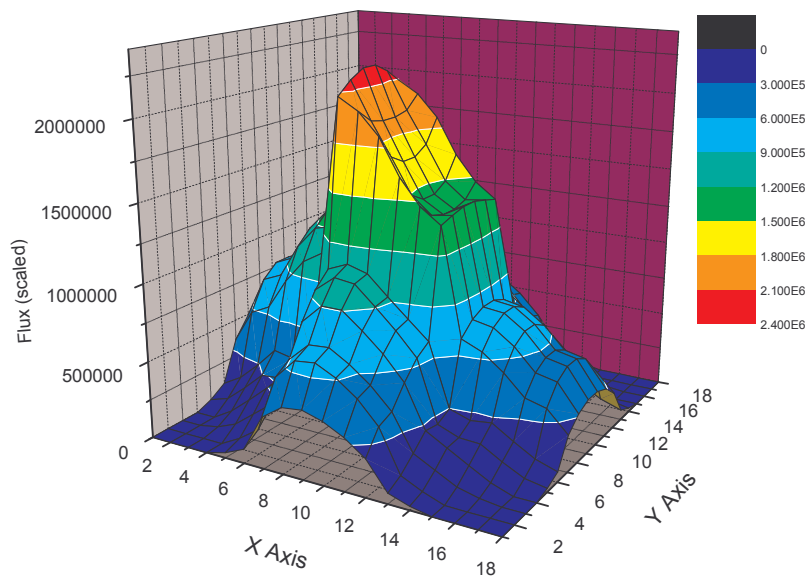


Fig. 4.23b. The thermal flux distribution ($270 < Z < 300$) at $t = 0.5$ s. The flux tilt is seen

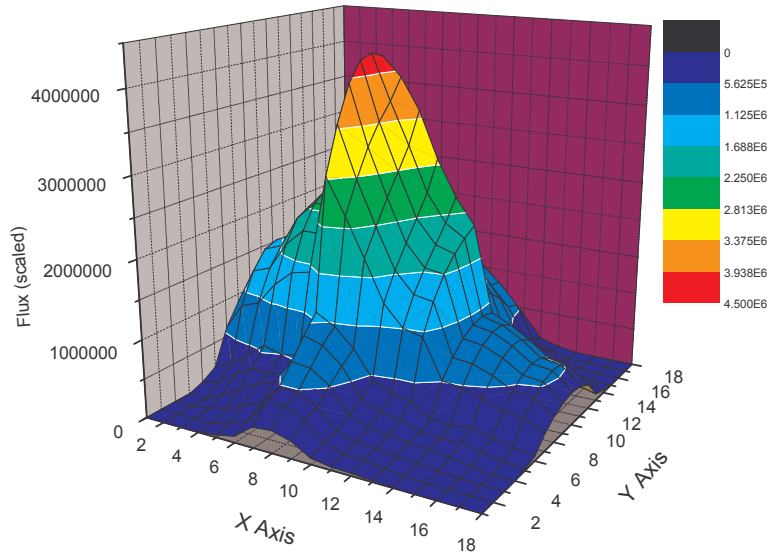


Fig. 4.23c. The thermal flux distribution ($270 < Z < 300$) at $t = 1.0\text{s}$.

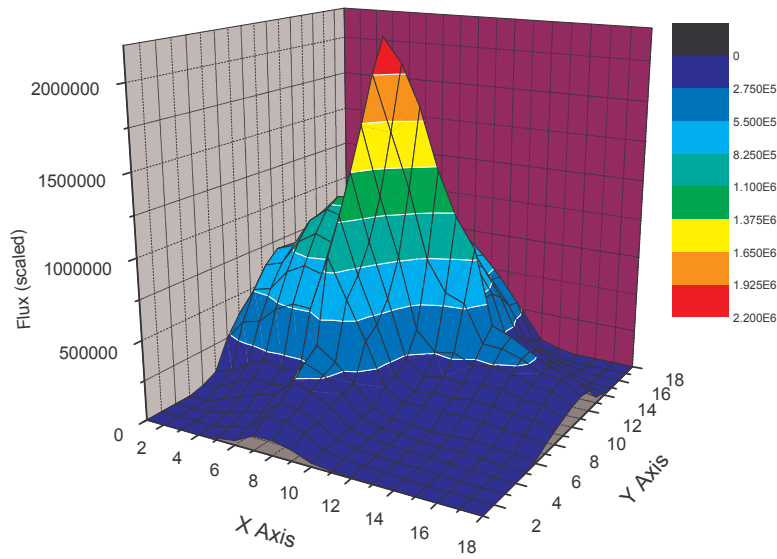


Fig. 4.23d. The thermal flux distribution ($270 < Z < 300$) at $t = 1.5\text{s}$.

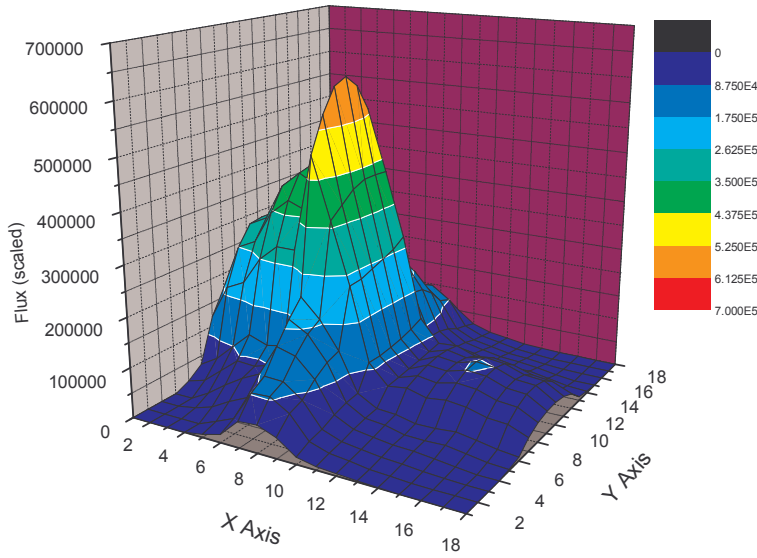


Fig. 4.23e. The thermal flux distribution ($270 < Z < 300$) at $t = 2.0s$

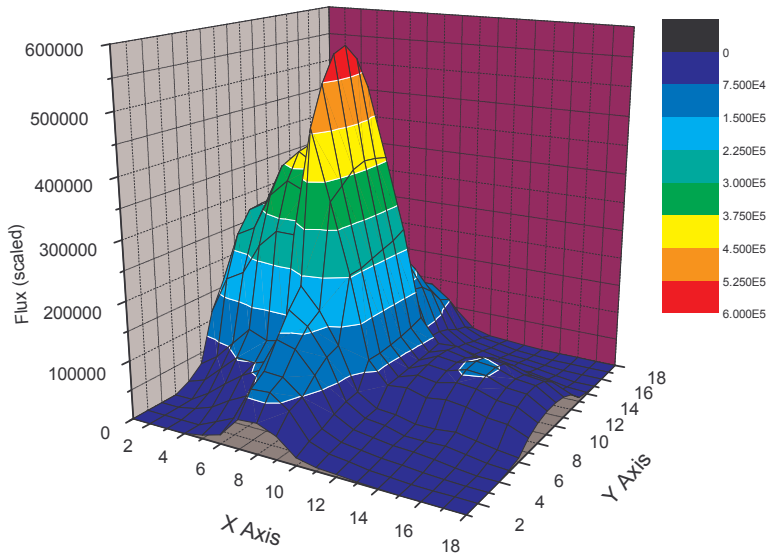


Fig. 4.23f. The thermal flux distribution ($270 < Z < 300$) at $t = 2.5s$

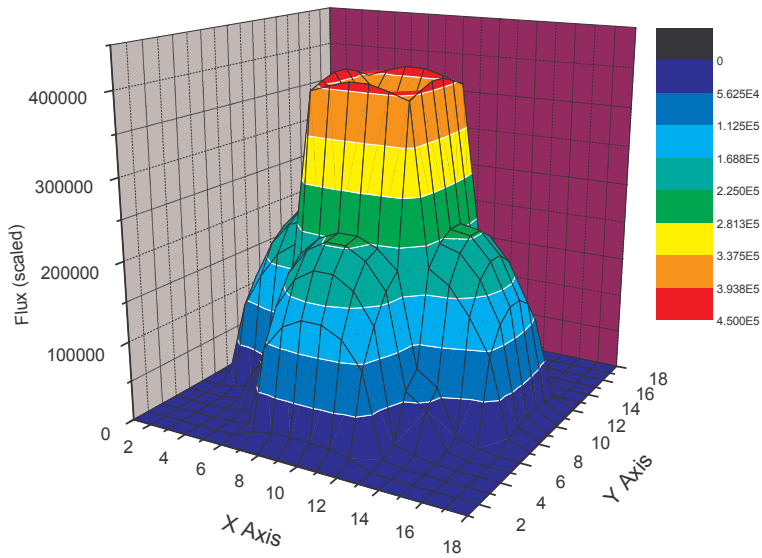


Fig. 4.24a. The fast flux distribution ($270 < Z < 300$) in CANDU PHWR at $t = 0.0\text{s}$

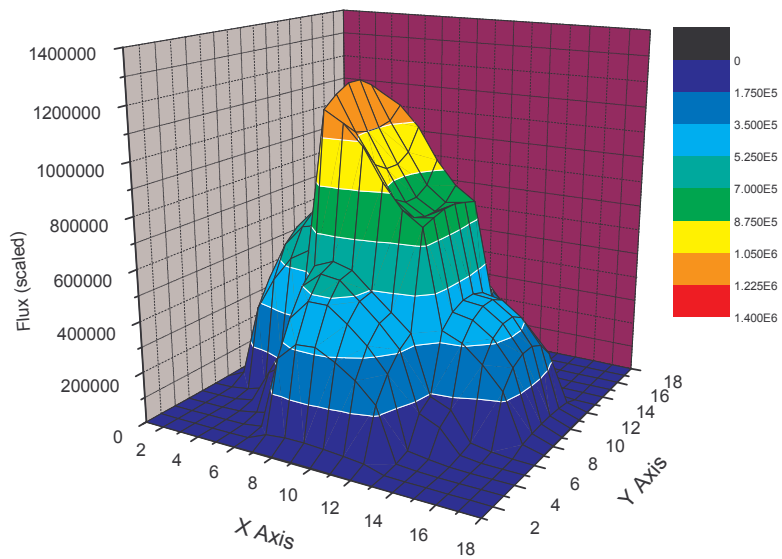


Fig. 4.24b. The fast flux distribution ($270 < Z < 300$) at $t = 0.5\text{s}$

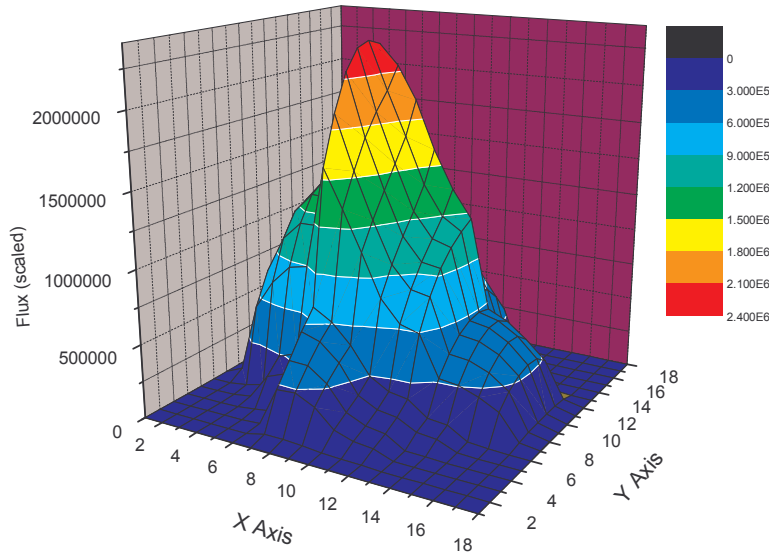


Fig. 4.24c. The fast flux distribution ($270 < Z < 300$) at $t = 1.0$ s

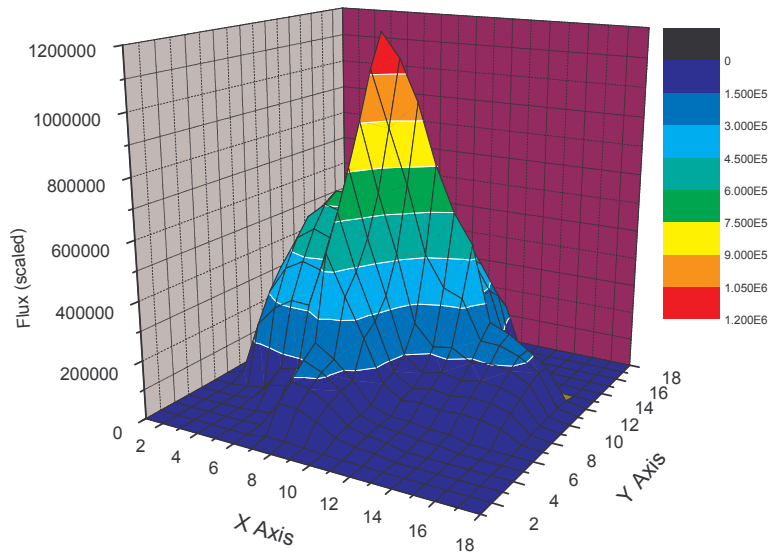


Fig. 4.24d. The fast flux distribution ($270 < Z < 300$) at $t = 1.5$ s

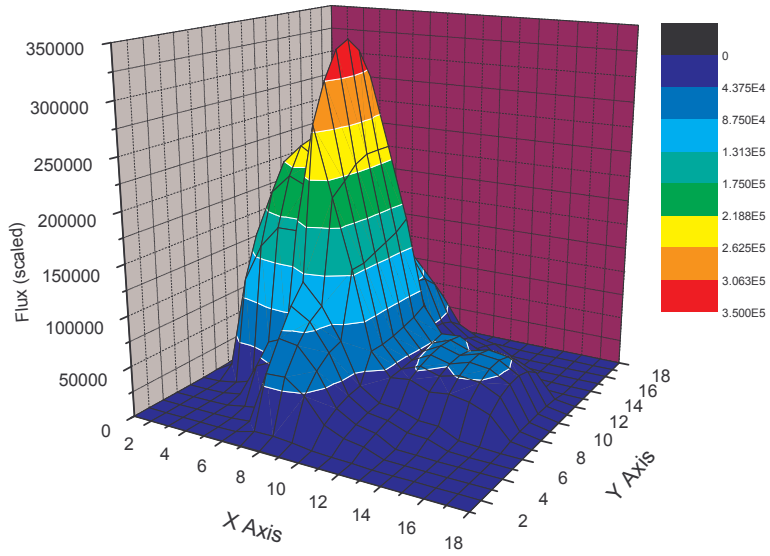


Fig. 4.24e. The fast flux distribution ($270 < Z < 300$) at $t = 2.0$ s

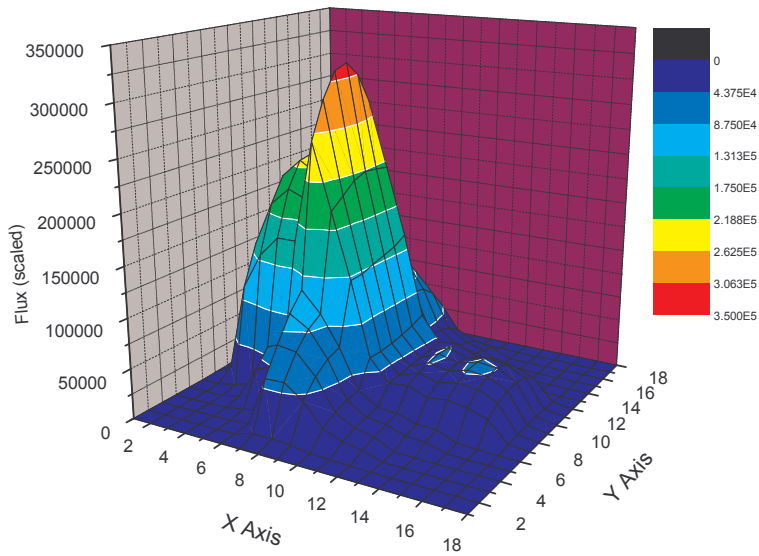


Fig. 4.24f. The fast flux distribution ($270 < Z < 300$) at $t = 2.5$ s

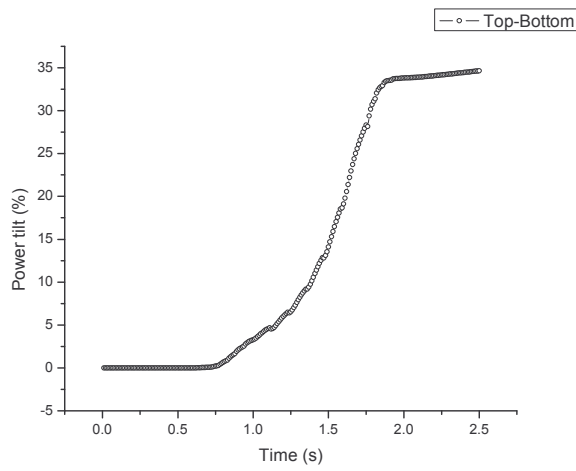


Fig. 4.25. The variation of power tilt (top-bottom) during the transient.

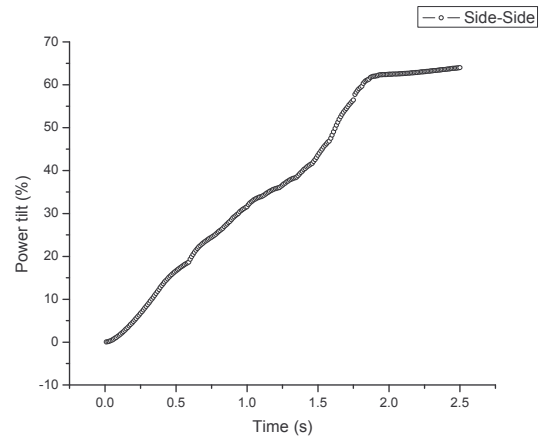


Fig. 4.26. The variation of power tilt (side-side) during the transient.

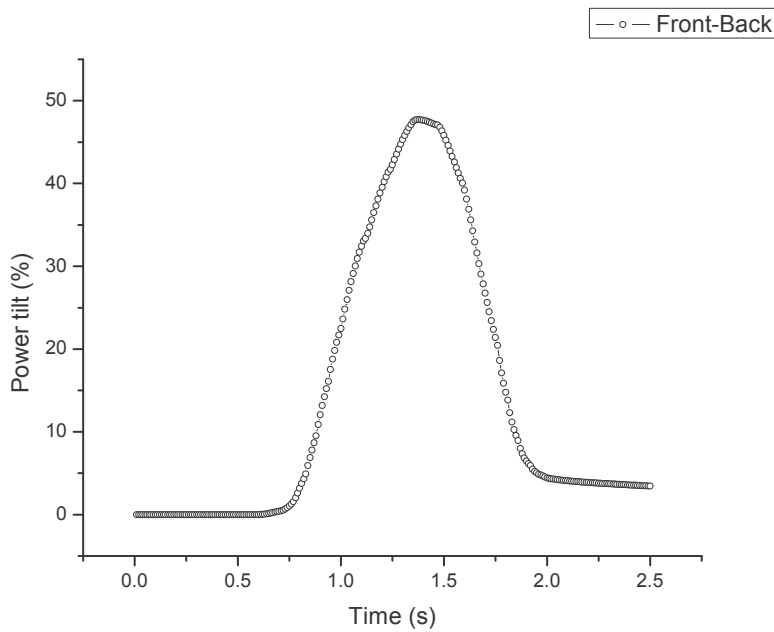


Fig. 4.27. The variation of power tilt (front-back) during the transient.

4.6 Summary

The transient in 3D homogeneous reactor is estimated using the modified exponential time differencing (ETD) method with improved quasi static model (IQS). The transient is estimated for two independent perturbations in the cross sections. The estimated transient is found to be in good agreement with the reference. In this case the effect of space part is found to be small in the estimation of transient.

The transient in 3D TWIGL benchmark reactor is estimated and the results agree well with the reported values. Here the perturbation in the cross section is localized. Here the effect of space part is found to be significant ($\sim 10\%$) in the estimation of transient. It may be due to the reason that the perturbation in the cross section is localized.

The transient in 3D LMW benchmark following control rod ejection accident is analyzed for longer duration of time. This benchmark contains complicated control rod movement. The transient is estimated for various micro and macro time steps and the results agree well with the reference. Here the space part contribution is found to be more in the estimation of transient.

The transient in CANDU 3D PHWR benchmark (AECL 7236) is analyzed following LOCA. The asymmetric insertion of control rod banks creates super delayed transients. The transient is estimated for various micro and macro time steps. The estimated transient is found to be in good agreement with the CERKIN code. It is observed that using the modified ETD method with IQS model, the transient can be estimated using large time step without losing the accuracy. Here the effect of space part is found to be more in the estimation of transient.

These results clearly indicate that the modified ETD method with IQS model can be used to estimate the transient for various types of reactivity insertions. The transient can be estimated

using large time step without losing the accuracy. This computational method is found to be stable in the sense that a small change in the micro time step or macro time step does not affect the accuracy very much.

CHAPTER 5

DYNAMIC UNCERTAINTY QUANTIFICATION AND SENSITIVITY ANALYSIS IN REACTOR TRANSIENTS

5.1 Introduction to uncertainty quantification and sensitivity analysis in reactor transients

The uncertainty analysis deals with assessing the uncertainty in the output of physical systems resulting from imprecisely known input variables or change of models or combination of both. Sensitivity analysis deals with the study of impact of input parameter-uncertainty in the output. The study of behaviour of reactor core to various types of input perturbations (cross sections, geometry etc) is important for the safe operation of research reactors as well as commercial nuclear reactors. Generally the safety requirements and licensing of commercial nuclear power plants are based on conservative approach [76]. Sometimes the conservative approach on safety analysis may be inaccurate [77]. The nuclear safety analysis using best estimate plus uncertainty (BEPU) analysis is in use since 1990 [77]-[79]. The study of safety analysis is important for quantifying the safety margins during reactor operation and accident scenarios. For example in the case of any postulated accidental scenario, the sudden rise of core power will lead to fuel temperature rise, cladding temperature rise, moderator density change etc. and if the rise in temperature or any parameter change is predicted with uncertainty, then the safety margins can be fixed more accurately. Generally a conservative error or uncertainty in the output parameter, (i.e. power, peaking factor, etc.) is assumed and based on this conservative error, the safety margins are fixed. But if the conservative error or uncertainty is evaluated in a more deterministic way, then the nuclear safety margins can be fixed in a high confidence level and the safety factors become more reliable than the conservative approach.

In any Nuclear Power Plant (NPP), it is essential to know the reactor behaviour when the input parameters are perturbed around their best estimate value. The best estimate plus uncertainty (BEPU) analysis method [78] has been developed for uncertainty quantification in support of regulatory rulemaking changes of safety analyses in the nuclear industry [80] and it has been applied to loss-of-coolant accidents (LOCA) [78], [79], [81], [82].

The reactor core behaviour is estimated by solving the neutron diffusion equation. Several computer codes exist to solve the neutron diffusion equations. The reactor physics parameters such as neutron multiplication factor (k_{eff}), core power, neutron flux, delayed neutron fractions, etc. are estimated using computer codes. The code prediction of reactor physics parameters is prone to several sources of errors or uncertainties in the input parameters as well as the methods adopted to calculate them. Some input parameter uncertainty may be more influential in affecting the multiplication factor, reactor power, peaking factor etc. and some parameter may be less influential in affecting them. The aim of the uncertainty analysis is to identify and quantify all potentially important input parameters with uncertainty, their range of variation, and their effect on core response and safety margins. Using this uncertainty analysis, the factors which are more influential may be identified and these factors may be estimated in a more accurate way. Based on uncertainty analysis, the upper limit for fuel temperature, clad temperature, can be set in a highly reliable way. The uncertainty and sensitivity analysis can be performed for any reactor physics parameter such as control rod worth, β_{eff} , k_{eff} , Λ etc. [83], [84]. Some input parameter uncertainty may not be influential as time progresses; but some uncertainty may be influential with time. The propagation of input parameter uncertainty with time may affect the reactor transient and in this case it is important to examine its effect on

uncertainty in reactor core power, peak mesh power, peaking factor etc. during transient to fix the safety margins. Here both static and dynamic sensitivity analysis is discussed in detail.

The sensitivity is defined as the change in the output response of some physical parameter with respect to change in the input parameter. The response of nuclear reactor may be taken as reactor power, reaction rate, production rate of isotopes, ratio of two reaction rates, etc. If ' R ' is the response of reactor, i.e. reactor power, then the sensitivity is estimated by computing the Gateaux [85], [86] differential of the response ' R ' as

$$\delta R = \lim_{t \rightarrow 0} R(\hat{e} + th) - R(\hat{e})$$

In the above equation, \hat{e} is function of flux and cross section and h is a function of perturbed flux and cross section. Following sensitivity, the sensitivity coefficient is defined as the ratio of relative change in the output response to the relative change in the input parameter and it is given as

$$\text{Sensitivity coefficient} = \frac{(\delta R/R)}{(\delta \Sigma/\Sigma)}$$

In the above equation, ' R ' refers to response; the response may be either directly measurable output parameter or any function involving the output parameter and δR refers to change in the output response. In the above equation, ' Σ ' refers to any input parameter and $\delta \Sigma$ is the input uncertainty. For a given model, the change in the response arises due to uncertainty in the input. The sensitivity coefficient may be estimated for many input parameters. Generally the sensitivity is further classified as local sensitivity and global sensitivity. In the case of local sensitivity, it refers to the factors affecting the behaviour of physical system (reactor core) in and around a localized area (confined area) within large system. In the case of global sensitivity it refers to the

factors affecting the complete system behaviour (whole reactor). In the present work the uncertainty and sensitivity analysis is performed with respect to the uncertainties in material properties (macroscopic cross sections) of reactor core and the uncertainties in reactor geometry and dimensions are not considered here. In this work, the local sensitivity is referred to peak mesh power in the reactor and the global sensitivity is referred to reactor power and total peaking factor, i.e. 3D peaking factor (3D PF).

5.2 Types of uncertainty analysis

The uncertainty analysis can be performed using (i) statistical method and (ii) deterministic method. Statistical methods are employed for conducting sensitivity analysis on large computational models. The statistical methods in fact depend on sampling approaches like (a) Simple random sampling (SRS), (b) Stratified importance sampling (c) Latin Hypercube sampling (LHS) [87]-[92]. Statistical methods for sensitivity analysis depend on number of iterations for each random sample. As the number of iterations or executions is large, better accuracy in the output parameter is obtained. Moreover these statistical methods are also subject to some drawbacks [93]. The major bottleneck in statistical methods for sensitivity analysis is that it is computationally expensive for even small systems and therefore they are also found impracticable for large time dependent systems. For time dependent systems, the statistical methods consume large computation time to estimate the results and in such cases deterministic approach is adopted.

In the case of deterministic approach, the exact equation governing the physical systems is solved with uncertainty in the input and the uncertainty in the output is estimated. In

deterministic approach, the following different kinds of methods are adopted for uncertainty analysis:

- (a) Brute Force method
- (b) Adjoint Sensitivity Analysis Procedure (ASAP)
- (c) Forward Sensitivity Analysis Procedure (FSAP)

Both static and dynamic uncertainty analysis can be performed using the above methods. In brute force method, the neutron diffusion equation is solved with perturbed input parameter and the perturbed output parameter is estimated. From the perturbed output parameter (i.e. flux) the uncertainty is estimated. In static (time independent) adjoint sensitivity analysis procedure (ASAP), the uncertainty in the output parameter is directly estimated without calculating the uncertainty in the flux. The static ASAP is the same as the first order perturbation theory [22] in estimating the uncertainty in the output parameter. In forward sensitivity analysis procedure (FSAP), the uncertainty in the input parameter is directly incorporated in the neutron diffusion equation and the uncertainty in the output is estimated. The detailed description of FSAP and ASAP is given by [85].

In this chapter, we first discuss the time-independent (static) uncertainty and sensitivity analysis using brute force method, ASAP and FSAP briefly. We then discuss the development of a new computational method to estimate the dynamic (time dependent) uncertainty in reactor transient by incorporating the improved quasi static (IQS) model with FSAP. From dynamic uncertainty, we perform the dynamic sensitivity analysis of reactor transients. The dynamic sensitivity analysis is performed for (i) 3D homogeneous reactor transient and (ii) 3D TWIGL

benchmark reactor transient. The above reactors are described in chapter 4. Both static (time independent) and dynamic sensitivity analyses are performed for the above mentioned reactors.

In the case of static sensitivity analysis, the uncertainty in the multiplication factor (k_{eff}), for various levels of uncertainties in the macroscopic cross sections (input parameters) is analyzed. It is observed that the sensitivity coefficient varies linearly with the uncertainty in the macroscopic cross section in the range 0.05%-0.5%. It is also observed that the more influential factor in affecting the multiplication factor is found to be the thermal fission cross section for the above mentioned reactors.

The dynamic sensitivity analysis is performed, for the above mentioned reactors, using FSAP. The uncertainty in the output parameter (i.e. flux) can be estimated by solving the FSAP directly (FSAP-direct) or by incorporating the IQS model in it (FSAP+IQS). In the case of dynamic sensitivity analysis, both local and global dynamic sensitivity analysis is performed for various levels of uncertainties in the input parameters (macroscopic cross sections). In the case of local dynamic sensitivity analysis, the sensitivity of peak mesh power with respect to uncertainty in cross sections is estimated. In the case of global dynamic sensitivity analysis, the sensitivity of reactor power and total peaking factor (3D Peaking Factor) is estimated. It is observed that in the case of dynamic sensitivity analysis in 3D homogeneous reactor, the uncertainty in total peaking factor is very small as the transient evolves with time. It is also observed to be true in the case of 3D TWIGL reactor. Since the results of dynamic sensitivity analysis are not available for the above mentioned reactors in the literature, the dynamic sensitivity analysis is also performed by directly solving the neutron diffusion equation with uncertainty (FSAP-direct) for the above mentioned reactors and the results are compared. For this first we quantify that the error between the two methods (FSAP + IQS model and FSAP-

direct) is negligible. To quantify this, the transients (without any uncertainty in cross sections) in the above mentioned reactors were estimated by the two methods and the relative error between the methods was found to be less than 0.2%. Since the relative error was found to be small ($< 0.2\%$), the two methods are considered to be similar. Hence any uncertainty that arises in the output is considered to be entirely due to the uncertainty in the input parameters (cross sections). The uncertainty and the sensitivity coefficient obtained using the FSAP with IQS model is found to be in good agreement with that of direct solution method (FSAP-direct). The dynamic uncertainty analysis using direct solution method is highly time consuming. On the other hand, the FSAP with IQS model is found to be less time consuming and this method serves as one of the fastest ways to perform the dynamic sensitivity analysis in transient with good accuracy. It is shown that the FSAP with IQS model can be used with large time step to perform the dynamic sensitivity analysis in reactor transients. This method can be simultaneously applied to perform the sensitivity analysis along with the transient estimation. The simultaneous estimation of reactor transient and its uncertainty is discussed in the following section.

5.3 Brute Force Method

It is a direct method of estimating the uncertainty and sensitivity. Both static and dynamic uncertainty can be estimated using this method. Here a direct solution of the equation governing the physical system with perturbation in the input parameter is obtained. The equation, governing the physical system, has to be solved with perturbation in the input. From the solution, the uncertainty and the sensitivity of the desired parameter can be estimated. Multiple perturbations in the input parameters can also be used here. Consider the time independent neutron diffusion equation (two-group, the constants carry usual meaning)

$$D_1 \nabla^2 \varphi_1 - \Sigma_{a1} \varphi_1 - \Sigma_{1 \rightarrow 2} \varphi_1 + \left(\frac{1}{k_{eff}} \right) (\nu \Sigma_{f1} \varphi_1 + \nu \Sigma_{f2} \varphi_2) = 0 \quad (5.1)$$

$$D_2 \nabla^2 \varphi_2 - \Sigma_{a2} \varphi_2 + \Sigma_{1 \rightarrow 2} \varphi_1 = 0 \quad (5.2)$$

In matrix form, the above equations (Eqs.(5.1) & (5.2)) are written as

$$\hat{A} \varphi = \frac{1}{k_{eff}} \hat{F} \varphi \quad (5.3)$$

\hat{A} is the neutron destruction operator, \hat{F} is the neutron production operator and k_{eff} is the eigen value. In the present case, our interest is that if some input parameter (macroscopic absorption or fission cross section) is perturbed, how it is affecting the multiplication factor (k_{eff}). With perturbed input parameter, (i.e. $\Sigma_{a1} \rightarrow \Sigma'_{a1}$) the resulting neutron diffusion equation is written as

$$\hat{A}' \varphi' = \frac{1}{k'_{eff}} \hat{F}' \varphi' \quad (5.4)$$

where \hat{A}' contains the perturbed input parameters (cross sections, $\hat{A}' = \hat{A} + \Delta \hat{A}$), \hat{F}' contains perturbed fission cross sections ($\hat{F}' = \hat{F} + \Delta \hat{F}$), φ' is the perturbed flux ($\varphi' = \varphi + \Delta \varphi$) and k'_{eff} is the new eigen value ($k'_{eff} = k_{eff} + \Delta k_{eff}$). Solution of Eq. (5.4), will give new k'_{eff} and the uncertainty in the multiplication factor can be estimated. The brute force method is applied to estimate the static uncertainty and sensitivity coefficient in 3D homogenous reactor as well as in 3D TWIGL benchmark reactor. Consider the 3D Homogeneous reactor in steady state condition. The detailed description of 3D homogeneous reactor is given in chapter 4. Here the uncertainty in the input parameters, D_1 , D_2 , Σ_{a1} , Σ_{a2} , $\Sigma_{1 \rightarrow 2}$ etc. is assumed to be 0.1% and the uncertainty in the eigen value is estimated. It is to be noted here that the uncertainty in the cross section is applied throughout the reactor. The sensitivity coefficient is calculated as

$$\text{Sensitivity coefficient} = \frac{\left(\frac{\Delta keff}{keff}\right)}{\left(\frac{\Delta \Sigma}{\Sigma}\right)}. \text{ The sensitivity coefficients of } keff \text{ are calculated for}$$

different macroscopic cross sections with 0.1% uncertainty and the results are given in Table 5.1a. The sensitivity coefficient, when the perturbation is negative, i.e. -0.1% is shown within the parenthesis in Table 5.1a. It is to be noted that whether the perturbation is positive or negative, keeping the magnitude same, the sensitivity coefficient almost remains constant.

It is observed from Table 5.1a that the thermal fission cross section ($v\Sigma_{f2}$) is more influential in affecting the eigen value ($keff$) and the second more influential factor affecting the eigen value is found to be the thermal absorption cross section (Σ_{a2}). This fact remains true as the uncertainty in the input is varied from 0.05% to 0.5%.

Table 5.1a. Uncertainty in $keff$ and the sensitivity coefficient for 3D Homogenous reactor

S.N	Parameter	Uncertainty	Brute Force $\frac{\Delta keff}{keff}$ (%)	Sensitivity coefficient
1	$\frac{\Delta D_1}{D_1}$	0.1% (-0.1%)	2.122E-2 (2.124E-2)	0.212 (0.212)
2	$\frac{\Delta D_2}{D_2}$	0.1% (-0.1%)	1.083E-2 (1.089E-2)	0.108 (0.108)
3	$\frac{\Delta \Sigma_{a1}}{\Sigma_{a1}}$	0.1% (-0.1%)	2.952E-2 (2.954E-2)	0.295 (0.295)
4	$\frac{\Delta \Sigma_{a2}}{\Sigma_{a2}}$	0.1% (-0.1%)	7.521E-2 (7.518E-2)	0.752 (0.751)
5	$\frac{\Delta(v\Sigma_{f1})}{v\Sigma_{f1}}$	0.1% (-0.1%)	1.386E-2 (1.386E-2)	0.138 (0.138)
6	$\frac{\Delta(v\Sigma_{f2})}{v\Sigma_{f2}}$	0.1% (-0.1%)	8.602E-2 (8.602E-2)	0.860 (0.860)
7	$\frac{\Delta \Sigma_{12}}{\Sigma_{12}}$	0.1% (-0.1%)	3.678E-2 (3.681E-2)	0.367 (0.368)

The uncertainty in the input parameters, D_1 , D_2 , Σ_{a1} , Σ_{a2} , and $\Sigma_{1 \rightarrow 2}$ is varied from 0.05% to 0.5% for the 3D homogeneous reactor and the sensitivity coefficient is estimated using Brute force method. The linear fit relating the sensitivity coefficient $\left(S(k_{eff}, \Sigma) = \frac{\left(\frac{\Delta k_{eff}}{k_{eff}} \right)}{\left(\frac{\Delta \Sigma}{\Sigma} \right)} \right)$ and the uncertainty in the input parameter is given below (Eq. 5.5a-5.5g). The constants in the linear fit are estimated by least square error minimization technique.

$$S(k_{eff}, D_1) = 0.21209 + (0.1714) * \left(\frac{\Delta D_1}{D_1} \right), \left[0.05\% \leq \left(\frac{\Delta D_1}{D_1} \right) \leq 0.5\% \right] \quad (5.5a)$$

$$S(k_{eff}, D_2) = 0.10866 + (0.0960) * \left(\frac{\Delta D_2}{D_2} \right), \left[0.05\% \leq \left(\frac{\Delta D_2}{D_2} \right) \leq 0.5\% \right] \quad (5.5b)$$

$$S(k_{eff}, \Sigma_{a1}) = 0.2957 + (0.2166) * \left(\frac{\Delta \Sigma_{a1}}{\Sigma_{a1}} \right), \left[0.05\% \leq \left(\frac{\Delta \Sigma_{a1}}{\Sigma_{a1}} \right) \leq 0.5\% \right] \quad (5.5c)$$

$$S(k_{eff}, \Sigma_{a2}) = 0.7519 + (0.1507) * \left(\frac{\Delta \Sigma_{a2}}{\Sigma_{a2}} \right), \left[0.05\% \leq \left(\frac{\Delta \Sigma_{a2}}{\Sigma_{a2}} \right) \leq 0.5\% \right] \quad (5.5d)$$

$$S(k_{eff}, v\Sigma_{f1}) = 0.1393 + (0.1374) * \left(\frac{\Delta v\Sigma_{f1}}{v\Sigma_{f1}} \right), \left[0.05\% \leq \left(\frac{\Delta v\Sigma_{f1}}{v\Sigma_{f1}} \right) \leq 0.5\% \right] \quad (5.5e)$$

$$S(k_{eff}, v\Sigma_{f2}) = 0.8606 + (0.78705) * \left(\frac{\Delta v\Sigma_{f2}}{v\Sigma_{f2}} \right), \left[0.05\% \leq \left(\frac{\Delta v\Sigma_{f2}}{v\Sigma_{f2}} \right) \leq 0.5\% \right] \quad (5.5f)$$

$$S(k_{eff}, \Sigma_{12}) = 0.3684 + (0.1734) * \left(\frac{\Delta \Sigma_{12}}{\Sigma_{12}} \right), \left[0.05\% \leq \left(\frac{\Delta \Sigma_{12}}{\Sigma_{12}} \right) \leq 0.5\% \right] \quad (5.5g)$$

The variation of sensitivity coefficient with the uncertainty in the thermal absorption cross section and thermal fission cross section are shown in Figs. 5.1 and 5.2 respectively.

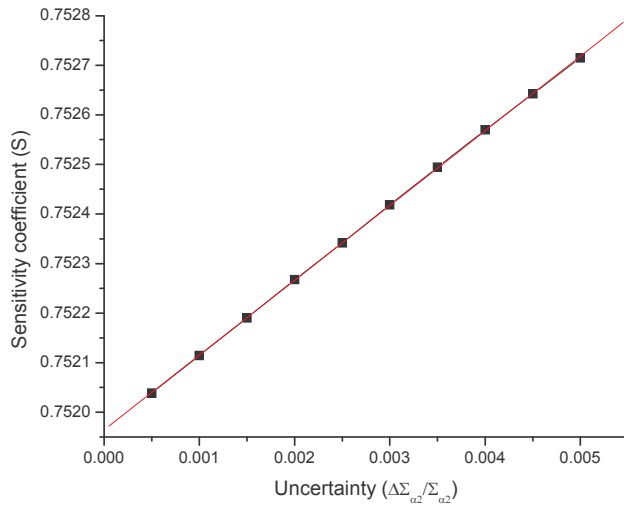


Fig. 5.1 The variation of sensitivity coefficient with uncertainty in Σ_{a2} for 3D homogeneous reactor. The linear fit is given as $S = 0.7519 + (0.1507) * \left(\frac{\Delta\Sigma_{a2}}{\Sigma_{a2}}\right), \left[0.05\% \leq \left(\frac{\Delta\Sigma_{a2}}{\Sigma_{a2}}\right) \leq 0.5\%\right]$

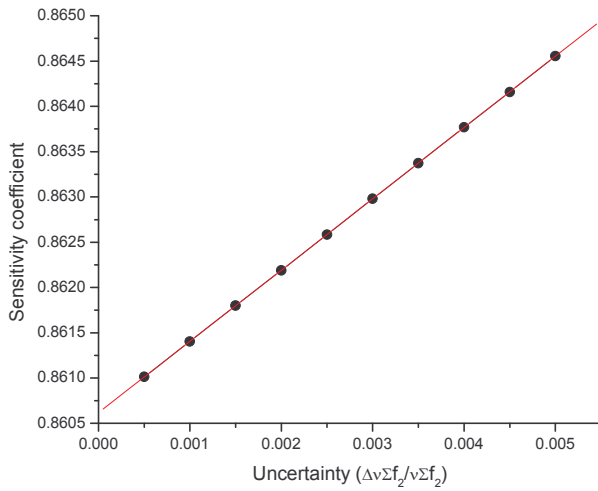


Fig. 5.2. The variation of sensitivity coefficient with uncertainty in $\nu\Sigma_{f2}$ for 3D homogeneous reactor. The linear fit is given as $S = 0.8606 + (0.78705) * \left(\frac{\Delta\nu\Sigma_{f2}}{\nu\Sigma_{f2}}\right), \left[0.05\% \leq \left(\frac{\Delta\nu\Sigma_{f2}}{\nu\Sigma_{f2}}\right) \leq 0.5\%\right]$

As a second example, consider the 3D TWIGL benchmark reactor. Its description is given in chapter 4. It is a two-group neutron problem. Here also the uncertainty in the input parameters D_1 , D_2 , Σ_{a1} , Σ_{a2} , and $\Sigma_{1 \rightarrow 2}$ is assumed to be 0.1%. The uncertainty is applied throughout the reactor. For 0.1% uncertainty in the input, the uncertainty in the eigen value ($keff$) and the sensitivity coefficient are estimated and they are given in Table 5.1b. The sensitivity coefficient, when the perturbation is -0.1% is also given in Table 5.1b within the parenthesis. It is to be noted that whether the perturbation is positive or negative, keeping the magnitude same, the sensitivity coefficient almost remains constant.

Table 5.1b. Uncertainty in $keff$ and sensitivity coefficient for 3D TWIGL reactor

S.N	Parameter	Uncertainty	Brute Force $\frac{\Delta keff}{keff} (\%)$	Sensitivity coefficient
1	$\frac{\Delta D_1}{D_1}$	0.1% (-0.1%)	8.584E-3 (8.66E-3)	8.584E-2 (8.66E-2)
2	$\frac{\Delta D_2}{D_2}$	0.1% (-0.1%)	1.008E-4 (2.57E-4)	1.008E-3 (2.57E-3)
3	$\frac{\Delta \Sigma_{a1}}{\Sigma_{a1}}$	0.1% (-0.1%)	4.433E-2 (4.45E-4)	0.443 (0.445)
4	$\frac{\Delta \Sigma_{a2}}{\Sigma_{a2}}$	0.1% (-0.1%)	6.837E-2 (6.855E-2)	0.683 (0.6855)
5	$\frac{\Delta(v\Sigma_{f1})}{v\Sigma_{f1}}$	0.1% (-0.1%)	3.146E-2 (3.12E-2)	0.314 (0.312)
6	$\frac{\Delta(v\Sigma_{f2})}{v\Sigma_{f2}}$	0.1% (-0.1%)	6.865E-2 (6.857E-4)	0.686 (0.6857)
7	$\frac{\Delta \Sigma_{12}}{\Sigma_{12}}$	0.1% (-0.1%)	2.166E-2 (2.16E-2)	0.216 (0.216)

It is observed from Table 5.1b that the thermal fission cross section is more influential in affecting the eigen value (k_{eff}) and the second more influential factor affecting the eigen value is found to be the thermal absorption cross section.

The sensitivity analysis was carried out for 3D TWIGL heterogeneous reactor by varying the uncertainty in D_1 , D_2 , Σ_{a1} , Σ_{a2} , $\Sigma_{1 \rightarrow 2}$, etc. from 0.05% to 0.5%. The sensitivity analysis was carried out using Brute force method and the variation of sensitivity coefficient with the uncertainty in the input parameter is given below (Eq. 5.6a-5.6g).

$$S(k_{eff}, D_1) = 0.08567 + (0.0694) * \left(\frac{\Delta D_1}{D_1}\right), \quad \left[0.05\% \leq \left(\frac{\Delta D_1}{D_1}\right) \leq 0.5\%\right] \quad (5.6a)$$

$$S(k_{eff}, D_2) = 0.0017 + (0.00198) * \left(\frac{\Delta D_2}{D_2}\right), \quad \left[0.05\% \leq \left(\frac{\Delta D_2}{D_2}\right) \leq 0.5\%\right] \quad (5.6b)$$

$$S(k_{eff}, \Sigma_{a1}) = 0.4444 + (0.2324) * \left(\frac{\Delta \Sigma_{a1}}{\Sigma_{a1}}\right), \quad \left[0.05\% \leq \left(\frac{\Delta D_2}{D_2}\right) \leq 0.5\%\right] \quad (5.6c)$$

$$S(k_{eff}, \Sigma_{a2}) = 0.6845 - (0.0341) * \left(\frac{\Delta \Sigma_{a2}}{\Sigma_{a2}}\right), \quad \left[0.05\% \leq \left(\frac{\Delta D_2}{D_2}\right) \leq 0.5\%\right] \quad (5.6d)$$

$$S(k_{eff}, \nu \Sigma_{f1}) = 0.3137 + (0.3248) * \left(\frac{\Delta \nu \Sigma_{f1}}{\nu \Sigma_{f1}}\right), \quad \left[0.05\% \leq \left(\frac{\Delta \nu \Sigma_{f1}}{\nu \Sigma_{f1}}\right) \leq 0.5\%\right] \quad (5.6e)$$

$$S(k_{eff}, \nu \Sigma_{f2}) = 0.6862 + (0.7230) * \left(\frac{\Delta \nu \Sigma_{f2}}{\nu \Sigma_{f2}}\right), \quad \left[0.05\% \leq \left(\frac{\Delta \nu \Sigma_{f2}}{\nu \Sigma_{f2}}\right) \leq 0.5\%\right] \quad (5.6f)$$

$$S(k_{eff}, \Sigma_{12}) = 0.2163 + (0.1182) * \left(\frac{\Delta \Sigma_{12}}{\Sigma_{12}}\right), \quad \left[0.05\% \leq \left(\frac{\Delta \nu \Sigma_{f2}}{\nu \Sigma_{f2}}\right) \leq 0.5\%\right] \quad (5.6g)$$

The variation of sensitivity coefficient with the uncertainty in the fast fission cross section and thermal fission cross section are shown in Figs. 5.3 and 5.4 respectively.

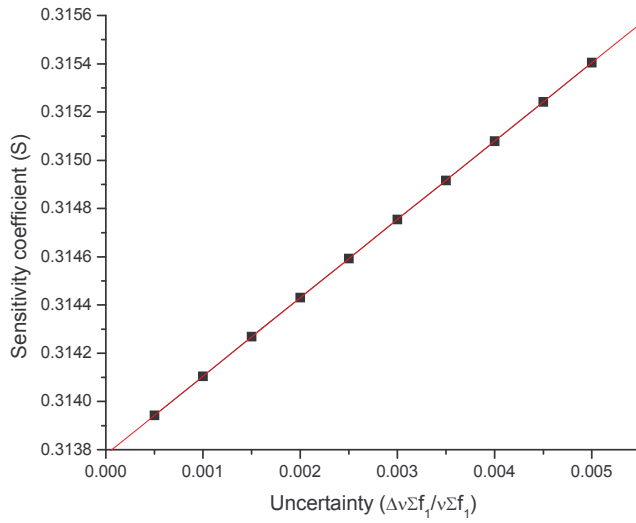


Fig. 5.3. The variation of sensitivity coefficient with $\frac{\Delta v\Sigma_{f1}}{v\Sigma_{f1}}$ for 3D TWIGL reactor. The linear fit

is given as $S = 0.3137 + (0.3248) * \left(\frac{\Delta v\Sigma_{f1}}{v\Sigma_{f1}}\right), \left[0.05\% \leq \left(\frac{\Delta v\Sigma_{f1}}{v\Sigma_{f1}}\right) \leq 0.5\%\right]$

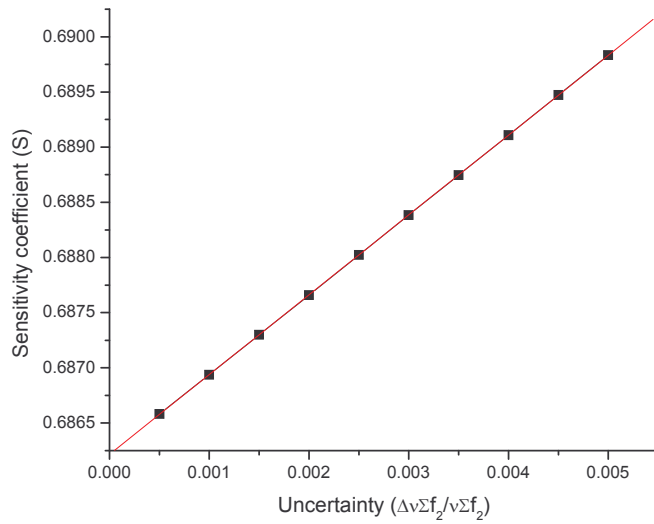


Fig. 5.4 The variation of sensitivity coefficient with $\frac{\Delta v\Sigma_{f2}}{v\Sigma_{f2}}$ for 3D TWIGL reactor. The linear fit is

given as $S = 0.6862 + (0.7230) * \left(\frac{\Delta v\Sigma_{f2}}{v\Sigma_{f2}}\right), \left[0.05\% \leq \left(\frac{\Delta v\Sigma_{f2}}{v\Sigma_{f2}}\right) \leq 0.5\%\right]$

5.4 Static Adjoint Sensitivity Analysis Procedure (ASAP)

In static ASAP, the uncertainty in the output parameter can be directly estimated without calculating the uncertainty in the flux, i.e. $\Delta\varphi_1$ and $\Delta\varphi_2$ (two-group neutron energy). This method is the same as the first order perturbation theory. To estimate the uncertainty in the output parameter, we solve the adjoint diffusion equation and estimate the adjoint flux. Consider the adjoint neutron diffusion equation (for the unperturbed system)

$$\hat{A}^\dagger \varphi^\dagger = \frac{1}{k_{eff}} \hat{F}^\dagger \varphi^\dagger \quad (5.7)$$

where \hat{A}^\dagger is the adjoint operator for \hat{A} and φ^\dagger is the adjoint flux. Now introducing the uncertainties in the operators and following the inner product notation, we get the neutron diffusion equation as (using Eqs. (5.3) & (5.4))

$$\langle \varphi^\dagger, (\hat{A} + \Delta\hat{A})(\varphi + \Delta\varphi) \rangle = \frac{1}{k_{eff} + \Delta k_{eff}} \langle \varphi^\dagger, (\hat{F} + \Delta\hat{F})(\varphi + \Delta\varphi) \rangle \quad (5.8)$$

$$\langle \varphi^\dagger, (\hat{A}\varphi + \hat{A}\Delta\varphi + \Delta\hat{A}\varphi + \Delta\hat{A}\Delta\varphi) \rangle = \frac{1}{k_{eff} + \Delta k_{eff}} \langle \varphi^\dagger, (\hat{F}\varphi + \hat{F}\Delta\varphi + \Delta\hat{F}\varphi + \Delta\hat{F}\Delta\varphi) \rangle \quad (5.8a)$$

Keeping only first order terms, the above equation (Eq. (5.8a)) can be re-written as

$$\langle \varphi^\dagger, (\Delta\hat{A})\varphi \rangle = \frac{1}{k_{eff}} \langle \varphi^\dagger, (\Delta\hat{F})\varphi \rangle + \left(-\frac{\Delta k_{eff}}{k_{eff}^2} \right) \langle \varphi^\dagger, (\hat{F})\varphi \rangle \quad (5.9a)$$

Eq. (5.9a) can be further simplified as

$$\langle \varphi, (\Delta\hat{A}^\dagger)\varphi^\dagger \rangle = \frac{1}{k_{eff}} \langle \varphi, (\Delta\hat{F}^\dagger)\varphi^\dagger \rangle + \left(-\frac{\Delta k_{eff}}{k_{eff}^2} \right) \langle \varphi, (\hat{F}^\dagger)\varphi^\dagger \rangle \quad (5.9b)$$

From Eq. (5.9b) the uncertainty in the multiplication factor is computed as

$$\frac{\Delta k_{eff}}{k_{eff}} = \frac{\langle \varphi, (\Delta\hat{A}^\dagger)\varphi^\dagger \rangle - \frac{1}{k_{eff}} \langle \varphi, (\Delta\hat{F}^\dagger)\varphi^\dagger \rangle}{\frac{1}{k_{eff}} \langle \varphi, (\hat{F}^\dagger)\varphi^\dagger \rangle} \quad (5.10)$$

and the sensitivity coefficient of multiplication factor with respect to input parameter Σ is computed as

$$S(k_{eff}, \Sigma) = \frac{\frac{\Delta k_{eff}}{k_{eff}}}{\frac{\Delta \Sigma}{\Sigma}} = \Sigma \left(\frac{\langle \varphi, \left(\frac{\Delta \hat{A}^\dagger}{\Delta \Sigma} \right) \varphi^\dagger \rangle - \frac{1}{k_{eff}} \langle \varphi, \left(\frac{\Delta \hat{F}^\dagger}{\Delta \Sigma} \right) \varphi^\dagger \rangle}{\frac{1}{k_{eff}} \langle \varphi, (\hat{F}^\dagger)\varphi^\dagger \rangle} \right) \quad (5.11)$$

The uncertainties in the cross section are absorbed in the operators $\Delta\hat{A}$ and $\Delta\hat{F}$. In Eq. (5.11), the known quantities are \hat{A} , $\Delta\hat{A}$, $\Delta\hat{F}$, \hat{F} , φ and φ^\dagger . It is to be noted here that the uncertainty Δk_{eff} is estimated without the requirement of $\Delta\varphi$.

5.5 Forward Sensitivity Analysis Procedure (FSAP)

In Forward Sensitivity Analysis Procedure (FSAP), the uncertainty in the input parameter is directly incorporated in the neutron diffusion equation and the uncertainty in the output is directly estimated. Consider the time independent neutron diffusion equations (5.1) and (5.2). Here the uncertainty in the input parameter is defined as $\Sigma \rightarrow \Sigma_0 + \Delta\Sigma$ and it is introduced in the neutron diffusion equation. Σ_0 represents the unperturbed cross section and $\Delta\Sigma$ represents the uncertainty in the cross section. Here the neutron diffusion equation is split into unperturbed part and perturbed part and it is written as

$$(\hat{A} + \Delta\hat{A})(\varphi + \Delta\varphi) = \frac{1}{k_{eff} + \Delta k_{eff}}(\hat{F} + \Delta\hat{F})(\varphi + \Delta\varphi) \quad (5.12)$$

In the above equation, \hat{A} is the unperturbed removal operator, \hat{F} is the unperturbed production operator, $\Delta\hat{A}$ and $\Delta\hat{F}$ are the perturbed operators, φ is the unperturbed flux, $\Delta\varphi$ is the perturbed flux and Δk_{eff} is uncertainty in k_{eff} . The solution of Eq. (5.12) will give the uncertainty in the output parameter, i.e. Δk_{eff} and the uncertainty in the flux, $\Delta\varphi$. Both time independent and time dependent uncertainty and sensitivity analysis can be performed using this method. Detailed description of time independent FSAP can be found in [85]. The time dependent uncertainty in the neutron flux, caused by uncertainty in the input parameters (macroscopic cross sections) is estimated by solving the time dependent neutron diffusion equation with uncertainties. Here we

make use of the improved quasi static (IQS) scheme for solving the uncertainty in the flux. The details are discussed in the following section.

5.6 Dynamic uncertainty and sensitivity analysis in reactor transient - Forward Sensitivity Analysis Procedure (FSAP) with IQS method

In this section we first discuss the dynamic (time-dependent) uncertainty in reactor transient. We then discuss the development of a new computational method to estimate the dynamic (time dependent) uncertainty and perform the associated sensitivity analysis in reactor transients by incorporating the IQS method in FSAP. The uncertainty in the input parameter may propagate with time and it may affect the reactor core power, peak mesh power, peaking factor etc. during transient which in turn may affect the safety factors. The sensitivity coefficient estimated in the static case (time independent) may not remain constant during the reactor transient. Hence for safe operation of nuclear reactor, it is essential to do the dynamic uncertainty and sensitivity analysis during transient and evaluate the safety factors. Based on the results of dynamic sensitivity analysis, the safety margins must be fixed. A direct solution of time-dependant neutron diffusion equation, with uncertainty in the input parameters, will give the uncertainty in the flux. But the direct solution of neutron diffusion equation will consume more time and one will encounter large round-off and truncation errors. Unless the time step is chosen very small, one may encounter stability issues in the solution. To overcome this difficulty, we develop a new computational method by incorporating the improved quasi static (IQS) method in FSAP and perform dynamic uncertainty and sensitivity analysis in reactor transient. For this we solve the time-dependent neutron diffusion equation with uncertainty using the IQS method. The solution of FSAP with IQS method will give the dynamic uncertainty in the flux. Using this computational method the dynamic uncertainty and sensitivity analysis can be performed in a

much faster way with good accuracy. Consider the following time independent neutron diffusion equation (in operator form)

$$\hat{A}_0 \varphi_0 = \frac{1}{k_0} \hat{F}_0 \varphi_0 \quad (5.13)$$

\hat{A}_0 is the unperturbed neutron removal operator, \hat{F}_0 is the unperturbed neutron production operator and φ_0 is the unperturbed neutron flux. Now small uncertainties are introduced in the removal and production operators and the perturbed neutron diffusion equation (time independent) is given as

$$\hat{A}' \varphi' = \frac{1}{k_0 + \Delta k} \hat{F}' \varphi' \quad (5.14)$$

where $\hat{A}' = \hat{A}_0 + \Delta A$, $\hat{F}' = \hat{F}_0 + \Delta F$, $\varphi' = \varphi_0 + \delta\varphi$, ΔA is the perturbation in the removal operator, ΔF is the perturbation in the production operator, $\delta\varphi$ is the uncertainty in the flux and Δk is the perturbation in k_0 . Let P_0 be the power in the unperturbed state and $P_0 + \Delta P$ be the power in the perturbed state, ΔP being the uncertainty in power. Subtracting Eq. (5.13) from Eq. (5.14), the dynamic uncertainty in the flux can be written as (two-group neutron energy, $k_0 = 1$, $\Delta k \ll 1$ and Δk is neglected)

$$\begin{aligned} \frac{1}{v_1} \frac{\partial(\delta\varphi_1)}{\partial t} = & (\delta D_1) \nabla^2 \varphi_1 + D_1 \nabla^2(\delta\varphi_1) - (\delta \Sigma_{a1}) \varphi_1 - \Sigma_{a1}(\delta\varphi_1) - (\delta \Sigma_{1 \rightarrow 2}) \varphi_1 - \Sigma_{1 \rightarrow 2}(\delta\varphi_1) + \\ & (1 - \beta) \chi_g^p ((\delta v \Sigma_{f1}) \varphi_1 + v \Sigma_{f1}(\delta\varphi_1) + (\delta v \Sigma_{f2}) \varphi_2 + v \Sigma_{f2}(\delta\varphi_2)) + (-\delta\beta) \chi_g^p (v \Sigma_{f1} \varphi_1 + \\ & v \Sigma_{f2} \varphi_2) + \sum_i \chi_{d,i}^g (\delta \lambda_i) C_i + \sum_i \chi_{d,i}^g \lambda_i (\delta C_i) \end{aligned} \quad (5.15)$$

$$\frac{1}{v_2} \frac{\partial(\delta\varphi_2)}{\partial t} = (\delta D_2) \nabla^2 \varphi_2 + D_2 \nabla^2(\delta\varphi_2) - (\delta \Sigma_{a2}) \varphi_2 - \Sigma_{a2}(\delta\varphi_2) + (\delta \Sigma_{1 \rightarrow 2}) \varphi_1 + \Sigma_{1 \rightarrow 2}(\delta\varphi_1) \quad (5.16)$$

$$\frac{\partial(\delta C_i)}{\partial t} = \beta_i((\delta v \Sigma_{f1})\varphi_1 + v \Sigma_{f1}(\delta \varphi_1) + (\delta v \Sigma_{f2})\varphi_2 + v \Sigma_{f2}(\delta \varphi_2)) + \delta \beta_i(v \Sigma_{f1}\varphi_1 + v \Sigma_{f2}\varphi_2) - \lambda_i \delta C_i - \delta \lambda_i C_i \quad (5.16a)$$

The constants, $D_1, \Sigma_{a1}, \Sigma_{a2}, \beta, \lambda_i$ etc. in the above equations carry usual meaning and they correspond to unperturbed state. χ_g^p denotes the fast neutron spectrum in the energy group ' g ' and $\chi_{d,i}^g$ denotes the delayed neutron spectrum in the energy group ' g ' for the i^{th} precursor. The time dependent uncertainty in the fast and thermal flux are denoted as $\delta \varphi_1$ and $\delta \varphi_2$. The uncertainties in the input parameters are denoted as $\delta D_1, \delta \Sigma_{a1}, \delta \Sigma_{a2}, \delta \beta, \delta \lambda_i$ etc. and φ_1 and φ_2 are the unperturbed fast and thermal flux. Equations (5.15) and (5.16) represent the time evolution of the uncertainty in flux. Eqs. (5.15)-(5.16a) represent the FSAP to estimate the dynamic uncertainty in the flux. As described earlier, Eqs. (5.15)-(5.16a) can be solved either directly (FSAP-direct) or by making use of IQS scheme (FSAP+IQS). Here Eqs. (5.15)-(5.16a) are solved subject to the following conditions: it is assumed that the uncertainties in the input parameters ($\delta D_1, \delta D_2, \delta \Sigma_{a1}, \delta \Sigma_{1 \rightarrow 2}$ etc.) come into effect only during the transient and under steady state conditions their effect is negligible. It is also assumed that the uncertainty in the neutron velocity is zero.

Eqs. (5.15) - (5.16a) can be solved, subject to the above conditions, if the initial uncertainty in the flux ($\delta \varphi|_{t=0}$) is known. The initial uncertainty in the flux ($\delta \varphi|_{t=0}$) can be obtained in many ways. But here the initial uncertainty in the flux ($\delta \varphi|_{t=0}$) is obtained from the initial uncertainty in the steady state power. The initial uncertainty in the steady state power is assumed to be 1% of initial power. The dynamic uncertainty in the fast flux and the thermal flux are written as (using IQS method)

$$\delta \varphi_1 = \psi_1(\delta T) + (\delta \psi_1)T \quad (5.17)$$

$$\delta\varphi_2 = \psi_2(\delta T) + (\delta\psi_2)T \quad (5.18)$$

In the above equation, T is the amplitude function, ψ is the shape function corresponding to unperturbed state, δT & $\delta\psi$ are independent unknown quantities which are to be determined. The uncertainty in the flux can be uniquely determined from the knowledge of either δT or $\delta\psi$ or both. For the sake of simplicity we assume $\delta\psi_1 = \delta\psi_2 = 0$ and hence the Eqs. (5.17) and (5.18) can be written as

$$\delta\varphi_1 = \psi_1(t)(\delta T) \quad (5.19)$$

$$\delta\varphi_2 = \psi_2(t)(\delta T) \quad (5.20)$$

Differentiating Eqs. (5.19) & (5.20) we get

$$\frac{\partial}{\partial t}(\delta\varphi_1) = \left(\frac{\partial}{\partial t}\psi_1(t)\right)\delta T + \left(\frac{d}{dt}(\delta T)\right)\psi_1(t) \quad (5.20a)$$

$$\frac{\partial}{\partial t}(\delta\varphi_2) = \left(\frac{\partial}{\partial t}\psi_2(t)\right)\delta T + \left(\frac{d}{dt}(\delta T)\right)\psi_2(t) \quad (5.20b)$$

Since $\frac{\partial\psi_1}{\partial t}$ is slowly varying with time (in the IQS method) and δT is small, the factors $\left(\frac{\partial\psi_1}{\partial t}\right) * \delta T$ and $\left(\frac{\partial\psi_2}{\partial t}\right) * \delta T$ are neglected. Hence Eqs. (5.20a) and (5.20b) are re-written as

$$\frac{\partial}{\partial t}(\delta\varphi_1) = \left(\frac{d}{dt}(\delta T)\right)\psi_1(t) \quad (5.20c)$$

$$\frac{\partial}{\partial t}(\delta\varphi_2) = \left(\frac{d}{dt}(\delta T)\right)\psi_2(t) \quad (5.20d)$$

Substituting Eqs. (5.19)-(5.20d) in Eqs. (5.15), (5.16) & (5.16a) and following the improved quasi static (IQS) method, described in chapter 2, we get a new kind of point kinetics equation, for calculating the uncertainty δT , as

$$\frac{d(\delta T)}{dt} = \left(\frac{\rho - \beta}{\Lambda} \right) \delta T + \sum_i \chi_d^i \lambda_i (\delta C_i) + \left[\left(\frac{\Delta \rho - \Delta \beta}{\Lambda} \right) T + \sum_i \chi_d^i (\delta \lambda_i) C_i \right] \quad (5.21)$$

$$\frac{d(\delta C_i)}{dt} = \left(\frac{\beta_i}{\Lambda} \right) \delta T - \lambda_i (\delta C_i) + \left[\left(\frac{\delta \beta_i}{\Lambda} \right) T - (\delta \lambda_i) C_i \right] \quad (5.22)$$

In the above Eqn. (5.21) & (5.22) ρ , β , Λ and T carry usual meaning (Eqs. (2.34)-(2.36)) and δT is denoted as the uncertainty in the amplitude function, δC_i is denoted as the uncertainty in the precursor concentration and $\Delta \rho$ and $\Delta \beta$ are given as

$$\Delta \rho = \frac{\langle \psi^\dagger \left(\{ \chi_g^p \} \delta \hat{F} - \delta \hat{L} \right) \psi_g(r, t) \rangle}{\langle \psi^\dagger \left(\{ \chi_g^p \} \hat{F} \right) \psi_g(r, t) \rangle} \quad (5.23)$$

$$\Delta \beta_i = \frac{\langle \psi^\dagger [(\delta \beta_i \hat{F}) + (\beta_i) \delta \hat{F}] \psi_g(r, t) \rangle}{\langle \psi^\dagger \left(\{ \chi_g^p \} \hat{F} \right) \psi_g(r, t) \rangle} \quad (5.24)$$

$$\Delta \beta = \sum_i \Delta \beta_i \quad (5.25)$$

The operators \hat{F} and \hat{L} in Eqs. (5.23) and (5.24) are defined in chapter 2. Equations (5.21) and (5.22) constitute a new kind of point kinetics equation and these equations are solved using the modified ETD method. The solution of Eqs. (5.21) & (5.22) along with the shape function will give the dynamic uncertainty in the fast flux and thermal flux. It is to be noted here that the new kind of point kinetics equations are solved only at macro time steps as described below and it is shown in Fig. 5.5.

5.6.1 Estimation of dynamic uncertainty in flux during transient

At macroscopic times T_0, T_1, T_2 etc. the solution of amplitude function and shape functions (T & Ψ) are made available. At macroscopic times T_0, T_1, T_2 , the solution of new kind of point kinetics equation is solved using the modified exponential time differencing method. The solution will give the uncertainty in the amplitude function, δT . The product of $\psi(t)$ and $\delta T(t)$ will give the uncertainty in the flux, i.e. $\delta\phi(t) = \psi(t)\delta T(t)$ (both fast and thermal, in the case of two group neutron diffusion equation) and the uncertainty in the flux is available at macroscopic times only. Since the time dependent neutron diffusion equation does not contain any feedback with uncertainty, it is sufficient that the dynamic uncertainty in the flux is estimated only at macroscopic times. In this way, the reactor transient as well as the dynamic uncertainty in the flux can be estimated simultaneously using this method. This method does not require any additional computation time for uncertainty estimation because only the new kind of point kinetics equation alone is to be solved (Eqs. (5.21) and (5.22)). This is schematically shown in Fig. 5.5.

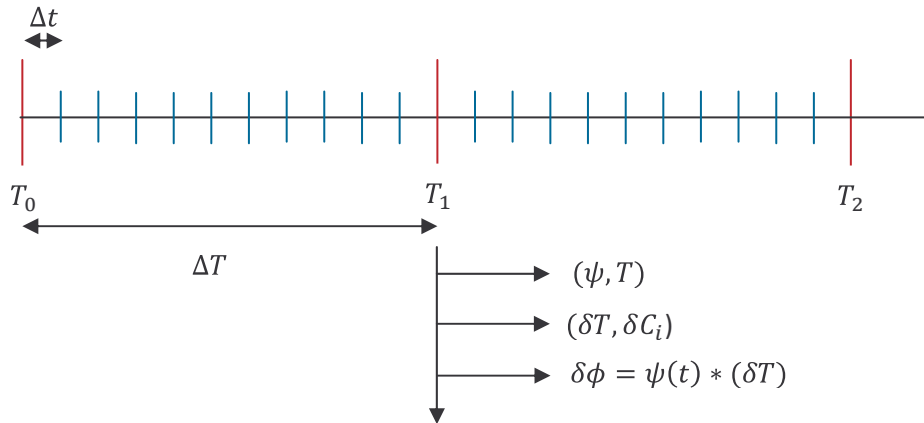


Fig. 5.5 Simultaneous estimation of reactor transient and dynamic uncertainty in flux. Δt denotes the micro time step and ΔT denotes the macro time step.

5.6.2 Dynamic uncertainty and sensitivity analysis in 3D Homogeneous reactor transient

Consider the 3D Homogeneous reactor (chapter 4). The transient in the reactor is created by decreasing the thermal absorption cross section (Eqs. (4.2)-(4.6)). Now small uncertainties are introduced in the macroscopic cross sections and the initial uncertainty in the flux is estimated. Here the uncertainty in core power, during transient, is estimated corresponding to uncertainty in the scattering cross section. One can also estimate the uncertainty in core power with respect to uncertainty in other cross sections. The uncertainty in $\Delta\Sigma_{1\rightarrow 2}$ is assumed to be 0.1%, 0.5% and 1.0%. The dynamic uncertainties in peak mesh power (local dynamic uncertainty), core power and 3D peaking factor, (global dynamic uncertainty) are estimated using FSAP with IQS method as well as with direct solution method. The results are compared.

As described earlier, before comparison of dynamic sensitivity results, it is shown that the error between the methods, FSAP with IQS model and direct solution is very small, i.e. $\leq 0.2\%$. For this, the transient in 3D homogeneous reactor is estimated without any uncertainty in the input parameter and it is given in Table 5.2a. The relative error is also shown. The relative error is found to be $\leq 0.2\%$ and hence the error between the methods is considered to be negligible. The uncertainty in core power during transient, estimated using FSAP with IQS method and direct solution method is given in Table 5.2b. It is observed from Table 5.2b, that the results agree to a good accuracy. The relative error in the estimation of uncertainty, between the two methods, is found to be small. From the comparison of results, it is observed that the new computational method, FSAP with IQS model is capable of estimating the dynamic uncertainty in transient to a good accuracy.

The time evolution of uncertainty in core power is given in Figs. 5.6 for $\Delta\Sigma_{1\rightarrow 2} = 0.1\%$, 0.5% and 1.0%. The dynamic sensitivity coefficient is given in Fig. 5.7. It is observed here that as the uncertainty is increased, the uncertainty in the reactor power increases and the sensitivity coefficient also increases. In a similar manner the uncertainty in the total peaking factor (3D Peaking Factor) is also estimated for various levels of uncertainties and it is given Table 5.3. It is observed that the uncertainty in the total peaking factor (3D peaking factor) is found to be of the order of 1.0E-6.

The uncertainty in the peak mesh power (PMP) is also estimated using the FSAP with IQS model and it is given in Table 5.4. The sensitivity coefficient, for peak mesh power, estimated from FSAP with IQS model and direct solution method agree to a good accuracy.

Table 5.2a Comparison of transients (without uncertainty)

S.N	Time (s)	Core power (Direct Soln.)	Core Power Modified ETD+IQS	% Error between two models
1	0.05	1.564859	1.566676	0.11611
2	0.10	1.952930	1.956036	0.15904
3	0.15	2.303640	2.307676	0.17520
4	0.20	2.621380	2.626111	0.18048
5	0.25	2.910100	2.915305	0.17886
6	0.30	3.173212	3.178775	0.17531

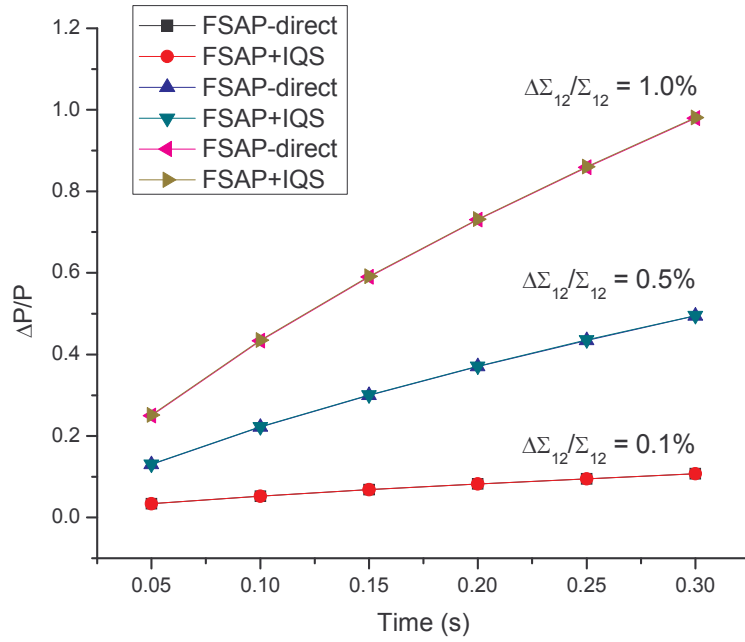


Fig. 5.6 The variation of $\Delta P/P$ with time for the various levels of uncertainty in $\frac{\Delta \Sigma_{12}}{\Sigma_{12}}$.

Table 5.2b. Dynamic uncertainty (%) in core power (global uncertainty) in 3D Homogeneous reactor (Initial power = 1.13444, $\Delta P|_{t=0} = 1.34\text{E-}02$). The uncertainty in core power ($\Delta P/P$) is estimated using FSAP with IQS model and direct solution method. The uncertainties are compared and the percentage error is also shown in the table.

S.N	Parameter	Uncertainty	Time (s)	FSAP (Direct soln.) $\Delta P/P$	FSAP with IQS model $\Delta P/P$	Absolute Error between two models
1	$\frac{\Delta \Sigma_{12}}{\Sigma_{12}}$	0.1%	0.05	3.4005E-02	3.4100E-02	9.5000E-5
			0.10	5.2348E-02	5.2463E-02	1.1500E-4
			0.15	6.7985E-02	6.8122E-02	1.3700E-4
			0.20	8.2005E-02	8.2162E-02	1.5700E-4
			0.25	9.4895E-02	9.5072E-02	1.7700E-4
			0.30	0.1069160	0.1071095	1.9350E-4

2	$\frac{\Delta\Sigma_{12}}{\Sigma_{12}}$	0.5%	0.05	0.1300493	0.1305024	4.5310E-4
			0.10	0.2217723	0.2223161	5.4380E-4
			0.15	0.2999649	0.3006125	6.4760E-4
			0.20	0.3700656	0.3708138	7.4820E-4
			0.25	0.4345179	0.4353645	8.4660E-4
			0.30	0.4946195	0.4955485	9.2900E-4
3	$\frac{\Delta\Sigma_{12}}{\Sigma_{12}}$	1.0%	0.05	0.2501040	0.2510049	9.00900E-4
			0.10	0.4335530	0.4346324	0.0011
			0.15	0.5899397	0.5912250	0.0013
			0.20	0.7301412	0.7316276	0.0015
			0.25	0.8590469	0.8607289	0.0017
			0.30	0.9792493	0.9810973	0.0018

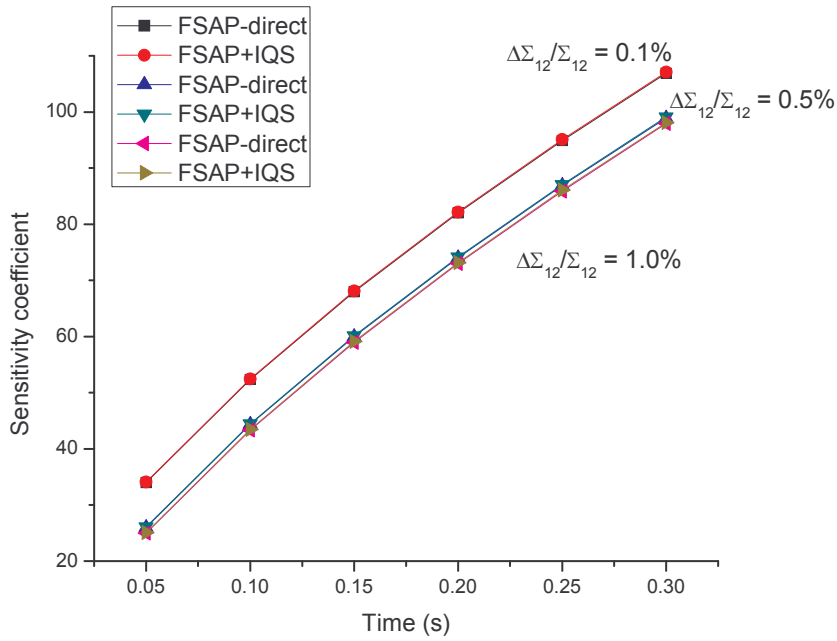


Fig. 5.7 The sensitivity coefficient with time for the various levels of uncertainty in $\frac{\Delta\Sigma_{12}}{\Sigma_{12}}$.

Table 5.3. The uncertainty in total peaking factor (3D peaking factor) for 3D Homogeneous reactor transient for various uncertainties in input parameters. (Initial power = 1.13444, $\Delta P|_{t=0} = 1.134\text{E-}02$)

S.N	Parameter	Uncertainty	Time (s)	FSAP Direct soln. $\frac{\Delta(3DPF)}{3DPF} \%$	FSAP with IQS model $\frac{\Delta(3DPF)}{3DPF} \%$
1	$\frac{\Delta\Sigma_{12}}{\Sigma_{12}}$	0.1%	0.05	1.2315E-06	1.2418E-06
			0.10	1.6561E-06	1.1467E-06
			0.15	3.6077E-06	3.9506E-06
			0.20	2.5665E-06	2.3463E-06
			0.25	2.9704E-06	2.4795E-06
			0.30	4.5458E-06	4.2381E-06
2	$\frac{\Delta\Sigma_{12}}{\Sigma_{12}}$	0.5%	--do--	8.6461E-06	8.8014E-06
				1.2752E-05	1.1595E-05
				1.7258E-06	1.0739E-05
				7.8773E-06	7.7501E-06
				1.2793E-05	1.8185E-05
				6.6591E-06	6.2112E-06
3	$\frac{\Delta\Sigma_{12}}{\Sigma_{12}}$	1.0%	--do--	1.1277E-05	1.6301E-05
				6.3350E-06	6.0000E-06
				2.2395E-05	2.9123E-05
				3.0640E-05	3.2678E-05
				1.2448E-05	1.2366E-05
				1.1670E-05	1.8439E-05

Table 5.4. The uncertainty in peak mesh power (PMP) for 3D Homogeneous reactor for various uncertainties in input parameters. (Initial power = 1.13444, $\Delta P|_{t=0} = 1.134\text{E-}02$))

S.N	Uncertainty in Parameter	Time (s)	FSAP Direct soln. $\frac{\Delta(PMP)}{PMP}$	FSAP with IQS model $\frac{\Delta(PMP)}{PMP}$	Sensitivity Coeff. (FSAP-Direct)	Sensitivity Coeff. FSAP+IQS
1	$\frac{\Delta\Sigma_{12}}{\Sigma_{12}} = 0.1\%$	0.05	3.4005E-2	3.405E-02	34.005	34.05
		0.10	5.2348E-2	5.239E-02	52.348	52.39
		0.15	6.7986E-2	6.803E-02	67.986	68.03
		0.20	8.2005E-2	8.207E-02	82.005	82.07
		0.25	9.4896E-2	9.497E-02	94.896	94.97
		0.30	0.10691	0.1070137	106.91	107.01
2	$\frac{\Delta\Sigma_{12}}{\Sigma_{12}} = 0.5\%$	0.05	0.13005	0.1305012	26.010	26.100
		0.10	0.22177	0.2223104	44.354	44.462
		0.15	0.29996	0.3006018	59.992	60.120
		0.20	0.37006	0.3707985	74.012	74.159
		0.25	0.43452	0.4353459	86.904	87.069
		0.30	0.49462	0.4955284	98.924	99.105
3	$\frac{\Delta\Sigma_{12}}{\Sigma_{12}} = 1.0\%$	0.05	0.250107	0.2510048	25.010	25.100
		0.10	0.433555	0.4346285	43.355	43.462
		0.15	0.589943	0.5912181	58.994	59.121
		0.20	0.730140	0.7316205	73.014	73.162
		0.25	0.859051	0.8607253	85.905	86.072
		0.30	0.979253	0.9811012	97.925	98.110

5.6.3 Dynamic uncertainty and sensitivity analysis in 3D TWIGL Benchmark reactor transient

Consider the 3D TWIGL heterogeneous reactor (chapter 4). The transient in the reactor is caused by decreasing the thermal absorption cross section. Here the uncertainty in the core

parameters is estimated with respect to uncertainty in scattering cross section. The uncertainty in the scattering cross section is assumed to be 0.1%. The uncertainties in core power (global uncertainty), total peaking factor (3D Peaking factor) and peak mesh power (PMP) (local uncertainty) are estimated using FSAP with IQS model and direct solution method. The results are given Table 5.5-5.7. It is observed that the results agree to a good accuracy. The relative error between the two methods is also found to be small. The results indicate that the FSAP with IQS model is capable of estimating the dynamic uncertainty and sensitivity coefficient to a good accuracy in heterogeneous reactor. The dynamic uncertainty and sensitivity coefficients for core power are computed and they are given in Figs. 5.8 and 5.9.

Table 5.5. Dynamic uncertainty in core power in 3D TWIGL reactor transient (Initial power = 1.13444, $\Delta P|_{t=0} = 1.134\text{E-}02$). The results are compared and the percentage error between the two methods is also shown in the table.

S.N	Parameter	Uncertainty	Time (s)	FSAP Direct soln. $\Delta P/P$	FSAP with IQS model $\Delta P/P$	Absolute Error between two models
1	$\frac{\Delta \Sigma_{1 \rightarrow 2}}{\Sigma_{1 \rightarrow 2}}$	1.0%	0.05	0.34537	0.3421439	0.0032
			0.10	0.42183	0.4150250	0.0068
			0.15	0.54328	0.5282437	0.0150
			0.20	0.76075	0.7223969	0.0384
			0.25	0.87556	0.8591789	0.0164
			0.30	0.88965	0.8793930	0.0103

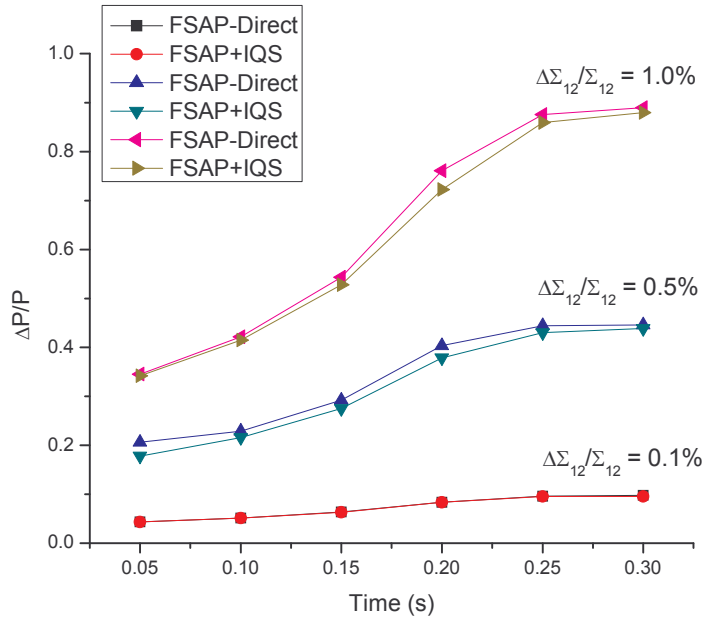


Fig. 5.8 The variation of $\Delta P/P$ with time for the various levels of uncertainty in $\frac{\Delta \Sigma_{12}}{\Sigma_{12}}$.

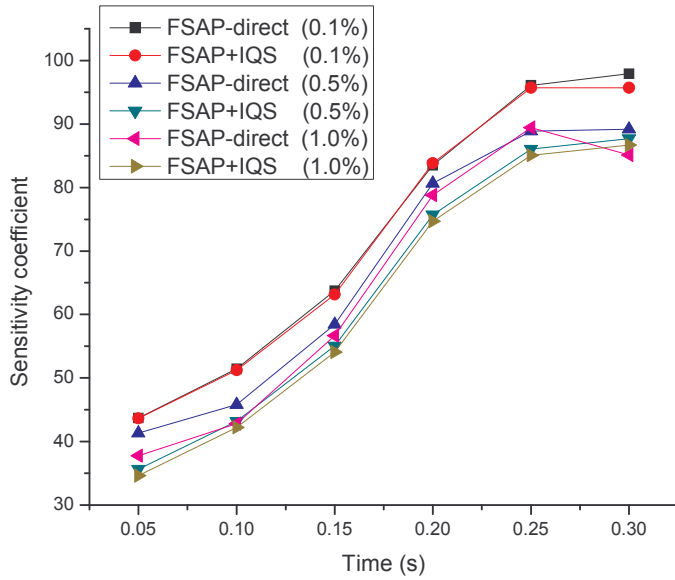


Fig. 5.9. The sensitivity coefficient with time for the various levels of uncertainty in $\frac{\Delta \Sigma_{12}}{\Sigma_{12}}$. The percentage of uncertainty is given in the inset.

Table 5.6. Dynamic uncertainty in total peaking factor (3D PF) in 3D TWIGL Reactor for 1.0% uncertainty in the scattering cross section (Initial power = 1.13444, $\Delta P|_{t=0} = 1.134\text{E-}02$).

S.N	Parameter	Uncertainty	Time (s)	FSAP Direct soln. $\frac{\Delta 3DPF}{3DPF} \%$	FSAP + IQS model $\frac{\Delta 3DPF}{3DPF} \%$
1	$\frac{\Delta \Sigma_{12}}{\Sigma_{12}}$	1.0%	0.05	1.145783E-5	1.7881E-05
			0.10	6.154134E-6	5.9604E-06
			0.15	1.709759E-6	1.4267E-06
			0.20	1.668029E-6	1.4149E-06
			0.25	4.146789E-6	3.9781E-06
			0.30	5.045297E-6	5.4923E-06

Table 5.7. Dynamic uncertainty in peak mesh power (PMP) in 3D TWIGL reactor for 1.0% uncertainty in the scattering cross section (Initial power = 1.13444, $\Delta P|_{t=0} = 1.134\text{E-}02$).

S.N	Parameter	Uncertainty	Time (s)	FSAP Direct soln. $\frac{\Delta(PMP)}{PMP}$	FSAP with IQS model $\frac{\Delta(PMP)}{PMP}$	Absolute error between two models
1	$\frac{\Delta \Sigma_{12}}{\Sigma_{12}}$	1.0%	0.05	0.345066	0.3421438	0.0029
			0.10	0.421043	0.4150250	0.0060
			0.15	0.539337	0.5282437	0.0111
			0.20	0.758517	0.7223970	0.0361
			0.25	0.873785	0.8591789	0.0146
			0.30	0.891265	0.8793930	0.0119

5.7 Summary

The uncertainty in neutron multiplication factor is estimated for various uncertainties in the macroscopic cross sections for 3D homogeneous and 3D TWIGL benchmark reactor. The sensitivity coefficient for neutron multiplication factor is found to follow a linear law. This linear fit can be used to estimate the uncertainty in the neutron multiplication factor for a given uncertainty in the macroscopic cross section.

A new computational method is developed for estimating the dynamic uncertainty in the flux during reactor transient. This computation method is developed by incorporating the IQS model in forward sensitivity analysis procedure (FSAP). Using this method, the dynamic uncertainties in core power, peak mesh power and total peaking factor are estimated for 3D homogenous and 3D TWIGL heterogeneous reactors. Here the dynamic uncertainties are estimated corresponding to uncertainty in the scattering cross section. The dynamic uncertainties are also estimated by directly solving the FSAP and the results are compared. The results agree to a good accuracy. The uncertainties in the core power, peak mesh power and total peaking factor match to a good accuracy. This study shows that this computational method can be used to estimate the uncertainty in the flux during transient with good accuracy. Use of large time step, in this method, in estimating the dynamic uncertainty saves computation time. Another advantage of this computational method is that the dynamic sensitivity analysis can be performed simultaneously along with the transient estimation. The methodology to simultaneously estimate the dynamic uncertainty along with the transient is described. This method can be used to perform the dynamic uncertainty analysis by applying multiple uncertainties simultaneously. This method serves as one of the fastest method to estimate the dynamic uncertainty in the flux during transient.

CHAPTER 6

SUMMARY AND CONCLUSIONS

6.1 Conclusions

A new computational method, the modified exponential time differencing method with improved quasi static (IQS) model, is developed for analyzing the transients in reactors and performing the sensitivity analysis in transients. Using this computational method the transient can be estimated with good accuracy using large time step. This method serves as one of the fastest and efficient method in analyzing the dynamic uncertainty and sensitivity in transient. According to this method, the time dependent neutron flux is split into two parts, i.e. the amplitude function and the shape function. The equation governing the amplitude function, i.e. point kinetics equations, is a stiff differential equation and it describes the fast time evolution of power. The shape function is a slowly varying function of time. The amplitude equation is solved using the modified exponential time differencing (ETD) method and the equation governing the shape function is solved using implicit scheme. Using the modified ETD method, the stiffness factor is efficiently handled and the point kinetics equation can be solved with large time step. The modified ETD method is capable of solving the point kinetics equation for different kinds of reactivity insertions, i.e. step, ramp and oscillatory. It is capable of estimating the transients for longer duration of time also. For constant and slowly varying reactivity perturbations, a scheme to choose the micro time step for solving the point kinetics equation is discussed and applied here to estimate the transients. This method is applied to estimate the transients of the well known CANDU 3D-PHWR kinetics benchmark, 3D LMW kinetics benchmark, 3D TWIGL kinetics benchmark and 3D homogenous reactor transients. These reactors have varying degrees of heterogeneities and the reactivity perturbations are also different.

The transients in CANDU 3D-PHWR, following LOCA, are estimated by this computational method for various micro and macro time steps. The transient estimated by this method is found to be in good agreement with the benchmark results [73] (CERKIN code). The relative errors in the estimation of peak power are found to be 2.02%, 1.53%, 0.94% and 0.98% while using the macro time steps 0.0125s, 0.025s, 0.05s and 0.1s. The effect of space part in estimating the transient is also discussed and is found to be more pronounced here. The error in the estimation of core power when the space part is neglected is also discussed. It is observed that an error of 33.87% is observed at peak power when the space part is neglected in estimating the transient.

The 3D LMW kinetics benchmark transient is analyzed using this method. Here the transient is created by control rod ejection accident (REA). This benchmark involves complicated control rod movements. Here the transient lasts for longer duration of time, i.e. 60s. It is observed that during the transient, the core power increases, reaches a maximum and then starts decreasing. The core power estimated by this method is found to be in good agreement with reference code. From the comparison of results it is established that this new computational method is capable of estimating the transients for longer duration of time. Here also the effect of space part in estimating the transient is analyzed. When the space part is neglected, an error of 7.6% is observed at peak power and an error of 20% is observed in the core power at the end of the transient. Here the effect of space part in estimating the transient is more pronounced. Similarly the maximum error in the estimation of total peaking factor is found to be 3.30% when the space part is neglected while estimating the transients.

The transients in 3D TWIGL heterogeneous and 3D homogeneous reactors are estimated by this new computational method. The estimated flux is found to be in good agreement with

other standard codes. In 3D TWIGL reactor the effect of space part, in estimating the transient, is found to be significant. A maximum error of 10% is observed in the estimation of core power when the space part is neglected. In the case of 3D homogeneous reactor, the error in the estimation of core power, when space part is neglected, is observed to be $< 0.10\%$ for both positive and negative reactivity perturbations.

From the results it is established that this new computational method, the modified exponential time differencing method with improved quasi static (IQS) model, is capable of estimating the transients to a good accuracy. Large time step can be used to estimate the transients without compromising the accuracy and this method serves as one of the fastest method in estimating the transients.

The static and dynamic sensitivity analysis associated with the transient is performed using this new computational method. Using this method, the uncertainty and sensitivity analysis can be carried out efficiently. The static and dynamic sensitivity analysis is performed for (i) 3D homogeneous reactor and (ii) 3D TWIGL reactor. In the case of static uncertainty and sensitivity analysis, the uncertainty in the neutron multiplication factor is estimated for various uncertainties in the input parameters (macroscopic cross sections). It is observed that the thermal fission cross section is more influential in affecting the multiplication factor and the second more influential factor is found to be the thermal absorption cross section for the above reactors considered here. It is also shown that the sensitivity coefficient is found to follow a linear law when the input uncertainty lies in the range 0.05%-0.5%. The sensitivity coefficient can be estimated using the linear law if the input uncertainty falls between 0.05% and 0.5%.

The propagation of macroscopic cross section uncertainty with time (dynamic uncertainty) and its impact on reactor transient is discussed in detail. The effect of macroscopic cross section uncertainty on core power, peak mesh power and total peaking factors during the transient is analyzed. The dynamic sensitivity analysis during transient is performed by incorporating the IQS model in forward sensitivity analysis procedure (FSAP). While incorporating the IQS model in FSAP, a new kind of point kinetics equations is developed. The new kind of point kinetics equations is solved using the modified ETD method. The solution of the new kind of point kinetics equation with the shape function gives the uncertainty in the flux. From the uncertainty in the flux, the uncertainties in core power, peak mesh power and peaking factor are estimated. The dynamic uncertainty and sensitivity analysis is performed for (i) 3D homogeneous reactor transient and (ii) 3D TWIGL reactor transient. Both local and global dynamic sensitivity analyses are performed using FSAP with IQS model as well as directly solving FSAP equations (FSAP-Direct). The results are compared and they are found to be in good agreement. The advantage of FSAP with IQS model is that the dynamic uncertainty and sensitivity analysis, during transient, can be performed in a much faster way without losing the accuracy. Using this new computational method, both the estimation of transient and the dynamic sensitivity analysis can be performed simultaneously. In the case of local dynamic sensitivity analysis, the sensitivity of peak mesh power with respect to macroscopic cross section uncertainty is estimated. In the case of global sensitivity analysis, the sensitivity of reactor core power and total peaking factor (3D peaking factor) are estimated for various macroscopic cross section uncertainties. The uncertainty in total peaking factor (3D PF) is found to be small during the transient in these reactors.

This study establishes that the FSAP with IQS model is capable of estimating the dynamic uncertainty in flux during the reactor transient to a good accuracy. This new computational method serves as one of the fastest method in performing dynamic sensitivity analysis during transient. It is also shown that both the transient analysis and dynamic sensitivity analysis can be performed simultaneously. The results clearly indicate that this method serves as one of the efficient method in evaluating the dynamic uncertainty deterministically. Using this computational method, the uncertainty in the core characteristics can be estimated and safety margins can be fixed more realistically.

6.2 Scope for further research

The modified exponential time differencing (ETD) method can be used to solve the burn-up equation and estimate isotope depletion and production.

The modified exponential time differencing method with IQS model can be applied to estimate the transient with thermal hydraulics feedback. The forward sensitivity analysis procedure (FSAP) with IQS model can be used to analyze the uncertainty in transient arising from the delayed neutron data. This method can be used to quantify the uncertainty in the core characteristics from multiple uncertainties in the macroscopic cross sections. This method can be used to estimate the uncertainty in the isotope production and depletion during fuel burn-up.

LIST OF FIGURES

2.1	Differential volume dV at location ' r '	8
2.2	The micro time step (Δt) and the macro time step (ΔT) adopted in the IQS model	22
3.1	The power transient of the Indian Prototype Fast Breeder Reactor (PFBR) computed by the modified ETD method and the Cohen's method for step reactivity $\rho(t) = 50 \text{ pcm}$	41
3.2	The power transient of the Indian Prototype Fast Breeder Reactor (PFBR) computed by the modified ETD method and the Cohen's method for positive ramp reactivity of 1 pcm/s	42
3.3(a)	The reactivity computed using modified ETD method for the desired power transient $P(t) = \exp(\omega t)$ with $\omega = 0.12353$.	
	(b). The relative error (%) between the reference and the solution obtained using modified ETD method	45
3.4(a)	The reactivity computed using modified ETD method for the desired power transient $P(t) = \exp(\omega t)$ with $\omega = 11.6442$.	
	(b). The relative error (%) in the estimation of reactivity	46
3.5(a)	The reactivity computed using modified ETD method for the desired power transient $P(t) = 1.44836 \times \exp\left(\frac{t}{17.06302}\right) - 0.16335$, $0 \leq t \leq 50s$ for Indian PFBR. (b) The relative error (%) in the estimation of reactivity	47
3.6	The neutron density $n(t)$ (with adiabatic feedback) with time for the external reactivity $\rho_{ex} = \frac{\beta}{2}$	47
3.7	The variation of temperature with time	48
3.8	The variation of estimated net reactivity with time	49
3.9	The variation of estimated feedback reactivity (ρ_{fb}) with time	49
3.10	The variation of feedback temperature coefficient of reactivity, i.e. $\left(\frac{\partial \rho_{fb}}{\partial T}\right)$ with time.	50
3.11	The synthetic power transients at different channels with 4% background noise	54

3.12	The power transient following a step reactivity of 50 pcm	55
3.13	The variation of temperature with time	55
3.14	The variation of net reactivity causing the power transient	56
3.15	The variation of feedback reactivity involved in the power transient	56
3.16	The estimated variation of feedback temperature coefficient of reactivity, $\frac{\partial \rho}{\partial t}$, with time	57
4.1	The relative error in reactor core power when the shape function is neglected in the case of positive reactivity perturbation	65
4.2	The relative error in reactor core power when the shape function is neglected in the case of negative reactivity perturbation	65
4.3	One quadrant of 3D-TWIGL reactor	67
4.4	The relative error (%) in core power (3D TWIGL) when the space part is neglected.	71
4.5	The variation of axial power (radially integrated) profile at $t = 0.4s$	72
4.6	One quadrant of the LMW core	75
4.7	The axial position of control rod before transient	76
4.8	The axial position of control rod at the end of the transient	76
4.9	The core power density (W/cm^3) with time	78
4.10	3D LMW core power with space-time kinetics and point kinetics	79
4.11	Relative error (%) in the estimation of core power when space part is neglected	79
4.12	Vertical cross section of CANDU 3D-PHWR	81
4.13	Vertical cross section (at $Z = 0$) of CANDU 3D-PHWR	82
4.14	Horizontal cross section (at $Y = 390\text{ cm}$) of CANDU 3D-PHWR	82
4.15	Vertical cross section of CANDU 3D-PHWR at $Z = 600\text{ cm}$.	83
4.16	Relative Power of CANDU 3D-PHWR using macro time step 0.0125s	86
4.17	Relative Power of CANDU 3D-PHWR using macro time step 0.0250s	87
4.18	Relative Power of CANDU 3D-PHWR using macro time step 0.05s	87
4.19	Relative Power of CANDU 3D-PHWR using macro time step 0.1s	88
4.20	Normalized thermal flux in XZ plane, $Y = 360\text{ cm}$, $Z = 270\text{ cm}$, $T = 2.5\text{ s}$.	88

4.21	The relative error (%) in power for various macro time steps	89
4.22	Relative error (%) in core power (CANDU 3D-PHWR) when space part is neglected	89
4.23a	The thermal flux distribution ($270 < Z < 300$) in CANDU PHWR at $t = 0s$	91
4.23b	The thermal flux distribution ($270 < Z < 300$) at $t = 0.5s$	91
4.23c	The thermal flux distribution ($270 < Z < 300$) at $t = 1.0s$	92
4.23d	The thermal flux distribution ($270 < Z < 300$) at $t = 1.5s$	92
4.23e	The thermal flux distribution ($270 < Z < 300$) at $t = 2.0s$	93
4.23f	The thermal flux distribution ($270 < Z < 300$) at $t = 2.5s$	93
4.24a	The fast flux distribution ($270 < Z < 300$) in CANDU PHWR at $t = 0.0s$	94
4.24b	The fast flux distribution ($270 < Z < 300$) at $t = 0.5s$	94
4.24c	The fast flux distribution ($270 < Z < 300$) at $t = 1.0s$	95
4.24d	The fast flux distribution ($270 < Z < 300$) at $t = 1.5s$	95
4.24e	The fast flux distribution ($270 < Z < 300$) at $t = 2.0s$	96
4.24f	The fast flux distribution ($270 < Z < 300$) at $t = 2.5s$	96
4.25	The variation of power tilt (top-bottom) during the transient	97
4.26	The variation of power tilt (side-side) during the transient	97
4.27	The variation of power tilt (front-back) during the transient	97
5.1	The variation of sensitivity coefficient with uncertainty in Σ_{a2} for 3D homogeneous reactor	110
5.2	The variation of sensitivity coefficient with uncertainty in $v\Sigma_{f2}$ for 3D homogeneous reactor	110
5.3	The variation of sensitivity coefficient with $\frac{\Delta v\Sigma_{f1}}{v\Sigma_{f1}}$ for 3D TWIGL reactor	113
5.4	The variation of sensitivity coefficient with $\frac{\Delta v\Sigma_{f2}}{v\Sigma_{f2}}$ for 3D TWIGL reactor	113
5.5	Simultaneous estimation of reactor transient and dynamic uncertainty in flux	121

5.6	The variation of $\Delta P/P$ with time for the various levels of uncertainty in $\frac{\Delta \Sigma_{12}}{\Sigma_{12}}$	124
5.7	The sensitivity coefficient with time for the various levels of uncertainty in $\frac{\Delta \Sigma_{12}}{\Sigma_{12}}$	125
5.8	The variation of $\Delta P/P$ with time for the various levels of uncertainty in $\frac{\Delta \Sigma_{12}}{\Sigma_{12}}$	129
5.9	The sensitivity coefficient with time for the various levels of uncertainty in $\frac{\Delta \Sigma_{12}}{\Sigma_{12}}$	129

LIST OF TABLES

3.1	The power transient of thermal reactor computed by the modified ETD method and the TSM method ($\rho_0 = -1\%$)	39
3.2	The power transient of thermal reactor computed by the modified ETD method and other methods ($\rho_0 = 0.003$)	39
3.3	The power transient of the Indian Prototype Fast Breeder Reactor (PFBR) computed by the modified ETD method and the Cohen's method (step reactivity = 50 pcm)	40
3.4	The power transient of the Indian Prototype Fast Reactor (PFBR) computed by the modified ETD method and other methods for positive ramp reactivity of 1pcm/s	40
3.5	The temperature coefficient of reactivity $\left(\frac{\Delta k/k}{^\circ C}\right)$ obtained using the modified ETD method along with the reference	48
3.6	The temperature coefficient of reactivity $\left(\frac{pcm}{^\circ K}\right)$ of the Indian PFBR, obtained using the modified ETD method for various background noise levels with beamforming	54
4.1	Two group constants for 3D Homogeneous Reactor	62
4.2	The fast and thermal flux estimated by the modified ETD method with IQS model for positive reactivity perturbation	62
4.3	The fast and thermal flux computed by the modified ETD method with IQS model for negative reactivity perturbation	63
4.4	Total peaking factor during transient for positive reactivity perturbation	63
4.5	Total peaking factor during transient for negative reactivity perturbation	64
4.6	Error in the peaking factor during the transient	64
4.7	Total peaking factor for various mesh sizes.	66
4.8	Two group constants for 3D TWIGL reactor at different regions	68
4.9	Comparison of k_{eff}	69
4.10	The thermal flux of 3D TWIGL reactor, estimated by modified ETD + IQS method along with other standard codes	69

4.11	Total peaking factors estimated with space-time kinetics and in the absence of space part	71
4.12	Material composition for LMW Benchmark reactor	74
4.13	Delayed neutron precursor data	75
4.14	Estimated k_{eff} along with the reference	76
4.15	Comparison of core power density with SKETCH code	77
4.16	Total peaking factor during the transient	78
4.17	Material composition of CANDU 3D-PHWR at different regions	83
4.18	Two group constants for CANDU 3D-PHWR	84
4.19	Delayed neutron fractions and precursor decay constants	84
4.20	Comparison of initial k_{eff} with other standard codes	86
5.1a	Uncertainty in k_{eff} and the sensitivity coefficient for 3D Homogenous reactor	108
5.1b	Uncertainty in k_{eff} and the sensitivity coefficient for 3D TWIGL reactor	111
5.2a	Comparison of transients (without uncertainty)	123
5.2b	Dynamic uncertainty (%) in core power in 3D Homogeneous reactor	124
5.3	The uncertainty in total peaking factor for 3D Homogeneous reactor	126
5.4	The uncertainty in peak mesh power (PMP) for 3D Homogeneous reactor	127
5.5	Dynamic uncertainty in core power in 3D TWIGL reactor transient	128
5.6	Dynamic uncertainty in total peaking factor in 3D TWIGL Reactor	130
5.7	Dynamic uncertainty in peak mesh power in 3D TWIGL Reactor	130